GROWTH MECHANISMS OF ATOMIC LAYER EPITAXY STUDIED IN SITU BY REFLECTANCE DIFFERENCE SPECTROSCOPY

by

Richard Arès

B.Sc., Physique, Université de Montréal, 1990
M.Sc., Physique, Université de Montréal, 1993

THESIS SUBMITTED IN PARTIAL FULFILLMENT OF THE REQUIREMENTS FOR THE DEGREE OF

Doctor of Philosophy

in the Department
of
Physics

© Richard Arès 1997

SIMON FRASER UNIVERSITY
August 1997

All rights reserved. This work may not be reproduced in whole or in part, by photocopy or other means, without permission of the author.

National Library of Canada

Bibliothèque nationale du Canada

Acquisitions and Bibliographic Services

Acquisitions et services bibliographiques

395 Wellington Street
Ottawa ON K1A 0N4
Canada

395, rue Wellington
Ottawa ON K1A 0N4
Canada

Your file Votre référence

Our file Notre référence

The author has granted a non-exclusive licence allowing the National Library of Canada to reproduce, loan, distribute or sell copies of this thesis in microform, paper or electronic formats.

L'auteur a accordé une licence non exclusive permettant à la Bibliothèque nationale du Canada de reproduire, prêter, distribuer ou vendre des copies de cette thèse sous la forme de microfiche/film, de reproduction sur papier ou sur format électronique.

The author retains ownership of the copyright in this thesis. Neither the thesis nor substantial extracts from it may be printed or otherwise reproduced without the author's permission.

L'auteur conserve la propriété du droit d'auteur qui protège cette thèse. Ni la thèse ni des extraits substantiels de celle-ci ne doivent être imprimés ou autrement reproduits sans son autorisation.

0-612-24289-7

Canada

APPROVAL

Name: Richard Arès

Degree: Doctor of Philosophy

Title of thesis: Growth Mechanisms of Atomic Layer Epitaxy Studied *In Situ* by Reflectance Difference Spectroscopy

Examining Committee:

Chair: Dr. Michael Plischke
Professor of Physics

Dr. Simon P. Watkins
Senior Supervisor
Associate Professor
Department of Physics

Dr. Michael L. W. Thewalt
Professor of Physics

Dr. Robert F. Frindt
Professor of Physics

Dr. Albert E. Curzon
Internal Examiner
Professor of Physics

Dr. Christine A. Wang
External Examiner
Senior Research Officer
Lincoln Laboratory
Massachusett Institute of Technology

date approved: 8 August 97

ABSTRACT

Metalorganic chemical vapor deposition (MOCVD) is a semiconductor growth technique that proceeds by exposing the surface of a heated substrate to vapors of different organic molecules. Atomic layer epitaxy (ALE) is a modification of MOCVD which alternates the exposure to vapors producing atoms of different columns in the periodical table in order to grow the crystal one atomic layer at a time.

The ALE growth of GaAs and InAs has been studied *in situ* by an optical technique called reflectance difference spectroscopy (RDS). For GaAs it is demonstrated that when trimethylgallium (TMGa) first arrives at the surface there is more than 1 monolayer (ML) of As terminating the crystal. The As lying in the topmost layer does not produce any extra Ga incorporation but plays an important role in the preservation of the 1 ML/cycle growth regime by inhibiting the desorption of As from the underlying layer.

The desorption of As from the topmost layer is facilitated by the presence of Ga on the surface. This is attributed to the chemical bonding of the As with methyl radicals produced by the decomposition of TMGa at the growth surface. The first 0.5 ML of incorporated Ga does not form dimers and remains invisible to the RDS measurements. The combined role of step edges and the redistribution of first layer As maintains the As termination of the surface until that point.

The presence of methyl radicals attached to the surface permits the deposition of a full ML of Ga and preserves the stoichiometry of the process. The methyl radicals are also observed to inhibit the formation of Ga droplets on the surface during exposure to the group III precursor.

A model using gas phase reactions exclusively is developed and shows that the experimental measurements of the incorporation of Ga during both the ALE and MOCVD processes can be reproduced, indicating that gas phase reactions have to be included in any complete picture of the ALE growth process.

The growth of ultrathin InAs/GaAs heterostructures by ALE has been characterized *in situ* for the first time using RDS. Significant In segregation is observed when InAs is

buried with GaAs and none is detected for the inverse structure. This asymmetry points to thermodynamic effects during growth favoring the exchange between the top and buried layers and bringing the In atoms to the surface.

The incorporation of In on GaAs proceeds without saturation for up to 4 ML coverage as opposed to the InAs surface where In stops entering the crystal after the surface is completely covered. The presence of strain stimulates the formation of islands on the surface during In exposure which disrupts the conditions for self-limiting growth.

DEDICATION

En mémoire de celle qui m'aura accompagné dans mes premiers pas sur la route de la connaissance et qui m'a transmis la curiosité et la persévérance nécessaires à la poursuite de mon chemin.

Madeleine Robillard-Arès

(1938-1996)

ACKNOWLEDGMENTS

When I first joined Prof. Watkins' lab in March 1993, the room that was to become the Simon Fraser University Semiconductor Growth Facility was still only an ordinary classroom. The amount of work as well as the many challenges that separated me from the completion of this degree was, thankfully, unknown to me at the time. The journey has been demanding but immensely rewarding. I am grateful to Prof Simon Watkins for providing me with the opportunity to participate in such an endeavor. His professional and personal support have been key ingredients in my progress as a young scientist.

I want to thank especially Dr. Chuong Tran showing me how to simultaneously operate every single piece of equipment in the lab without losing my mind. His friendship and scientific insight have been most valuable.

A big thank you to Dr. Georg Soerensen and Mike Bilany for their impressive technical expertise and for being so much fun to work with.

I thank and salute the personnel of the Physics office: Shauna, Sada, Sharon, Audrey for being so helpful (tactful?) when I could not get my act together.

To my fellow lab members who joined Simon and I along the way, Dave, James, Wenkai, Phil, Jinsheng, I say: "hang on! There is a life after the Ph.D."

And most importantly I want to acknowledge the contributions, without which my life would have no sense, of all the people that have crossed my path and nourished me with their love and wisdom. My mother who has shown early that learning was fun. My father and brother whose love and trust gave the confidence to carry on. Raymond, Eric Stéphane, Yves, Moyra, pour votre amitié qui me nourrit et m'a permis de survivre à 7 mois de pluie continuelle a chaque hiver.

À tous les êtres eveillés qui me guident et me rapellent que l'essentiel est le chemin et non la destination.

À toi, Michèle, chère "spirit sister", je dis: Gassho!

TABLE OF CONTENTS

APPROVAL ii

ABSTRACT iii

DEDICATION v

ACKNOWLEDGMENTS vi

TABLE OF CONTENTS vii

LIST OF TABLES xi

LIST OF FIGURES xii

1. INTRODUCTION 1

2. EPITAXY OF III–V SEMICONDUCTORS 4

2.1 Metalorganic Chemical Vapor Deposition 4

2.1.1 Delivery of the precursor molecule 6

2.1.2 Hydrodynamics in the reactor chamber 8

2.1.3 Chemistry of dissociation of the precursor molecule 9

2.1.4 Surface reactions 11

2.2 Atomic Layer Epitaxy 12

2.2.1 The ALE cycle 14

2.2.2 Self–limiting growth 15

2.2.2.1 Selective adsorption model 16

2.2.2.2 Adsorbate inhibition model 17

2.2.2.3 Flux balance model 18

2.2.3 Carbon incorporation 18

3. *IN SITU* MONITORING 20

3.1 Surface reconstructions 21

3.1.1 Charge neutrality of the surface: missing dimer model 23

3.2 Optical anisotropy: reflectance difference spectroscopy 24
3.2.1 Theoretical analysis 24
3.2.2 Spectral information 25

4. EXPERIMENTAL DETAILS 28

4.1 Epitaxy system 28
4.1.1 MOCVD reactor and gas handling system 28
4.1.2 Supplying the precursors to the growth chamber 29
4.1.3 Growth chamber: technical details 30
4.1.4 Sample preparation 32

4.2 Reflectance difference spectroscopy 33
4.2.1 Description of the optical setup 33
4.2.2 Analysis of the optical response 35
4.2.3 Determination of the zero 38
4.2.4 Time resolved spectral measurements 40

4.3 X-ray diffraction 41
4.3.1 X-ray diffractometer 41
4.3.2 Growth rate measurements 43
4.3.2.1 Kinematic description of the rocking curves 43

4.4 Atomic force microscopy 47
4.4.1 Contact and non-contact modes 47
4.4.2 Description of the microscope and data acquisition 48

5. GROWTH MECHANISMS 51

5.1 Arsenic desorption 52
5.1.1 GaAs 53
5.1.2 InAs 55

5.2 Group III incorporation 60
5.2.1 GaAs 60
5.2.2 InAs 67

5.3 Preservation of the stoichiometry 69
5.3.1 GaAs 70
5.3.2 InAs 77

5.4 Model for the chemisorption of the group III atoms 80

5.5 Morphology study of the self-limiting process 85
5.5.1 Droplet formation 87
5.5.2 Effect of methyl radicals 89

5.6 Alkyl desorption 91
5.6.1 GaAs 91
5.6.2 InAs 95

5.7 Conclusions 96

6. KINETIC STUDY OF THE GROWTH PROCESS 97

6.1 Introduction 97

6.2 Literature review 98
6.2.1 Other models 98
6.2.2 Precursor mediated approach 99

6.3 Gas phase based model 101
6.3.1 Theoretical description 101
6.3.2 Comparison with growth rate data 106
6.3.3 Comparison with ALE growth rate 109

6.4 Conclusion 110

7. HETEROEPITAXY 113

7.1 Indium segregation 114

7.1.1 Background 114

7.1.1.1 Segregation models 115

7.1.2 *In situ* study 116

7.1.2.1 Measurement of the segregation coefficient 122

7.1.3 Conclusions 124

7.2 Breakdown of self-limiting behavior for ALE heteroepitaxy 126

7.2.1 Experimental results 128

7.2.2 Conclusions 134

8. CONCLUDING REMARKS 135

APPENDIX A: ELECTRONIC FEEDBACK FOR THE RDS SETUP 139

REFERENCES 142

LIST OF TABLES

Table 2-1 Summary of the physical parameters of the different precursors used in this study 7

Table 6-1 Fitting parameters used to model the growth rate data. The values in bold were allowed to vary while the other values were kept constant. 108

LIST OF FIGURES

Fig. 2.1 Side view of the vessel used to store and supply the organometallic precursors. 6

Fig. 2.2 Comparison of the dissociation mechanisms for TMGa (homolytic fission) and TEGa (β-hydride elimination). 10

Fig. 2.3 AFM image of the surface of a GaAs layer grown at 580°C by MOCVD. 14

Fig. 3.1 Simplified view of the surface reconstruction of a zincblende semiconductor like GaAs. The circles and squares represent Ga and As atoms respectively. Dimers are illustrated by full symbols 22

Fig. 3.2 RDS energy spectra of surface reconstructions of GaAs as identified by RHEED. 26

Fig. 3.3 Surface reconstructions commonly observed in UHV GaAs. The As and Ga atoms are respectively represented by squares and circles. Dimerized atoms have solid symbols. 27

Fig. 4.1 Schematic view of the gas handling system for the MOCVD reactor. The RDS setup is mounted vertically on a metal plate over the growth chamber 29

Fig. 4.2 Side view of the growth chamber. The inlets with their respective gas species are identified. 31

Fig. 4.3 RDS optical setup as it is configured on the vertical plate. Each component is identified by a label and discussed in the text. 33

Fig. 4.4 Propagation of the polarization through the different components of the RDS setup. The reference frames are aligned with the main axes of the sample surface. 36

Fig. 4.5 Example of the procedure used to measure the contributions of the component misalignment and imperfection to the RDS signal 40

Fig. 4.6 Schematic view of the x-ray diffractometer. The sample and detector stages are rotated through angles of θ and 2θ respectively. 42

Fig. 4.7 Kinematic justification for the modulation of the diffracted beam when a thin marker layer is inserted in a single crystal. The wave fields diffracted from the cap and buffer layers interfere. 45
Fig. 4.8 Modulation of the diffracted x-ray intensity by the presence of a thin InAs layer in GaAs. The dots represent the experimental data and the solid line the simulation using the dynamical theory.......... 46
Fig. 4.9 Interatomic force acting on the cantilever as a function of the distance between the tip and the sample. 48
Fig. 4.10 Basic components of the atomic force microscope. 49
Fig. 5.1 *In situ* RDS monitoring of the desorption of As from the GaAs surface. The top panel shows the time transient at 2.6 eV. The specific instants during the transients are: (i) 0 s, (ii) 3.7 s, (iii) 30 s, and (iv) 180 s. The corresponding energy spectra are shown in the lower panel. 54
Fig. 5.2 RDS energy spectra of the InAs surface with (solid) and without (dotted) TBAs overpressure. The corresponding recontruction for the purged surface has been identified as (4×2). The other spectrum is called "As super rich" (ASR) in this work. 56
Fig. 5.3 *In situ* RDS monitoring of the desorption of As from the InAs surface. The roman numerals correspond to specific instants and their energy spectra are displayed in the lower panel. 57
Fig. 5.4 Arrhenius plot of the two parts of the RDS transient for the desorption of As from the InAs surface. 59
Fig. 5.5 Growth rate as a function of exposure time to the group III exposure at 470°C. The arrows are positioned at the time needed for the RDS transient to saturate. 61
Fig. 5.6 RDS signal monitored at 2.6 eV during an ALE cycle for the three precursors. The energy spectra of the different instants of interest are compared in Fig. 5.7. 64
Fig. 5.7 RDS energy spectra of the surface during the ALE cycles illustrated in Fig. 5.6. The letters identify the specific instants. 66

Fig. 5.8 *In situ* RDS monitoring of the InAs surface during ALE. 68

Fig. 5.9 RDS spectra of the surface of GaAs after a long purge with different TMGa pulse durations (given in the insets with the RDS transient). 71

Fig. 5.10 RDS spectra of the purged GaAs surface as a function of TMGa exposure length at 470°C. The dotted lines are fits according to the ratio discussed in the text. The values of the ratio are plotted in Fig. 5.11 73

Fig. 5.11 Overlay of the Ga incorporated in the layer as measured by XRD (solid line) with the fitted ratio (dots). The RDS transient at 2.6 eV (dashed line) is included for comparison 74

Fig. 5.12 RDS transient for the desorption of As from the GaAs surface with no TMGa (dot-dashed line), 0.25 ML TMGa (solid line) and > 1 ML (dotted line) 77

Fig. 5.13 RDS spectra of the purged InAs surface as a function of TMIn exposure length at 390°C. The dotted lines are fits according to the ratio discussed in the text. The values of the ratios are plotted in Fig. 5.14 79

Fig. 5.14 Overlay of the In incorporated in the layer as measured by XRD (thick line) with the fitted ratio (triangles). The RDS transient (thin line) is included for comparison 80

Fig. 5.15 Schematic illustration of our model for the incorporation of Ga during ALE of GaAs 82

Fig. 5.16 Mechanism inhibiting the formation of Ga dimers through the redistribution of As atoms from the step edges 84

Fig. 5.17 AFM pictures of the GaAs surface after 1 ALE cycle with a group III exposure equivalent to 2 ML. Picture (a) shows the buffer layer only. The group III precursors are TEGa (b), TMGa (c), and TNPGa (c). 87

Fig. 5.18 AFM pictures of the GaAs surface for a 1ML exposure to TMGa (b) and TEGa (c). Picture (a) shows only the buffer layer. 89

Fig. 5.19 AFM picture of the GaAs surface after the exposure to 1 ML of TMGa and 1 ML of TEGa separated by 0 s (a), 2 s (b), and 10 s (c) of hydrogen purge. 91

Fig. 5.20 Arrhenius plot of the time constant of the RDS transient during the surface purge following the group III exposure for TMGa (empty) and TNPGa (solid). The solid line is a least square fit. The inset shows a typical RDS transient with the fit given by the solid line. 93

Fig. 5.21 Decomposition of the mononeopentylgallium via the β-methyl elimination process. 94

Fig. 5.22 Arrhenius plot of the slope of the RDS signal during the hydrogen purge following TMIn exposure in ALE of InAs. 96

Fig. 6.1 Schematic view of the gas dynamics near the surface during the MOCVD process. On the left side a graph gives a qualitative illustration of the precursor partial pressure as a function of distance from the surface 102

Fig. 6.2 Growth rate measurements for GaAs grown with TMGa as a function of temperature obtained by XRD (solid dots) and RDS (circle). The solid line shows the best fit using the model outlined in the text. 107

Fig. 6.3 Growth rate measurements for GaAs grown with TNPGa as a function of temperature obtained by XRD (solid dots) and RDS (circle). The solid line shows the best fit using the model oulined in the text. 108

Fig. 6.4 ALE growth rate of GaAs using TMGa as the group III precursor. The solid line is the fit from the model outlined in the text. The dotted line shows the prediction of the standard Langmuir theory. 109

Fig. 6.5 Temperature dependence of the growth rate. The cross hatched regions indicate purely limited regimes. The square shows approximately the temperature window for ALE of GaAs. 112

Fig. 7.1 Schematic view of the heterostructure. 117

Fig. 7.2 RDS signal measured at 2.6 eV during the growth of a InAs SMQW in GaAs. 118

Fig. 7.3 RDS signal measured at 2.6 eV during the growth of 1 ML of GaAs in InAs. 119

Fig. 7.4 RDS energy spectra of the TBAs exposed surface as a function of the number of ALE cycles for the InAs SMQW in GaAs. 120

Fig. 7.5 RDS energy spectra of the TBAs exposed surface as a function of the number of ALE cycles for the GaAs ML in InAs. 121

Fig. 7.6 RDS signal at 2.6 eV monitored during the growth of InAs/GaAs heterostructures with different TMIn pulse durations. 123

Fig. 7.7 Variation of the shift in the RDS signal as a function of growth thickness for the heterostructures of Fig. 7.5. The solid lines represent a least square fit to the data. 124

Fig. 7.8 RDS signal monitored at 2.6 eV during the ALE growth of InAs SMQW's in GaAs at different growth temperatures. The time axis has been normalized to the number of cycles. 127

Fig. 7.9 Growth rate measurements for homo- (dots) and heteroepitaxy (triangles) of InAs by ALE at 360°C. 129

Fig. 7.10 Growth rate measurements for homo- (dots) and heteroepitaxy (triangles) of InAs by ALE at 390°C. 130

Fig. 7.11 Low temperature photoluminescence emission spectra of InAs SMQW's in GaAs as a function of TMIn pulse length. The asterisk identifies the QW related emission. 131

Fig. 7.12 Comparison of heteroepitaxial growth rate of InAs on GaAs at 360°C and 390°C. The lines are linear square fits to the data. The cross symbol shows a result at 470°C. 133

Fig. A.1 Simplified schematic representation of the circuit detailed in Fig. A.2. 140

Fig. A.2 Electronic circuit used to regulate the DC signal in the RDS setup. 141

1. Introduction

The level of miniaturization attained in electronics over the last decades has been astounding. In 1989 the price per unit function had shrunk by more than seven orders of magnitude compared to the transistors of the late 50's [1]. The trend has remained on an exponential growth in the last decade and ever more stringent requirements are imposed on the characteristics and performance of the devices fabricated from thin semiconductor films. Of all the different techniques available today to grow such structures only two have displayed a level of control over the growth conditions sufficient to aspire at contributing to the next generations of devices. These techniques are molecular beam epitaxy (MBE) with its hybrid form chemical beam epitaxy (CBE) or organometallic molecular beam epitaxy (OMMBE), and metalorganic chemical vapor deposition (MOCVD) with its various acronyms (OMVPE, MOVPE).

The ultra high vacuum (UHV) prevailing in MBE permits the use of electron beam based measurement techniques which gives it a definite edge over MOCVD in terms of diagnostics tools to optimize the growth. On the other hand MOCVD is more flexible, allowing the growth of phosphorous compounds more easily and because of the simplicity of the equipment reducing the initial capital cost. In the last decade or so optical techniques have been developed as *in situ* monitoring tools to be used in MOCVD, paving the way for more detailed studies of the growth process.

Atomic layer epitaxy (ALE) was first tried on a III/V system using organometallics in the 80's copying a technique developed for ZnO [2]. The goal was to acquire total control of the layer thickness, composition and doping over a large area of the wafer. ALE makes use of a growth environment similar to MOCVD but

proceeds by alternate exposure to species of different groups separated by short purges. Since the process is supposed to self regulate itself, stopping the incorporation of an element when the surface is fully covered, both the value and the uniformity of the layer thickness are perfectly controlled [3]. The issue of doping is a little more complicated. Even if some material has been grown with purity levels adequate for device fabrication high levels of carbon contamination is still a problem today. The use of alkyl precursors such as trimethylgallium (TMGa) combined with the central role played by surface reactions in ALE create a situation where the surface is exposed to carbon-containing groups for significant amounts of time. However, as we will show in this work, the presence of these organic radicals, if undesirable from a purity standpoint, is critical to the preservation of a well controlled cycle.

Other effects such as segregation at the growth interface create challenges for the ALE process. Ideally the nature of the ALE cycle should allow for a perfect control of the crystal composition at a monolayer (ML) accuracy. Vertical movement of atoms through the surface, e.g. segregation, complicates the growth severely. As an example of such a detrimental effect consider the case of the single ML InAs quantum well in GaAs (SMQW). This structure is believed to be a good candidate to improve the efficiency of active layers in some devices by confining the carriers in the InAs where they have a much larger mobility. The performance of such a structure depends heavily on the abruptness of the interface. With a well thickness of only a few angstroms any variation is expected to strongly affect the dynamics of the carriers.

This work focuses on the use of reflectance difference spectroscopy (RDS) as an *in situ* probe to study the microscopic mechanism governing ALE, and more specifically, the incorporation of the group III atom in the crystal. Substantial efforts have been made in the last decade to improve the knowledge of the process in the hope of improving the performance of the technique. The state of the surface at each stage of the incorporation is investigated with RDS and some conclusions can be drawn from the data. This constitutes the main topic of this work.

Starting from the results of the previous study we then push the investigation of the Ga incorporation in GaAs a step further. The kinetics of the growth process have

been explained with two different approaches depending on whether MOCVD or ALE was considered. Our ALE results suggest that the distinction is not as clear as was first assumed. Using conditions thought to be exclusive to the MOCVD process we try build a model to explain ALE in terms of gas phase diffusion exclusively.

In the last part of the thesis we report on some work that was done in the *in situ* monitoring of the growth of actual structures. In this case the structure was the SMQW heterostructure. Indium segregation is a major problem in the growth of such layers, and any characterization tool that can provide immediate *in situ* information regarding surface properties is extremely valuable.

The thesis is divided in the following way. The first two chapters deal with some of the theoretical background pertaining to the processes under study. Chapter 2 explains the basics of epitaxy with an emphasis on MOCVD and ALE. The overview is structured so the main concepts related to the present study are discussed. The concepts that generated the development of RDS as well as some theoretical treatment of the measurements are presented in chapter 3.

A detailed description of the different measurement techniques is given in chapter 4 along with some information on the experimental conditions of the growth. The growth reactor is described as well. The different topics of investigation are presented in their own chapters. The main project of the *in situ* study of the growth mechanisms of ALE is treated in chapter 5. Chapter 6 gives a description and a discussion of a simple model to explain the kinetics of the growth processes in MOCVD and ALE. The experimental results end with chapter 7 where SMQW growth is studied with an *in situ* point of view. Finally some concluding remarks and comments on future work are outlined in chapter 8. This works has a single appendix where a detailed description of the electronic feedback control of the RDS signal is presented.

2. Epitaxy of III–V semiconductors

2.1 Metalorganic Chemical Vapor Deposition

The idea of growing a crystal by exposing an existing matrix to a vapor of molecules is straightforward. The first challenge one meets, though, comes from the nature of semiconductors themselves. Since the electrical properties of these crystals are intimately linked to the number of impurities present in them, the "cleanliness" of the technique is crucial. In order to illustrate the kind of performance demands that will have to be met one has to get a feel for the extreme sensitivity of semiconductor to any kind of impurity. A crystal having an impurity level of 1 ppm, or in other words a dopant concentration of about 10^{16} cm^{-3}, is considered significantly if not heavily doped. Layers that are labeled "pure" or "undoped" have impurity contents in the 10^{13} to 10^{15} cm^{-3} range. Since the MOCVD process is performed in an environment where the pressure varies from 10 to 760 Torr, the purity of the different components (gasses, precursors) used has to be very high.

The use of large organic molecules as a source for the elements to enter the crystal makes the success of such a task even more challenging,especially since carbon is a dopant for semiconductors of the III-V family. The natural approach to such a growth would be to proceed under an ultra high vacuum (UHV) environment using sources made of single atoms or simple molecules. This technique has already been developed and is called molecular beam epitaxy (MBE). The improvement of crystal purity there, is partly a question of vacuum quality. Both MBE and MOCVD rely on source purity as well. Apart from the complexity and costly nature of the equipment

there are a number of problems that arise from the UHV technique as well. MOCVD has turned out to be not only more cost effective compared to MBE but more flexible, permitting the growth of a wider variety of materials. This has created today's situation where MOCVD claims ever increasing parts of the world's semiconductor thin films industry and is expected to continue doing so into the next century.

ALE has been borrowed from work done initially on II-VI semiconductors. The physical conditions are the same as the ones used in MOCVD except that the vapors are not introduced in the chamber simultaneously. Each precursor is supplied sequentially to the surface, separated by a purge. In this way no interaction is possible between the different molecules in the gas phase. Under well controlled conditions, the growth produces one atomic layer of the crystal at a time over the entire surface of the substrate. The ideal result is a perfect control over the layer thickness and composition. The reality is considerably different, as will become obvious in the following pages.

The technique has been used with variable success over several different systems. The development of novel *in situ* techniques such as RDS provides supplementary means of gaining knowledge on the intimate workings of the growth, and improves the odds of solving the different problems.

The following chapter will give a brief review of the principal ideas behind both techniques. The first section will give a simple picture of the MOCVD process. The concepts are presented in semi chronological way: i.e. the different topics are discussed in the order that they appear in the lifetime of a precursor molecule in MOCVD, from its extraction from the liquid phase in the bubbler to its dissociation and incorporation into the crystal. The description is not intended to be complete. Only the basic principles will be discussed in order to provide the reader with the necessary tools to appreciate the different topics of this study. A more complete discussion has been published by Stringfellow [1].

The last section of the chapter will give a description of the experimental setup used for the different projects. The procedure used to calculate the different flows from the precursor vapor pressure will be summarized along with details on the

different organometallic compounds used. The chapter ends with a description of the pre–growth sample preparation in the case where the wafer used were not "epi ready".

2.1.1 Delivery of the precursor molecule

The first part of the MOCVD process is concerned with delivering the organic molecules used in the growth. This must be done in a quantitatively accurate manner in order to keep control over the growth process on the surface of the wafer, at the other end of the line. The method is very simple and uses basically only ideal gas law principles.

The precursors are stored, in liquid form, in stainless steel vessels which are kept at a stable temperature by being immersed in a temperature controlled ethylene glycol bath. The control system has an accuracy better than 0.1 °C. Fig. 2.1 shows a schematic description of the setup. The vessel is equipped with two stainless steel

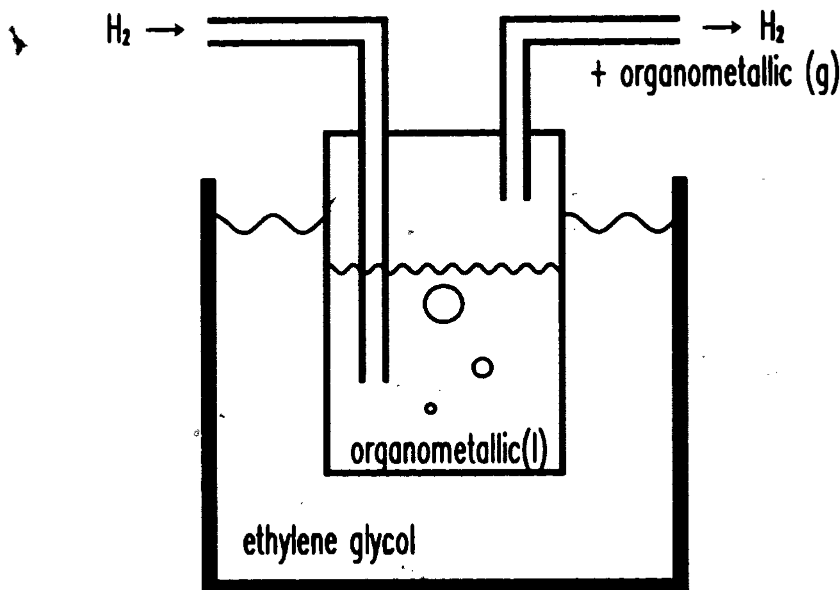

Fig. 2.1 Side view of the vessel used to store and supply the organometallic precursors.

access ports: an inlet port which goes deep into the liquid, and an outlet port that collects the vapor. Hydrogen is forced into the precursor liquid and the bubbles that form float to the surface, becoming saturated with precursor vapor along the way. The gas phase on top of the liquid is assumed to be in thermodynamic equilibrium with the

liquid. The precursor vapor is then collected from the outlet and injected into the growth system.

The exact flow of precursor vapor (f_p) in the gas mixture coming out of the bubbler can be calculated from the ideal gas law and the assumption that the vapor reaches its equilibrium partial pressure at the outlet.

$$f_p = \frac{F}{22407.47} \frac{P_l(T_b)}{\left(P_B + P_l(T_b)\right)} \quad (mol/min) \tag{2-1}$$

The parameters that need to be controlled precisely are: the temperature of the bath (T_b), the pressure in the bubbler (P_B), and the flow of gas passing through it (F). The partial pressure (P_l) of the liquid is taken from the literature or from the manufacturer and is a function of the bath temperature. The accuracy of control of each of these parameters determines the total precision in the flow of molecules extracted from the bubblers. We have already stated that the temperature is kept within 0.1 °C of the nominal value. The pressure controllers have an accuracy better than 0.5% and the mass flow controllers are used in the top 90% of their range where their accuracy is better than 1% of nominal. The given value for the precursor vapor pressure is assumed to have an accuracy much better than that of the bubbler pressure so it can be neglected. The calculated value for the molecular flow coming out of the bubblers is therefore better than 1.5% for all flows. Values for the different precursors used in our study are summarized in table 2-1.

Precursor	T_b (°C)	P_b (Torr)	P_l (Torr)	$\bar{f}_p$ (10^{-7} mol/min/sccm)
trimethylgallium (TMGa)	-10	1200	37.1	14.3
triethylgallium (TEGa)	15	780	2.4	1.4
trisneopentylgallium (TNPGa)	28	800	0.03*	0.01*
trimethylindium (TMIn)	18	800	1.47	0.82
tertiarybutylarsine (TBAs)	7	800	71.9	44.1

Table 2-1 Summary of the physical parameters of the different precursors used in this study
* Values obtained from kinetic studies (see chapter 6).

2.1.2 Hydrodynamics in the reactor chamber

The accurate modeling of the gas flow dynamics in a MOCVD reactor has been the subject of several studies with both vertical [4, 5], and horizontal chamber geometries [6, 7]. For the vertical reactor used in this work the gas is injected through the top and comes down towards the susceptor as a laminar flow. A more detailed description of the growth chamber is given in Fig. 4.1. The gas reaches the surface of the susceptor (sample stage) and is diverted sideways. The region immediately above the susceptor is the region where the details of the gas flow influence the growth parameters. This is also where they are the most complex. The contact between the gas and the surface of the susceptor produces a layer where the gas velocity is greatly reduced, and is negligible at least in the direction normal to the surface. This region is called the "stagnant flow" or boundary layer. In this region the precursor molecules are not dragged along with the carrier gas, since there is no noticeable amount movement of the gas towards the surface. They must diffuse through the boundary layer in order to reach the surface. This is a fundamental difference between MOCVD and other UHV techniques like CBE that use organometallic molecules as precursors. In the latter case the dynamics are in a molecular flow regime where the precursor molecules reach the surface in a ballistic fashion without any interactions with a carrier gas.

Several other effects can affect the dynamics of the gas over the surface. Because the susceptor is heated, there is a strong temperature gradient in the region of the boundary layer which generates convection flows. Even with the use of several simplifying assumptions, the solving of the hydrodynamic equations requires the computing power of supercomputers. We will present a very simplified picture of gas dynamics in chapter 6 as part of a simple model for the incorporation of Ga in GaAs MOCVD and ALE. The main point to remember is that the precursor travels through the whole system as a diluted part of the carrier–precursor gas mixture, and once it is near the surface, only diffusion within the mixture brings it to the surface. The strongest evidence of this aspect of MOCVD is the temperature independence of the growth rate over a certain temperature range. In this range the precursor is incorporated so quickly into the crystal, because of the extremely high reaction rates on

the surface, that the rate limiting factor becomes the diffusion of the molecules through the boundary layer, which depends only on the pressure of the gases. More details on the effects of gas dynamics on the growth rate will be given in chapter 6.

2.1.3 Chemistry of dissociation of the precursor molecule

The chemistry of the reactions taking place over and on the heated substrate surface is quite complex and still the subject of debate today. We discuss in this section the way the precursor molecule dissociates prior to its incorporation in the matrix. We leave the processes happening at the surface, such as the formation of kinks and the adsorption, migration and incorporation of the atoms in the crystal for the next section. We deal specifically with reactions taking place in the gas phase immediately over the surface.

Several studies have considered the decomposition of organometallic molecules in a heated gas environment. Of the precursors used in this study, all but trisneopentylgallium (TNPGa) have been studied extensively. The number of different decomposition pathways and the nature of the reaction products are varied and depend on several conditions such the nature of the molecule, the carrier environment, the temperature, the pressure etc. The details of such reactions lies beyond the scope of this work so we will restrict the review to two dissociation paths, namely homolytic fission and β–elimination, since they characterize the decomposition of all the precursors that we have used.

A molecule in a gas environment at high temperature collects significant amount of energy that can become large enough trigger its dissociation. Because it is moving through a gas it undergoes numerous collisions with other molecules and ions as well. These kinds of reactions are of two basic kinds called unimolecular and bimolecular. The unimolecular reaction happens when a molecule uses its internal energy to dissociate. The generic equation for such a reaction is:

$$AR \rightarrow A + R . \qquad (2\text{-}2)$$

The first–order rate constant for such reactions is given by:

$$k_{AR} = \frac{kT}{h} e^{\Delta S/R} e^{-\Delta H/RT}, \tag{2-3}$$

where k and h are Boltzmann and Planck constants and ΔS and ΔH represent respectively the change in entropy of the system and the thermodynamic enthalpy difference which is the difference between the activation energies of the forward and inverse reactions. Two examples of unimolecular reactions are homolytic fission, and

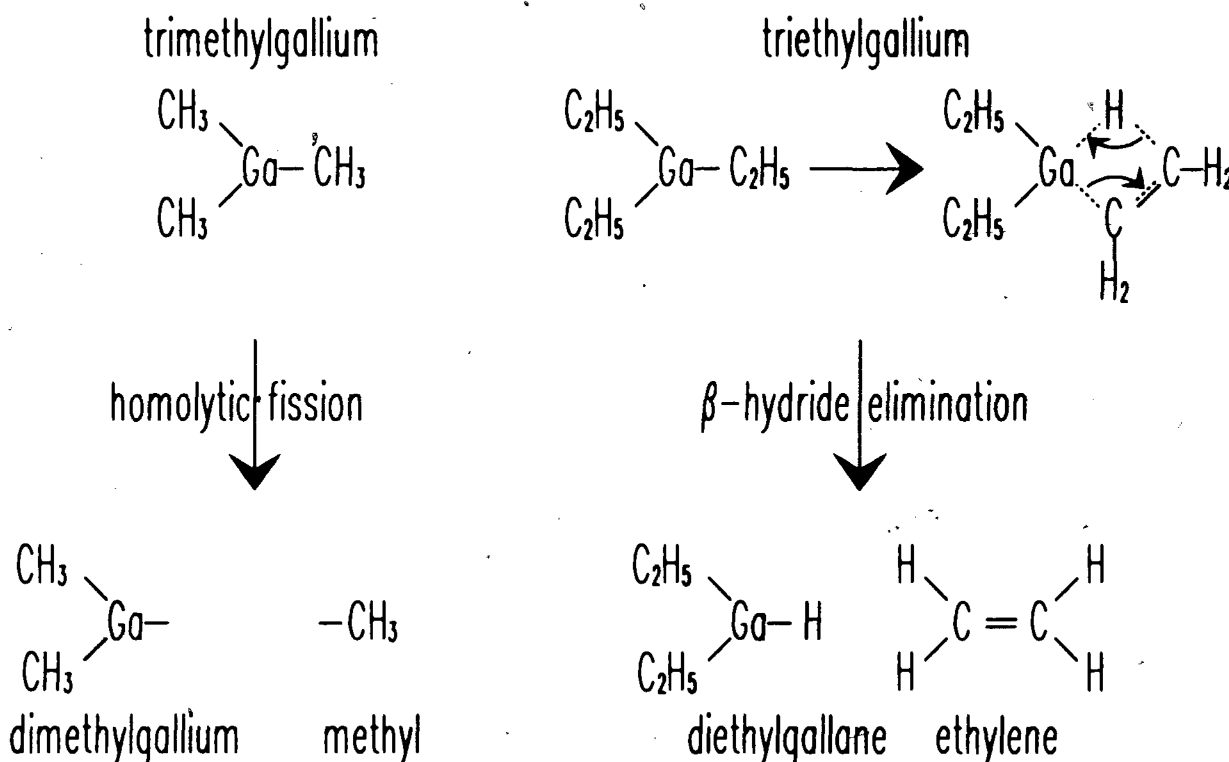

Fig. 2.2 Comparison of the dissociation mechanisms for TMGa (homolytic fission) and TEGa (β-hydride elimination).

β–elimination. In the first case the reaction consists in breaking one of the molecule's chemical bonds by stripping a part of the molecule from the other. β–elimination on the other hand, proceeds through a rearrangement of the bond structure in the molecule. Fig. 2.2 shows an example of each reaction. First, homolytic fission governing the dissociation of TMGa and a process called β–hydride elimination suspected to dominate the dissociation of TEGa. In the former case, one of the ethyl radicals is slightly distorted so 4 different atoms interact together. This type of unimolecular reaction is called a "four center" reaction. When the molecule reaches the proper configuration through slight modifications of bond angles, the bond structure is

modified so two distinct stable molecules are formed. In the example, one of the hydrogen atoms from the ethyl radical's tip transfers its bond from the second carbon to the Ga atom. Meanwhile the first carbon of the radical does likewise, transferring its bond from the Ga to form a double bond with the second carbon. The products formed in this way are diethylgallane and ethylene. Since no bonds have been severed during the reaction the total activation energy is expected to be lower than straight homolytic fission. This is confirmed by the fact that TEGa is observed to decompose at around 300°C compared to 450°C for TMGa, which decomposes through homolytic fission.

In the case of a bimolecular reaction, the molecule undergoes a collision with another species. In this case the equation looks like this:

$$A + B \rightarrow AB. \qquad (2\text{-}4)$$

The reaction takes place during a collision between two molecules so the equation rate is scaled by the collision frequency in the gas Z_{AB}:

$$k_{AB} = P_{AB} Z_{AB} e^{-E/RT}. \qquad (2\text{-}5)$$

The steric factor P_{AB} represents the probability that two reactants having enough energy will be in a favorable configuration for the reaction to occur. In both cases the rate of reaction depends exponentially on temperature. When plotted against 1/T the logarithm of the rate constant k_{AB} follows a straight line with a slope that is proportional to the activation energy of the reaction. This type of plot is called an Arrhenius plot and is the standard method of measuring E.

2.1.4 Surface reactions

MOCVD usually operates in the temperature regime where the growth is limited by mass transport. The molecules dissociate during their diffusion through the boundary layer and enter the matrix rapidly upon contact with the surface. The precursor flows are adjusted so the number of molecules from the group V dominates the group III by a factor of 5 to 40 for arsenides. The ratio of the number of molecules from the two groups is called the "V/III ratio". Because of this dominance the surface is considered to be continuously covered with As during the growth. The growth rate is then limited

by the rate of incorporation of the group III species. Any molecule from that group arriving at the surface rapidly finds a chemisorption site, incorporates into the crystal and is immediately covered by another As atom.

The sites that are most likely to favor chemisorption are the step edges and kinks. At these locations there is a larger number of bonds available, resulting in more favorable conditions for chemisorption. The incoming species can create new bonds with atoms underneath it as well as immediate neighbors. The growth therefore proceeds in a fashion where existing atomic step edges propagate along the surface until they meet another and coalesce, or reach the edge of the sample. Since the incoming species must migrate on the surface to reach the proper chemisorption sites, the evolution of the step structure during growth will vary depending on the mean free path of the migrating molecules. When the mean free path is large the molecules can travel very long distances to reach a step edge. This leads to a growth mode where the existing step edges grow at similar rates and the surface sees a succession of long step edges traveling across it. This growth mode is called "step flow growth regime". When the mobility of the species is reduced and a significant number of them cannot reach an edge, they incorporate in the middle of a terrace and start the growth of a small island as more species collect around its edges. This growth mode is labeled "island growth mode". Under most conditions MOCVD proceeds in the step flow mode with terraces reaching microns in size. An example of such a growth is given in Fig. 2.3 by an AFM picture of the surface of a GaAs layer grown by MOCVD at 580°C using TEGa as the Ga precursor. The terraces are several thousands of angstroms in size, testifying to the large surface mobility of the chemical species.

2.2 Atomic Layer Epitaxy

Most of the previous discussion still applies for the ALE process. The molecules are extracted from the liquid in the same fashion and carried to the growth chamber through the same system as for the MOCVD process. The main differences between the two growth methods reside in the chemistry taking place over and on the surface.

The first concern in ALE is to remove the reactions in the gas phase by performing the growth at low temperature and using fast gas velocity. These conditions reduce the thickness of the boundary layer and make the dissociation of the diffusing molecules in the gas phase less likely because of the shorter time taken to reach the surface and the smaller amount of thermal energy available for dissociation. Surface kinetics and chemistry therefore play a central role in ALE. In fact, as we will show, a careful study of the growth rates in ALE as well as MOCVD show that this last claim might have to be modified somewhat. In chapter 6 we propose a model based exclusively on gas phase reactions to explain the experimental growth rate measurement and obtain surprising results suggesting that gas phase reactions cannot be totally discarded in the understanding of the ALE process. The ALE process is much less understood than MOCVD and considerable work remains to be done to obtain a satisfactory picture of the growth. Other problems such as large amounts of carbon contamination of GaAs layers grown by ALE demand a more fundamental understanding of the growth process if a solution is to be found. The main topics that will be outlined in this section cover the basic principles behind ALE. The first section deals with the components of the ALE cycle and the role of each parameter in the growth. The following section will explain what is meant by self–limiting growth and will outline the different models that have been proposed in the literature to explain this behavior. This explanation will act as a backdrop for our own efforts to try to gain more insights in the self–limiting behavior of ALE. The last section will summarize the problems that need to be solved if ALE is to be used extensively in the production of devices. The most notorious of these is the large amount of carbon that contaminate GaAs layers when TMGa is used as the Ga precursor. Even if the reason for such high incorporation is relatively well known, the exact process of carbon incorporation is still under investigation at this point in time.

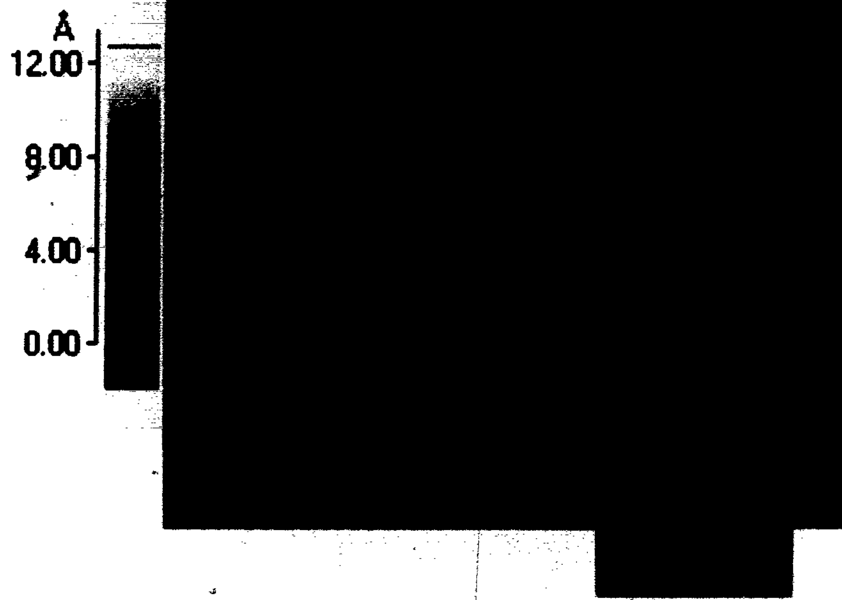

Fig. 2.3 AFM image of the surface of a GaAs layer grown at 580°C by MOCVD.

2.2.1 The ALE cycle

ALE proceeds by alternatively exposing the surface to flows from group III and group V vapors. If the process is well controlled each exposure is expected to fully cover the surface and a full ML of material is grown during each cycle. This is done while all the unwanted species present at the surface are rejected to the gas phase and prevented from entering the crystal and contaminating it. This process seems at least as unlikely as the basic idea behind MOCVD. It is nonetheless the result that is intended with such a method. The cycle is made of four time-steps involving different gases in the growth chamber. The cycle starts with the surface held at equilibrium under a flow of the group V precursor. In the case of GaAs in our system that precursor is tertiarybutylarsine (TBAs). The surface state is stable and the surface coverage is constant. The TBAs flow is then terminated and the chamber is purged of this precursor. During that period the surface state evolves according to the growth conditions. After this hydrogen purge cycle, the group III precursor, TMGa for

example, is introduced into the chamber. Ga atoms are added to the surface until it is completely covered and, if the conditions are properly maintained, no more incorporation occurs beyond this point regardless of the duration of the exposure or the TMGa concentration. This property of the ALE cycle is called self–limiting growth behavior. A more detailed description of the process is given in the next section.

Once saturation is reached the chamber is again purged of the group III precursor to prepare it for the group V exposure. The same criteria apply to this exposure as well. The surface becomes saturated with As and the cycle is repeated. The optimization of such a process can be quite challenging considering that the number of parameters to vary is considerable. There are the flow rates and exposure times for all precursors. The length of the different purge times and the growth temperature need to be adjusted as well, making the determination of the optimal set of parameters for a given compound a serious endeavor. The cycle needs to be adjusted so that the surface is fully covered during each precursor exposure. Since carbon incorporation has been attributed to the long exposure of the surface to carbon-containing radicals, shortening the group III exposure and the following purge step is more likely to diminish such an effect. Growth rate is also a factor to take into account when determining the ALE cycle, since it depends on the total time needed to complete each ML. Shorter cycles will produce a higher growth rate and make it possible to grow complicated structures in a more reasonable time.

2.2.2 Self–limiting growth

The ability of the surface to self regulate the incorporation of atoms is the key to an efficient ALE process. In this fashion some variation in the different parameters used during the growth is possible without affecting the condition of 1 ML of material being grown at each cycle. This strong control over the growth rate provides ALE with extremely good uniformity in the layer thickness. Variations of a few percent in the thickness of a layer over a 3" wafer has been measured under ALE mode compared with a change of about 50 % for conventional MOCVD in the same reactor. [8] The determination of the different parameter ranges over which the growth rate remains at

1 ML/cycle is usually performed by measuring the thickness of a layer grown with different values of a chosen parameter. This method is very time consuming and requires significant post growth treatment of the samples. We demonstrate in this work the use of *in situ* RDS to probe the surface in order to reach the optimal set of parameters in a small fraction of the time normally necessary for such a task.

The physical and chemical factors that explain the capacity of a crystal surface to protect itself from continuous incorporation of atoms after it has been covered by a monolayer is still a very active area of study today. Surface science methods have been used to probe the chemical properties of the different surface structures produced by exposure to the different precursors with results that are so varied that no consensus has emerged in the understanding of self-limiting growth behavior. We now outline the different arguments that form the basis for the three main proposed pictures for self-limiting growth. In each case the experimental evidence that stimulated the formulation of the models will be given along with a brief description of the mechanism. The pictures have been developed to explain results obtained for the growth of GaAs using TMGa as the Ga precursor, but the basic principles can be applied to other As-based semiconductors and different precursors.

2.2.2.1 Selective adsorption model

When an As-terminated surface is exposed to TMGa, the molecules join the crystal, modifying the surface stoichiometry from an As to a Ga termination. Once this process has been completed the TMGa molecules, which are still supplied to the surface, change their dissociation behavior. In the selective adsorption (SA) model it is assumed that TMGa stops decomposing if it can't find a site on the surface terminated by As. At complete coverage the TMGa molecules no longer stick to the surface and return to the gas phase without producing any further Ga incorporation.

In support of this model, As-terminated GaAs surfaces were exposed to TMGa for a time longer than that needed to completely cover it with Ga. The samples were then taken under UHV to a different chamber where surface measurements such as x-ray photoelectron spectroscopy (XPS) were performed on them. These measurements

have not detected any amount of excess Ga or C. [9, 10] The absence of excess Ga indicates that no droplets are formed on the surface, and the low carbon content implies that alkyl radicals are absent from the surface. Since the surface appears to be completely "bare", the only possible mechanism responsible for self–limiting growth has to be some kind of site selectivity on the part of the incoming molecules. This model has several shortcomings as pointed out by Creighton *et al.*. [11] The first problem with such measurement is the fact that it is performed *ex situ*. The time required to cool the sample down to room temperature and to transfer it to a different chamber is sufficient to allow the desorption of most volatile species from the surface. In the case of GaAs grown with TMGa the measured lifetimes of methyl radicals on the surface are of the order of a few seconds at 450°C so it is likely that most radicals present have left the surface by the time the measurement is performed. Creighton *et al.* further argue that droplets with small dimensions (< 0.5μm) are virtually invisible to techniques such as XPS.

2.2.2.2 Adsorbate inhibition model

Since the TMGa molecule reaches the surface at varying stages of decomposition it is expected to adsorb on the surface while still attached to one or more methyl radicals. The radical(s) then act as a shield against further reactions with other molecules. The proponents of the adsorbate inhibition (AI) model attribute an even more important role to the radical by claiming that because of their size, the undecomposed groups effectively block a certain number of neighboring sites and prevent their interactions with incoming molecules. The coverage of the surface then becomes limited by the rate of desorption of the radicals. We will discuss this approach further in this work and show that this argument is not necessary to explain the kinetic results. Previously reported high temperature ALE of GaAs [12] cannot be explained by this process alone since the lifetime of methyl radicals beyond 500°C becomes negligible. It has been argued that a difference in the method of measuring growth temperature could explain such a discrepancy. We treat this problem and suggest an alternative interpretation later in this work.

2.2.2.3 Flux balance model

According to the previous two pictures the surface becomes totally non reactive when it is saturated with Ga. Yu *et al.* have measured the dissociation probability of TMGa on a Ga saturated surface and found that it remained high (0.6) at normal ALE temperature (425°C) [13] meaning that TMGa dissociates even on a Ga terminated surface. According to the other models this probability should drop to zero when the surface becomes entirely covered with Ga and the TMGa molecules should return intact to the gas phase after interacting with the surface. This result means that even when covered with Ga the surface still reacts with TMGa molecules but does not include more Ga atoms. This is why they proposed a model saying that TMGa does decompose on the surface but one of the reaction products ($Ga(CH_3)$) that is returned to the gas phase contains a Ga atom. The balance that is established between incoming and rejected Ga atoms, preserves the stoichiometry of the surface.

2.2.3 Carbon incorporation

GaAs layers grown by ALE with TMGa as the Ga precursor are typically p–type with a hole concentration around 10^{18} cm^{-3}. This level of residual incorporation is too high for many possible applications. Secondary ion mass spectrometry (SIMS) has shown that the residual dopant was carbon. [14] Carbon atoms having four valence electrons are called "amphoteric" because they would act as a donor on a Ga site (C_{Ga}), and as an acceptor on an As site (C_{As}). In GaAs grown under our conditions the acceptor C_{As} is preferentially obtained. Unintentional carbon incorporation is one of the main challenges facing ALE at present and a better understanding of its mechanism is the first step towards a solution to the problem. Some trends have been observed by varying different components of the ALE and measuring the effect on the carrier concentration. The main results can be summarized as follows:

The carbon concentration increases with

- longer TMGa exposure time,
- higher TMGa flow,
- shorter AsH_3 exposure time,

- lower AsH_3 flow.

These effects can be explained by the long contact of the surface with methyl radical adsorbates. The most obvious way to solve this problem would appear to be to purge the surface for a long time after the TMGa exposure to remove methyl radicals from the surface. Experiments have shown, however, that long purges following TMGa exposure have little or no effect on the carbon incorporation, suggesting that carbon incorporation occurs during the TMGa exposure, possibly simultaneously with the chemisorption of the molecule. [15] Since methyl radicals are recognized as the carbon source, the use of alternate precursors producing different kinds of adsorbates could constitute part of the solution to the problem. TEGa has been used to grow layers by MOCVD with significantly lower carbon concentration, but the lack of self–limiting growth with this compound makes it a poor candidate. In the present study we report the characterization of a new precursor, trisneopentylgallium (TNPGa) as a possible candidate for the growth of high purity GaAs by ALE. The rationale behind the use of such a molecule is twofold: 1) The neopentyl radicals have a weaker bond to the Ga atom making their desorption from the surface easier. 2) The configuration of the molecule is expected to produce a dissociation through homolytic fission which will preserve the neopentyl radicals which can then act to maintain self–limiting growth. The details of the study are given in chapter 5.

3. *In situ* monitoring

MBE and other UHV epitaxy methods have benefited greatly from the development of electron beam based techniques such as reflection high energy electron diffraction (RHEED) and surface chemical analysis like XPS and Auger electron spectroscopy (AES). The wide range of *in situ* tools available has provided the crystal growers with a wealth of information on the microscopic mechanisms of UHV epitaxy. MOCVD on the other hand has been developed mainly on *ex situ* measurements and post growth diagnostics, since the lack of a UHV environment precluding the use of electron beam techniques. This situation prevailed until the late 80's when the first *in situ* measurement technique, namely reflectance difference spectroscopy (RDS) was developed by Aspnes. [16] Since then several alternatives have been proposed, increasing the number of options available to study MOCVD growth. [17–21]

The surface sensitivity of RDS comes from the intrinsic anisotropy of the top layer of the semiconductor. Because there are unfilled electronic bonds in the topmost layer, this layer will lower its collective energy by forming pairs of atoms, called dimers. As it turns out under most situations, all the dimers are formed along the same direction creating a strongly anisotropic layer. The underlying atomic layers, being part of the bulk zincblende structure, are optically isotropic. By measuring the optical anisotropy of the crystal, one gets information coming from the surface layer exclusively. This forms the rationale behind a technique such as RDS.

The present chapter is structured in the following fashion. We first give a brief review of the main concepts involved in the reconstruction of the top layer of a crystal,

since this constitutes the basis for RDS measurements. A simple theoretical analysis of the RDS setup follows and shows how the surface anisotropy information is extracted.

3.1 Surface reconstructions

When the surface of a semiconductor crystal is allowed to relax at high temperature it can lower its total energy by forming dimers. This section explains phenomenologically how these pairs are formed and shows how they are interesting from the point of view of optical anisotropy. A simple interpretation is illustrated in Fig. 3.1.

Let us assume for clarity that the circle represent Ga atoms and the squares As atoms. If a crystal with the zincblende structure, say GaAs is cut across the (001) direction the top atomic plane has a square structure. An example of such a plane is illustrated in Fig. 3.1a. In this case the Ga atoms have two bonds coming out of the image that are aligned in the (110) direction and two bonds going into the image aligned along the $(1\bar{1}0)$ direction. These two directions constitute the main axes of the surface. This plane has the same configuration as any other Ga plane in the bulk crystal. The RDS measures the average signal coming from all the bonds, and since there are as many bonds in one direction as there are in the other, any anisotropy coming from one type of bond is cancelled by the signal coming from the other type.

When an As plane is overlaid on the original surface, each atom from this plane has two bonds with the first layer. In the example the bonds are along the (110) axis. The remaining two bonds remain unfilled. These dangling bonds are represented by lobes in Fig. 3.1b and they are all oriented along the $(1\bar{1}0)$ crystal axis. Interactions between these orbitals from first neighbors create dimers with energy levels similar to a diatomic molecule as seen in Fig. 3.1c. The surface reconstruction is then labeled "(2×1)" to represent the change in period of the surface symmetry. In order to preserve the charge neutrality of the surface it has been shown that one dimer in every four has to be removed. [22–24] An example of the reconstructed surface is given in Fig. 3.1d. A dotted box shows the unit cell of the surface which is labelled as (2×4) symmetry.

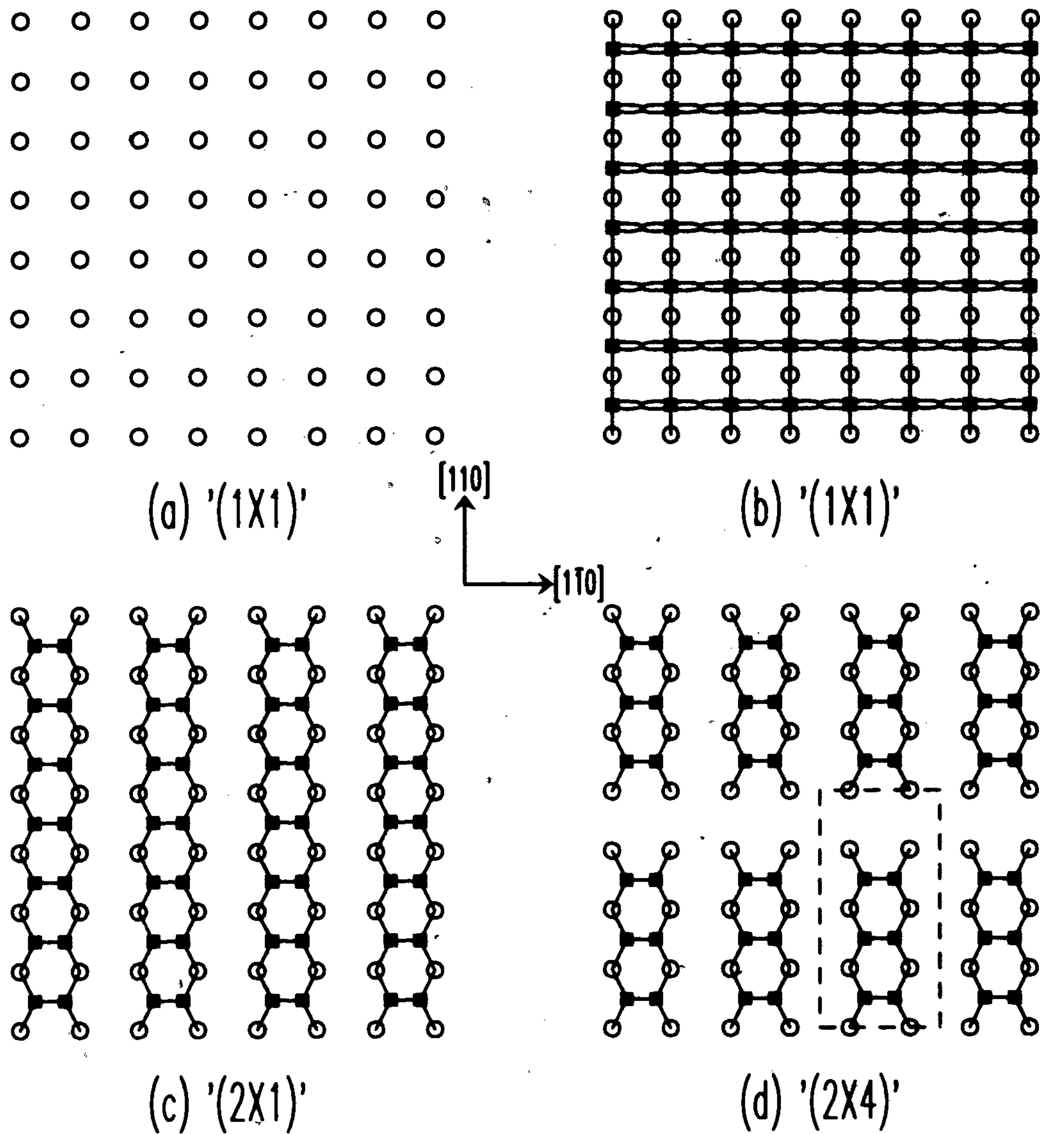

Fig. 3.1 Simplified view of the surface reconstruction of a zincblende semiconductor like GaAs. The circles and squares represent Ga and As atoms respectively. Dimers are illustrated by full symbols.

Termination with either chemical group has been observed on surfaces with techniques such as scanning tunneling microscopy (STM). [24, 25] The labeling of the different symmetries is based on their unit cells. The two indices correspond to the number of periods along each direction in the unit cells. The reconstruction shown in Fig. 3.1d is labeled (2×4) because the unit cell is 2 periods long in the $(1\bar{1}0)$ direction and 4 periods in the (110) direction. This labeling scheme is justified by the nature of the other measurements used normally to obtain structural information on surface reconstructions.

3.1.1 Charge neutrality of the surface: missing dimer model.

Reflection high energy electron diffraction (RHEED) observations made on the GaAs surface reveal that several As-terminated reconstructions have a (2×4) type of symmetry, inverting the indices for the Ga terminated surface. Before the advent of high spatial resolution techniques such as STM, different models had been proposed for such reconstructions. One of these models used groups of dimers separated by vacancies as the reason for such symmetries and were later confirmed by direct STM measurements. Simple energetic arguments were invoked to explain the missing dimers. [22, 23] We give a brief summary of the concepts motivating the missing dimer models. The example is discussed for the As terminated surface but the same reasoning applies to the Ga termination.

In the zincblende structure each atom has 4 nearest neighbors. The As atom has five valence electrons in its *4s* and *4p* orbitals. In the crystal these orbitals reconfigure to form the 4 lobes of the tetrahedral sp^3 hybrid orbital. Each lobe contains on average 5/4 electrons. When the As is on the surface, only two of the four lobes form bonds to the Ga in the bulk with 2 1/2 electrons as part of these bonds. When forming a dimer, the remaining 2 lobes of the sp^3 orbital rearrange into two orbitals of different types. One lobe (*p*-like) extends towards the other As atom in the dimer and contributes 1 electron to form a covalent bond. The last part of the orbital takes a *s*-like spherical shape and takes the remaining 1 1/2 valence electrons. The energy in this last orbital is well below the Fermi level. It should therefore be completely filled. There is a deficit of 1/2 electron in the structure for it to be balanced.

The way to accomplish this balance is to remove every fourth As dimer. When this is done, four Ga atoms from the underlying layer have each one lobe of their sp^3 orbital exposed. For a Ga atom there is 3/4 electrons in each lobe. The energy in these orbitals lies higher than the Fermi level forcing them to remain empty. The 3 electrons obtained from these orbitals are used to fill the 6 *s*-like orbitals in the remaining 3 As dimers and full charge balance is achieved.

This state is considered stable since all the levels that lie above the Fermi level are then empty and the ones that are below are filled. This type of argument has been

used to explain the presence of reconstructions such as the (2×4) As terminated and the (4×2) Ga terminated. Other types of reconstructions are observed in GaAs as will be discussed in the next section. The principles governing their structures can be quite complex, and lie beyond the scope of the present work.

3.2 Optical anisotropy: reflectance difference spectroscopy

We have seen in the last section that the dimers forming on a reconstructed surface do so along one of the crystal axes (110), or $(1\bar{1}0)$. Since each individual dimer is similar to a diatomic molecule, it is expected to exhibit electronic energy levels having both bonding and antibonding character. Interaction with polarized light having the electric field oscillating along the dimer direction is likely to generate transitions between the different states which would not be stimulated by light polarized in the other direction. Transitions within the dimers affect the absorption characteristics of the surface and therefore the reflectivity. The reflectivity of the surface is thus different for the two polarizations. It is this difference that is measured by RDS. Energy spectra of the difference can then characterize specific surface reconstructions, since each of them has a different arrangement of dimers which have different chemical or structural signature.

It is worth noting here that although the information comes almost exclusively from the top few angstroms of the crystal, the light still penetrates deeply into the material. The strength of RDS is to extract the surface related signal very selectively.

3.2.1 Theoretical analysis

The detailed treatment of electromagnetic waves passing through anisotropic media has been done at length in the literature. [26–28] In the case of a semiconductor and its surface the reflectance can obtained by decoupling the isotropic bulk and the reconstructed surface layer. The three media are then the ambient, the surface, and the bulk layers. For the RDS measurements we are concerned with the reflection of polarized light from the crystal. The angle of incidence is small and can be considered to be normal to the surface. We use a and s as indices for the ambient and substrate media respectively. The surface being anisotropic, the two crystalline axes are

identified separately. The reflectance difference $\Delta r/r$ between the two main crystal axes is given by:

$$\frac{\Delta r}{r} = 2\frac{r_{1\bar{1}0} - r_{110}}{r_{1\bar{1}0} + r_{110}} = \frac{4\pi i d n_a}{\lambda}\frac{\varepsilon_{1\bar{1}0} - \varepsilon_{110}}{\varepsilon_s - \varepsilon_a}, \quad (3\text{-}1)$$

where r_{110} and $r_{1\bar{1}0}$ represent the complex reflectance for light polarized along the two main crystalline axes, ε_i is the dielectric constant of the different regions, λ is the wavelength of the light, n_a is the index of refraction of the ambient and d is the thickness of the layer that is considered as the surface and is assumed to be much smaller than λ.

For the different surface reconstructions the only variation in the preceding equation comes from the surface dielectric constants ε_{110} and $\varepsilon_{1\bar{1}0}$. Interpretation of the RDS signal relies on the accurate estimation of these parameters, but their accurate value is difficult to obtain. This is the main reason why very few attempts have been made at modeling measured RDS energy spectra. RDS still remains a mainly qualitative technique today.

Equation 3-1 relates the surface anisotropy to the difference in the complex reflectance for light polarized along the two main axes. The purpose of the optical setup is to measure that difference. A simple analysis of the setup used for this work is given in chapter 4. The setup that we used is based on a design by Aspnes *et al.*. [29]

3.2.2 Spectral information

By varying the frequency of the light monitored by the RDS setup we can obtain spectral information on the state of the surface. Each reconstruction has a characteristic spectral signature that has been catalogued by comparing the RDS spectrum with RHEED [30] and grazing incidence x-ray scattering (GIXS) measurements. [31] Different features in the RDS spectrum have been attributed to transitions within the dimers. [32]

Fig. 3.2 is an overview of the main spectra encountered in this study for GaAs. The corresponding proposed reconstructions are labeled for each spectrum. Features appear mainly at three different energies, 1.9, 2.6, and 4.2 eV. The first two energies have been related to electronic transitions within Ga and As dimers respectively. [30] Note the inversion of sign of the 2.6 eV part of the spectrum between the (2×4) and c(4×4)/d(4×4) surfaces because of the orientation of the As dimer in the latter case that is rotated by 90°. The 4.2 eV feature has been thought to be related to transitions in the As dimer [30] but since it does not show the same change in sign as the 2.6 eV feature, such a relation is unlikely. The exact origin of that feature remains uncertain at

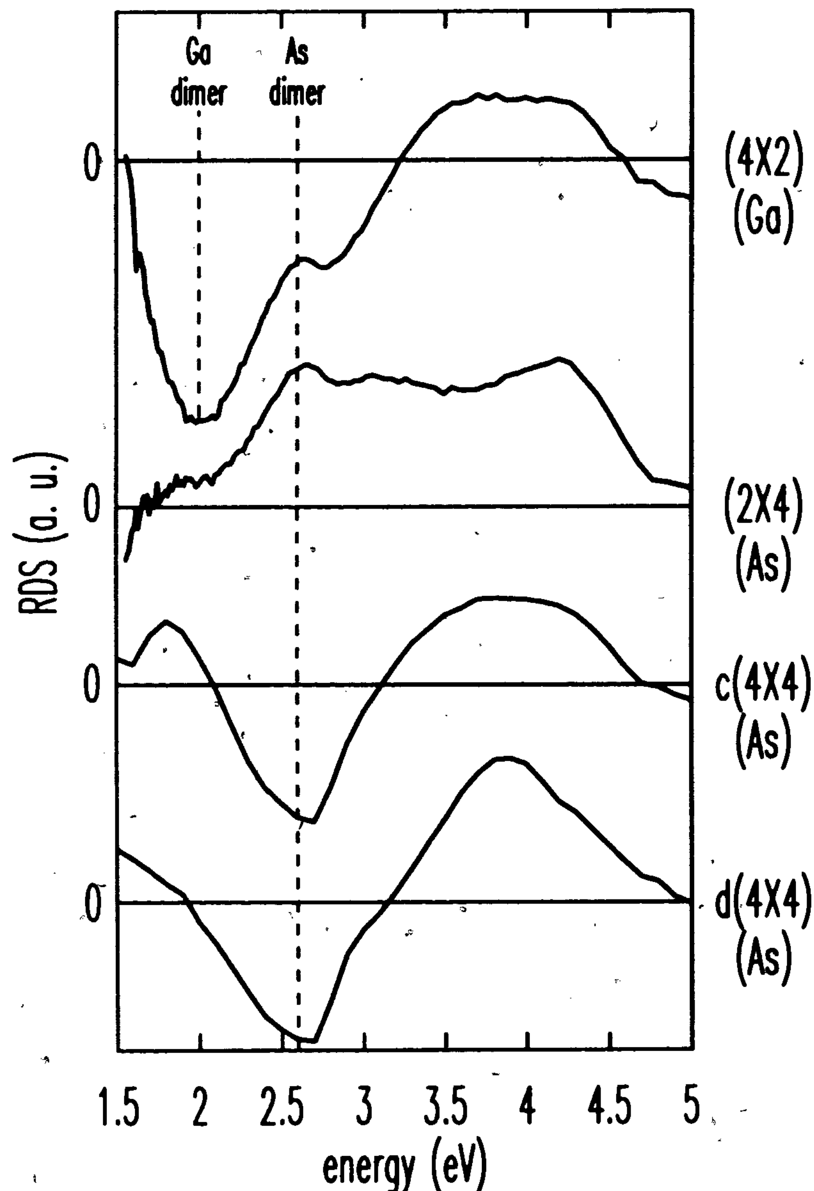

Fig. 3.2 RDS energy spectra of surface reconstructions of GaAs as identified by RHEED.

this point. For the purpose of the present work we will use uniquely the first two energies.

Fig. 3.3 shows examples of each of the main reconstructions of GaAs. Only the top two atomic layers are represented. The squares symbolize As atoms while the circles represent Ga. The solid symbols highlight the dimerized atoms of the surface. The unit cell of the reconstruction symmetry is given by a dotted box and justifies the different labels used for the identification of the reconstructions.

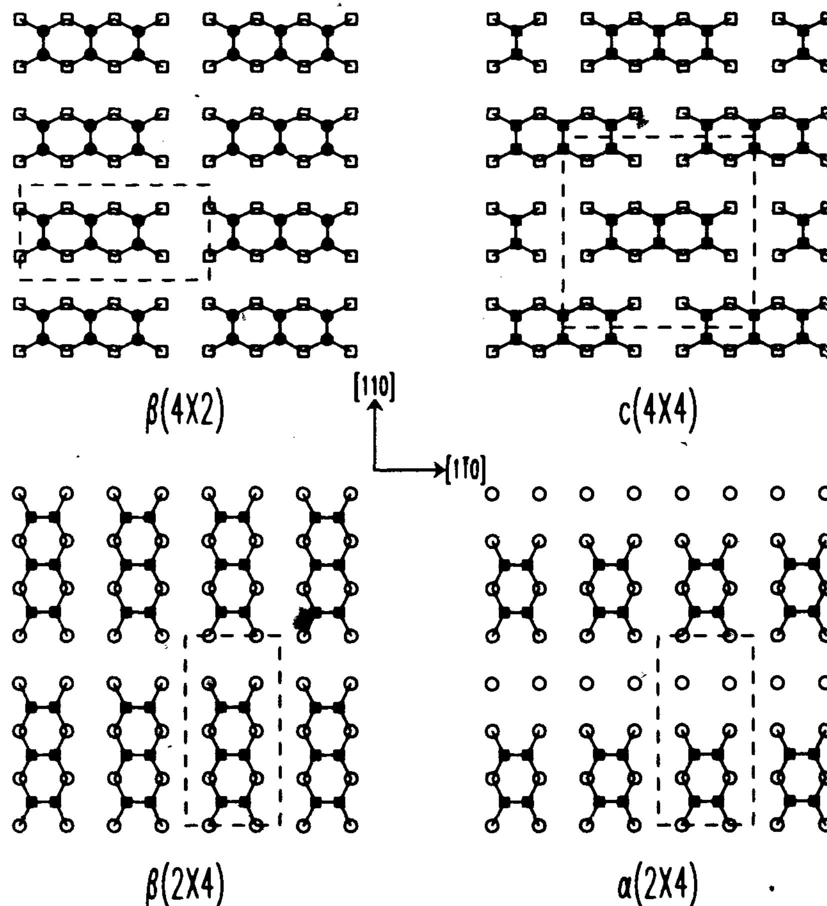

Fig. 3.3 Surface reconstructions commonly observed in UHV GaAs. The As and Ga atoms are respectively represented by squares and circles. Dimerized atoms have solid symbols.

4. Experimental Details

4.1 Epitaxy system

4.1.1 MOCVD reactor and gas handling system

The MOCVD reactor was manufactured by Thomas Swan (UK) in 1993 and consists of a commercial gas handling unit coupled with a reactor chamber customized for the specific needs of research. The carrier gas was ultra high purity (UHP) compressed hydrogen stored in interlocked gas cabinets. The nitrogen used in the different purge and vent lines is obtained by evaporating liquid nitrogen from a conventional tank. The gas handling system consists of high purity stainless steel tubing butt welded together and using VCR™ fittings to reduce dead volumes. The exhaust gases from the reactor are purified through an activated carbon scrubber.

A schematic view of the growth setup is given in Fig. 4.1. Hydrogen is supplied to the carrier lines as well as the bubblers for extraction of the precursors. Pressure in the bubblers is controlled electronically and the bubbler temperature is kept constant by ethylene glycol baths. The flow from each bubbler can be directed either to the carrier line where it is brought towards the growth chamber or exhausted to a vent line when not needed. The carrier lines enter the reactor chamber through the top and several hydrogen purge lines are added to maintain the gas flows laminar in the reactor and to keep the windows clean. Section 4.1.3 is devoted to the detailed description of the growth chamber. The RDS setup is mounted vertically over the reactor.

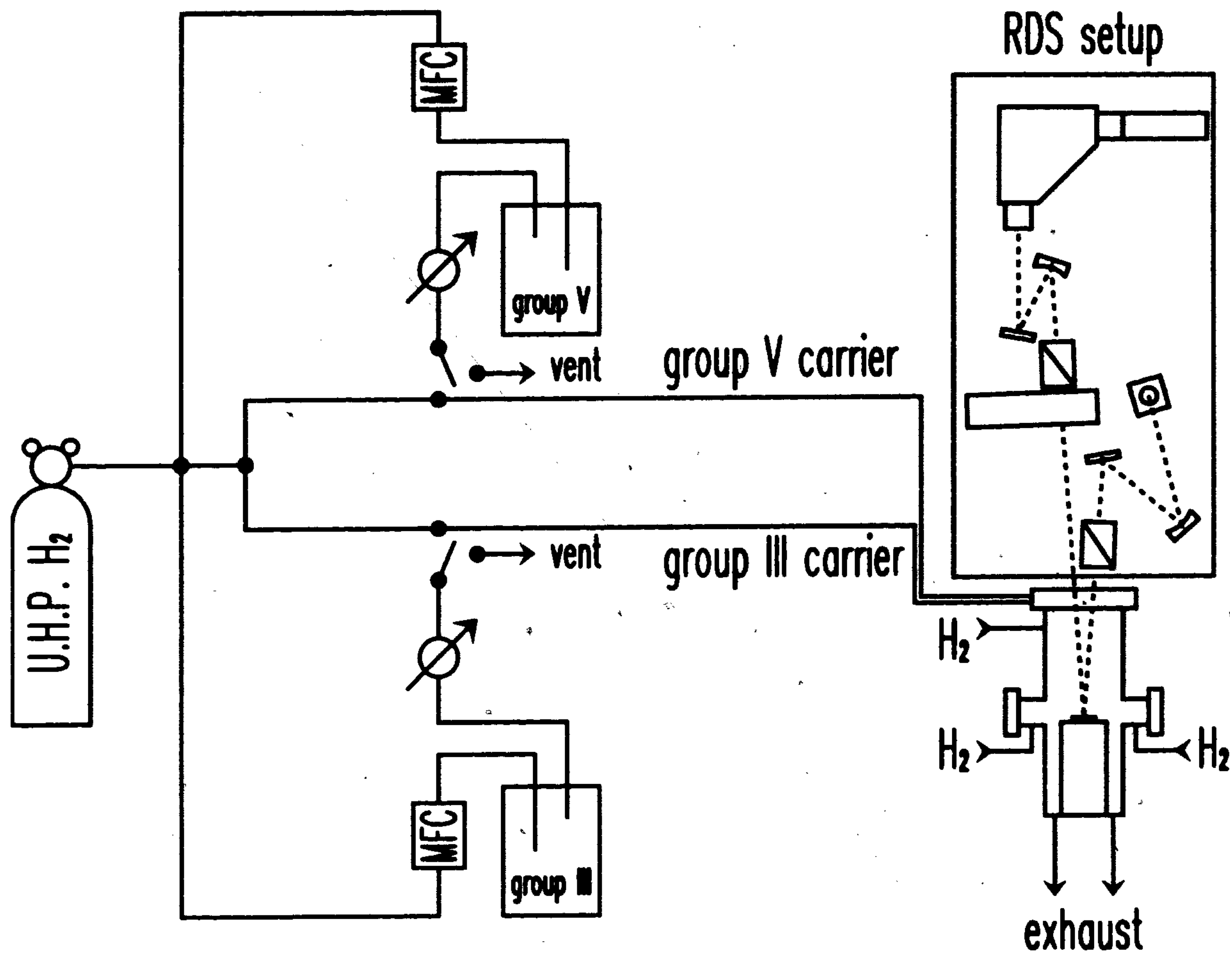

Legend:

Fig. 4.1 Schematic view of the gas handling system for the MOCVD reactor. The RDS setup is mounted vertically on a metal plate over the growth chamber.

4.1.2 Supplying the precursors to the growth chamber

Hydrogen is continuously passed through the bubbler during a growth run. The mixture of hydrogen and precursor vapor is then introduced in a carrier line going to the reactor chamber or diverted to vent according to the needs of the growth. Two carrier lines, one for the group III precursors and one for the group V precursors, direct the flows to the growth chamber. In order to suppress any fluctuations in pressure the total gas flow passing through both carrier lines is kept constant by a

computer controlled makeup flow. When the precursor flow is removed from the carrier line and directed to vent, the makeup line injects an amount of gas identical to the one that was removed, preserving the total flow of the line and suppressing any turbulence in the gas dynamics. In order to further minimize the flow transients, the vent line is kept at the same pressure as the carrier line by a differential pressure controller. A feedback loop adjusts the vent flow to achieve the pressure balance.

4.1.3 Growth chamber: technical details

The details of flow control and prevention of pressure fluctuation are given in the experimental details in the previous section. We use different carrier lines for elements from each groups to prevent any early reaction between the precursors and to better control gas switching in ALE and as well as unwanted memory effects. A delay of 0.35 s was observed between the gas switching and the time of subsequent surface transients measured by RDS when using a gas velocity of 50 cm/s in the growth chamber.

A side view of the growth chamber can be seen in Fig. 4.2. The chamber configuration is inspired by a design proposed by Brennan *et al.* for *in situ* x-ray measurements. [33] It is composed of a stainless steel vertical reactor equipped with optical ports to allow both normal and Brewster angle access. The carrier flows are introduced through different lines in the top of the chamber where they mix and proceed down a quartz nozzle in a laminar flow pattern. The use of a nozzle serves the purpose of decreasing the amount of material necessary to perform the growths by bringing the major part of the precursor molecules directly on the susceptor. To maintain the laminar flow of gas in the chamber, H_2 is supplied to the ring shaped volume surrounding the nozzle with a flow that generates the same gas velocity as the carrier flow through it. Other H_2 flows are supplied to the side window ports to maintain a pressure slightly higher than that of the chamber in order to prevent the formation of deposits on the side windows. We have found that using a purge flow of 10 sccm would keep the windows reasonably clean for about 10-30 runs, depending on their lengths, without disrupting the gas flow in the chamber.

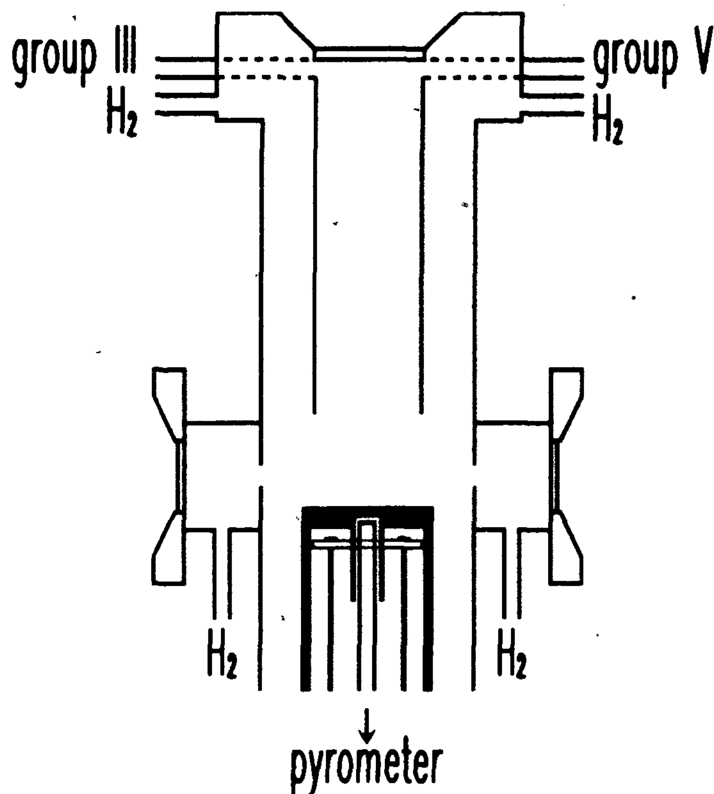

Fig. 4.2 Side view of the growth chamber. The inlets with their respective gas species are identified.

The sample sits on a graphite susceptor heated from the back by a resistive graphite heater. The temperature is monitored by a pyrometer looking at the back of the susceptor through a quartz light pipe. The pyrometer was calibrated periodically using a thermocouple in contact with the top surface of the susceptor under the same flow and pressure conditions used for the growths. The variation with time was observed to be typically less than a few degrees and always inferior to 10°C. The main source of variation was the coating of the susceptor during subsequent growths, decreasing its thermal conductivity. A summary of the growth parameters is given below:

Reactor pressure:	50 Torr
Alkyl total flow:	600 sccm
Hydride total flow:	600 sccm
Total gas flow:	5 slm
Window purge flow:	10 sccm
Gas velocity:	50 cm/s

4.1.4 Sample preparation

GaAs substrates, approximately 1 cm^2 in size, were taken from semiinsulating vertical gradient freeze wafers either exactly oriented in the (001) direction or with a 2° miscut towards the (110) direction. The nominal etch pit density of the wafers was below 5000 cm^{-2}. The InAs substrates were exactly cut in the (001) direction. In all cases the new wafer was quoted as "epi ready" by the manufacturer so the early samples taken from the wafers were directly introduced in the reactor without pre–treatment. After some time, though, the surface of the wafer started to collect some oxide. The samples were then prepared using the following procedures.

For GaAs wafers:

1) 5 min. in an ultrasound activated acetone bath,
2) 5 min. in an ultrasound activated methanol bath,
3) rinsed in deionized water,
4) 2 min. in a 5:1:1 (H_2SO_4:H_2O_2:H_20) solution,
5) rinsed in deionized water,
6) blown dry with nitrogen.

For InAs wafers:

1) 5 min. in an ultrasound activated acetone bath,
2) 5 min. in an ultrasound activated methanol bath,
3) rinsed in deionized water,
4) 2 min. in HF (10% vol. in deionized water),
5) 2 min. in a 19:1 (methanol:Br) solution,
6) rinsed in deionized water,
7) blown dry with nitrogen.

4.2 Reflectance difference spectroscopy

4.2.1 Description of the optical setup

Fig. 4.3 shows a schematic representation of the RDS setup used in our experiments. The evolution of the polarization of the light as it passes through the system is represented in Fig. 4.4. In the figure letters corresponding to the labelling of Fig. 4.3 are assigned to each components. The light is emitted by a wide emission (200-800 nm) Xe arc lamp (model L2174, Hamamatsu) (a) and is linearly polarized using a MgF_2 Rochon prism (b). The light is then directed on the sample (s) whose main axes are positioned at a 45° angle with respect to the polarization of the light. The components of the polarization along the two crystal directions are therefore equal. When the light is reflected, its polarization is slightly shifted because of a small difference in its components created by the anisotropic reflectivity. Note that this effect is greatly exaggerated in Fig. 4.4 for clarity. The actual difference between the two components is of the order of one part in 10^4. The next device along the line is a device called a photoelastic modulator (PEM) which consists of a fused silica bar that can be made birefringent by a piezoelectric cell that induces a stress through the material (c). This stress is modulated in a sinusoidal fashion at 50 kHz and the maximum retardation can be adjusted by an electronic

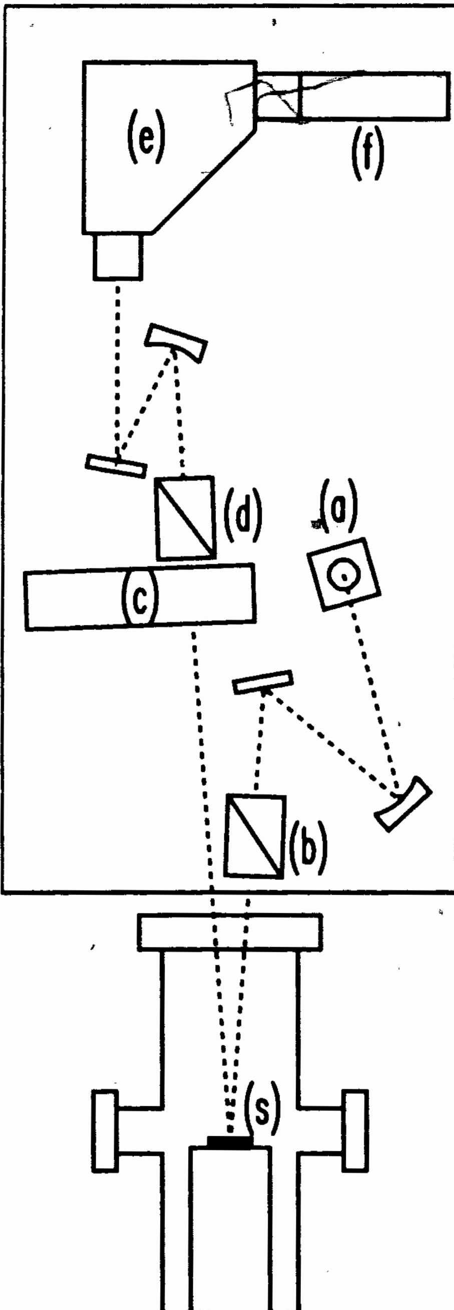

Fig. 4.3 RDS optical setup as it is configured on the vertical plate. Each component is identified by a label and discussed in the text.

controller. We used the PEM-90 model sold by Hinds Instrument. In our case the PEM maximum retardation is set at $\lambda/2$. Thus the retardation oscillates between $-\lambda/2$ and $+\lambda/2$ with a frequency of 50 kHz. The axis along which the stress is applied is positioned to be perpendicular to the direction of the original polarization of the light prior to reflection. Any shift in the polarization induced by the sample anisotropy is modulated by the PEM at 50 kHz. The analyzer (d) is made of a quartz Rochon prism set to choose the polarization along one of the sample's main axes. A specific wavelength is then monitored by a 0.25 m grating spectrometer (e) in conjunction with a wide spectral response multialkali photocathode photomultiplier tube (Hamamatsu, #R374) (f). The intensity of the light reaching the detector consists of a DC signal corresponding to the light reflected by the bulk portion of the sample which is isotropic, and a small modulation coming from the anisotropic surface layer. Using a simple lock–in amplifier technique the amplitude of the modulated signal can be measured efficiently. The ratio of the amplitude of the modulated to the DC signal is of the order of 10^{-4}-10^{-5} which is well within the range of commercial lock–in amplifiers. The instrument that was used in the present work is the SR830 digital lock-in amplifier manufactured by Stanford Research. Since the value measured is the ratio of the amplitude of the oscillation to the DC signal, provisions have to made to either measure the DC directly or maintain it at a given value during the experiment.

Several factors can affect the DC component of the signal. Since it mainly originates from the bulk, absorption or interference effects can change its intensity. Interference modulates the DC signal when a layer of a given material is grown over one of a different kind. Light waves reflected by the surface and the interface between the materials interfere and produce a modulation of the reflected intensity as the layer thickness changes in a Fabry-Perot-like fashion. Since RDS measures $\Delta R/R$, this modulation of R will affect the RDS signal with an effect coming from the bulk that will be visible during the growth of thick layers. This kind of phenomenon has been used in our lab as a tool to control the reproducibility of growth rates. In the experimental

conditions of the present work though, the thickness of the layers grown is so small that those modulations are negligible.

The emission spectrum of the arc lamp includes several features and varies in intensity across the energy range we use, also changing the value of the DC signal hitting the detector. The easiest way work around such variations is to maintain the DC level of the signal by varying the sensitivity of the detector. We hold the DC level constant by varying the photomultiplier gain via the tube voltage with the use of an electronic control circuit. The details of the circuit used in our setup are given in appendix A.

In order to avoid any modification of the light polarization from birefringence coming from other components, we used front surface spherical and flat mirrors coated against oxidation of the aluminum surface, using a special coating for use in the UV range of the spectrum.

4.2.2 Analysis of the optical response

The electric field of a uniform transverse electromagnetic plane wave can be represented in the Jones vector notation by:

$$\mathbf{E}(z,t)=\begin{bmatrix} \tilde{E}_{110}\cos\left(\omega t-\frac{2\pi}{\lambda}z+\delta_{110}\right) \\ \tilde{E}_{1\bar{1}0}\cos\left(\omega t-\frac{2\pi}{\lambda}z+\delta_{1\bar{1}0}\right) \end{bmatrix}. \qquad (4\text{-}1)$$

Since the present analysis deals exclusively with monochromatic waves, ω remains the same so the time dependence can be suppressed. It can be restored by multiplying any vector by $e^{i\omega t}$ and taking the real part of the expression. Furthermore since the spatial dependence is the same for both components of the polarization it can be taken out of the vector. The wave is then given by:

$$\mathbf{E}(z)=\begin{bmatrix} \tilde{E}_{110}e^{i\delta_{110}} \\ \tilde{E}_{1\bar{1}0}e^{i\delta_{1\bar{1}0}} \end{bmatrix} e^{-\frac{2\pi}{\lambda}z}. \qquad (4\text{-}2)$$

Here again expression 4-1 can be obtained by taking the real part of (4-2). The vector contains all the information on the direction, amplitude and phase of the

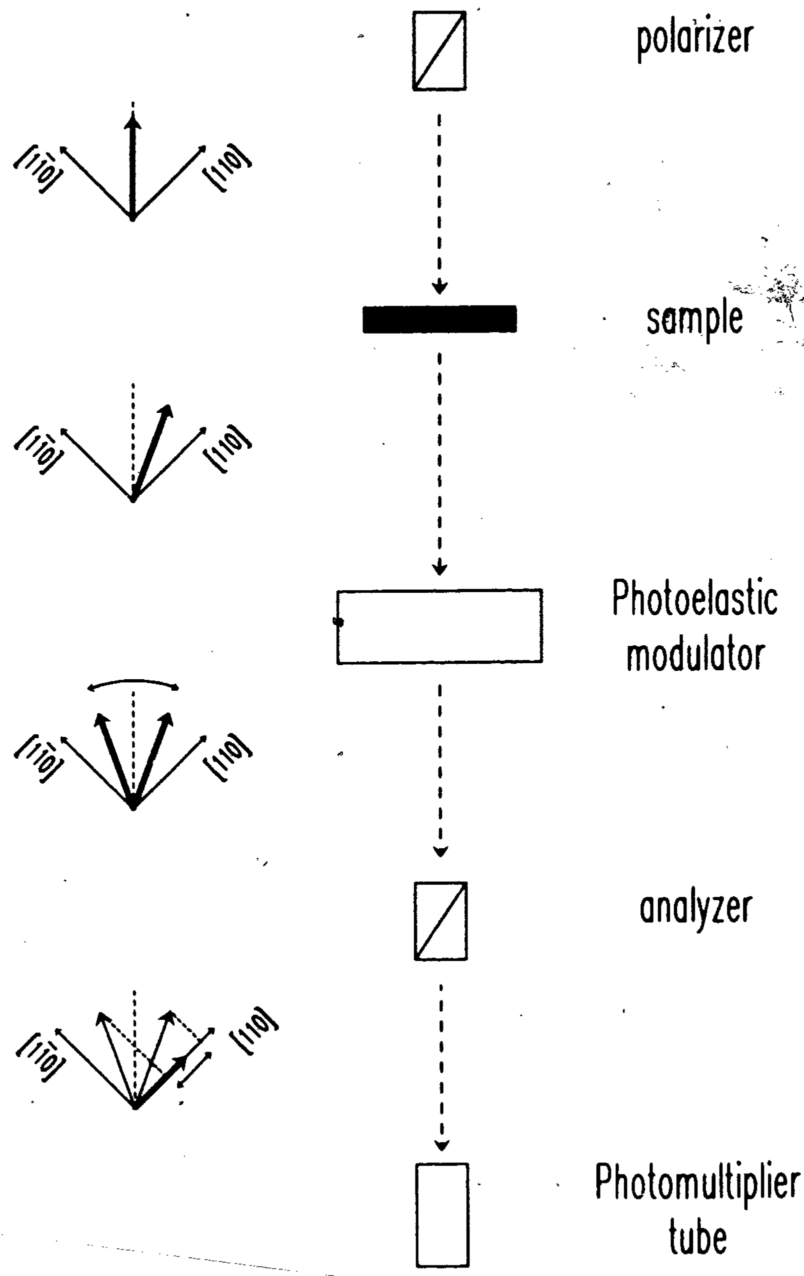

Fig. 4.4 Propagation of the polarization through the different components of the RDS setup. The reference frames are aligned with the main axes of the sample surface.

polarization. Since none of the components in the RDS setup affect the wavelength of the light and the measurement is strictly concerned with the amplitude of the of the light, we need only use the vector part of the expression. Under the Jones notation every optical component can be expressed by a 2×2 matrix and the optical setup can be analyzed simply by multiplying the matrices of each components. [28]

A schematics of the different stages of the setup is shown in Fig. 4.4. First we consider the wave coming out of the polarizer expressed as:

$$\mathbf{E}_1 = \begin{bmatrix} E_{110} \\ E_{1\bar{1}0} \end{bmatrix} = E_0 \begin{bmatrix} 1 \\ 1 \end{bmatrix}. \tag{4-3}$$

where we have used $E_a = \tilde{E}_a e^{i\delta_a}$. We chose the main axes of the surface as the basis for the vector representation. The light is polarized at 45° from the main axes so that the components are equal in both directions. Using r_{110} and $r_{1\bar{1}0}$ for the complex reflectance along the two directions we obtain for the reflected light:

$$\begin{aligned} \mathbf{E}_2 &= E_0 \begin{bmatrix} r_{110} & 0 \\ 0 & r_{1\bar{1}0} \end{bmatrix} \begin{bmatrix} 1 \\ 1 \end{bmatrix} \\ &= E_0 \begin{bmatrix} r_{110} \\ r_{1\bar{1}0} \end{bmatrix}. \end{aligned} \tag{4-4}$$

The PEM is oriented so its main axis is at 45° off the crystal axes. The wave coming out of it is given by:

$$\begin{aligned} \mathbf{E}_3 &= \frac{E_0}{\sqrt{2}} \begin{bmatrix} 1 & 0 \\ 0 & e^{i\delta_C} \end{bmatrix} \begin{bmatrix} 1 & 1 \\ -1 & 1 \end{bmatrix} \begin{bmatrix} r_{110} \\ r_{1\bar{1}0} \end{bmatrix} \\ &= \frac{E_0}{\sqrt{2}} \begin{bmatrix} r_{110} + r_{1\bar{1}0} \\ \left(r_{1\bar{1}0} - r_{110}\right) e^{i\delta_C} \end{bmatrix}. \end{aligned} \tag{4-5}$$

The factor $e^{i\delta_C}$ corresponds to the retardation applied by the PEM which is modulated so $\delta_C = \pi \sin \omega t$. The preceding expression shows that the (110) component of the light is constant in time and corresponds to the sum of the complex reflectances. The other component is modulated between the two limits $\pm\left(r_{1\bar{1}0} - r_{110}\right)$.

Likewise the analyzer is positioned to select one of the main axes so the light entering the spectrometer and ultimately the detector is expressed as:

$$\begin{aligned} \mathbf{E}_4 &= \frac{E_0}{2} \begin{bmatrix} 1 & 0 \\ 0 & 0 \end{bmatrix} \begin{bmatrix} 1 & -1 \\ 1 & 1 \end{bmatrix} \begin{bmatrix} r_{1\bar{1}0} + r_{110} \\ \left(r_{1\bar{1}0} - r_{110}\right) e^{i\delta_C} \end{bmatrix}, \\ &= \frac{E_0}{2} \begin{bmatrix} r_{1\bar{1}0} + r_{110} - \left(r_{1\bar{1}0} - r_{110}\right) e^{i\delta_C} \\ 0 \end{bmatrix}. \end{aligned} \tag{4-6}$$

The detector signal is proportional to the intensity of the wave so:

$$I(t) = I + \Delta I(t),$$
$$= \frac{E_0^2}{2}\left[\left|r_{1\bar{1}0}\right|^2 + \left|r_{110}\right|^2 + \left(\left|r_{1\bar{1}0}\right|^2 - \left|r_{110}\right|^2\right)\cos\delta_C + i\left(r_{110}^{*}r_{1\bar{1}0} - r_{110}r_{1\bar{1}0}^{*}\right)\sin\delta_C\right]. \quad (4\text{-}7)$$

The trigonometric functions can be expanded in their Bessel-function series as:

$$\cos\delta_C = \cos(\pi \sin\omega t)$$
$$= J_0(\pi) + 2\sum_{m=1}^{\infty} J_{2m}(\pi)\cos(2m\omega t) \quad (4\text{-}8)$$
$$\sin\delta_C = \sin(\pi \sin\omega t)$$
$$= 2\sum_{m=1}^{\infty} J_{2m+1}(\pi)\sin((2m+1)\omega t) \quad (4\text{-}9)$$

and the expression for ΔI becomes a series of the type:

$$I = I_{DC} + I_{\omega} + I_{2\omega} + \ldots \quad (4\text{-}10)$$

We need to retain only the first two frequency terms for the RDS measurements. The expression for $\Delta I/I$ is given by the expression:

$$\frac{\Delta I}{I} = -2\frac{\left|r_{110}\right|\left|r_{1\bar{1}0}\right|}{R}\sin\left(\theta_{1\bar{1}0} - \theta_{110}\right)J_1(\pi)\sin(\omega t) + 2\frac{\Delta R}{R}J_2(\pi)\cos(2\omega t), \quad (4\text{-}11)$$

where we have used:

$$\Delta R = \left|r_{1\bar{1}0}\right|^2 - \left|r_{110}\right|^2, \quad \text{and} \quad R = \frac{\left|r_{1\bar{1}0}\right|^2 + \left|r_{110}\right|^2}{2}. \quad (4\text{-}12)$$

The term in ω depends on the phase change through the reflection and the second harmonic depends on the difference in reflectance. The measurements of our study only monitor the 2ω term. The great majority of the catalogued spectra have been measured with the second harmonic. It is also this term that has the lowest level of error induced by imperfections in the components or retardation because of stress induced birefringence in the window. [34]

4.2.3 Determination of the zero

Several conditions can affect the RDS in a systematic way. Components can be poorly aligned or can have intrinsic imperfections. The reactor windows, because of the

vacuum inside the chamber, are under stress. Just as the PEM uses stress to generate birefringence, the window can modify the polarization of the light. The component intrinsic imperfections have been calculated to affect the second harmonic signal only to the second order and can be neglected. [34] The misalignment of both the polarizer and the PEM shift the signal as a whole and are not expected to have a frequency dependency. The stress induced birefringence in the window will likely have a spectral response and can modify the shape of the collected spectrum. The procedure to remove such effects from the data uses the capability of our system to rotate the sample. In principle a rotation of 90° changes the sign of the RDS signal coming from the sample but leaves the other effects unchanged.

Before each experiment the surface is stabilized and a RDS spectrum is collected. The sample is then rotated by 90° and a second spectrum is measured. Let S_{tot} be the total measured RDS signal and conversely S_{sam} and S_{opt} the signal coming from the sample and the optics respectively. The optics contribution can be extracted in the following way:

$$S_{opt} = \left(\frac{S_{tot}(0^{\circ}) + S_{tot}(90^{\circ})}{2} \right) = \left(\frac{S_{sam} + S_{opt} - S_{sam} + S_{opt}}{2} \right); \qquad (4\text{-}13)$$

An example of such a procedure is illustrated in Fig. 4.5. The two RDS spectra are of opposite signs and the average of the signals gives the spectral response of the other effects combined. Since the setup is aligned at the beginning of an experiment the procedure needs to be applied only once and the obtained background can be subtracted from each spectrum taken during the experiment.

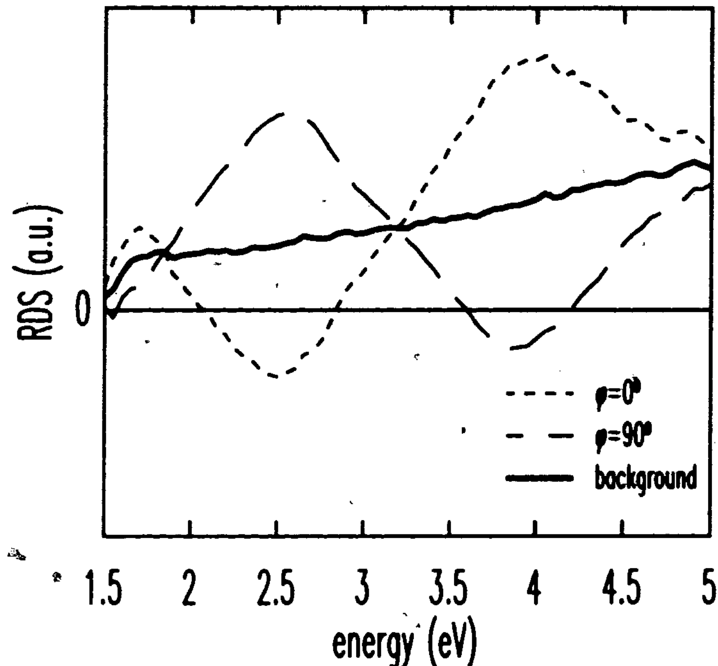

Fig. 4.5 Example of the procedure used to measure the contributions of the component misalignment and imperfection to the RDS signal.

4.2.4 Time resolved spectral measurements

The RDS energy spectrum of a surface can be obtained when its state is stable enough to permit data collection. With our setup the time needed to collect a spectrum from 1.5 to 5 eV is about 1 min. It is obvious that the standard procedure can't be used to obtain information on the surface at all instants of an ALE cycle for instance. The surface is changing continuously during the cycle and only single frequency monitoring can be done. This state of affairs does not necessarily preclude obtaining time resolved energy spectra however.

Aspnes has used RDS with a procedure that indirectly produces the spectral information during a certain growth sequence. [35, 36] If the sequence produces a series of surface states that are highly reproducible it can be repeated an unlimited number of times without generating any cumulative effects that would affect the RDS spectrum. The procedure uses the fact that each sequence is highly reproducible to its

advantage. Single energy RDS monitoring can collect data with a frequency of up to 8 measurements per second. Each individual measurement is taken by an electronically triggered A/D converter within the digital lock-in amplifier, making it very regular in time. Each individual cycle is monitored at a different energy. In order to assure that the time measurements all coincide between the different sequences, a triggering signal is sent to the lock-in sampling system to initiate the monitoring at the beginning of each sequence. This trigger is linked to the switching of one of the valves on the reactor. Once a complete set of energies have been monitored during the sequence, the RDS spectra can be extracted by building them from corresponding time points. This is done after the experiment using a computer program. In this fashion we can obtain complete energy spectra over the entire ALE cycle only 0.125 s apart.

4.3 X-ray diffraction

X-ray diffraction (XRD) is a characterization technique that is essential to any growth facility. Its ease of use combined with its powerful capabilities make it the tool of choice as an *ex situ* feedback for crystal growth. It can quickly provide the crystal grower with important information such as layer thickness and composition, the presence of strain relaxation or contamination of the layers. Recent improvements of the equipment has also allowed very accurate lattice constant measurements and reciprocal space mappings, which push the diagnostic ability of XRD even further. As we will discuss later in this section XRD can even be sensitive to fractions of a ML of material buried within a crystal. This section describes the diffractometer that we used to measure the growth rates on our samples as well as the amount of material embedded in the crystal by heteroepitaxy. The procedure to gain such information is outlined as well.

4.3.1 X-ray diffractometer

The machine that we used is the model 300 manufactured by BEDE Scientific in the UK. A schematic view of the setup is shown in Fig. 4.6. The x-rays are generated from a 2 kW electron beam hitting a Cu target. The x-rays are emitted by the Kα

transitions in the Cu and have a wavelength of 1.514 Å. Two channel cut Si (220) single crystals are used to both collimate the beam and make it monochromatic. The conditioned beam is then directed towards the sample. The angle of incidence is accurately controlled by a multiple axis goniometer. The diffracted beam is detected by an extended dynamic range (EDR) detector which consists a the combination of a scintillator with a photomultiplier tube. The unit is sensitive to x-rays in the range of 4 to 25 keV. The use of small slits before the detector cuts down the noise due to scattered x-rays. The sample is rotated using the high precision stage to an angle θ and the detector is positioned to remain at the specular angle 2θ. Both angles are varied simultaneously and the signal is collected to obtain what is commonly called a "rocking curve". Using a high quality GaAs single crystal we have obtained linewidths as small as 15 arcseconds with this setup. Using the higher resolution mode, the linewidth can be improved to as narrow as 4 arcseconds but with a significant reduction in the intensity of the signal. All the measurements of this study have been made in the low resolution/high dynamic range mode where resolution is sacrificed to allow higher signal intensity.

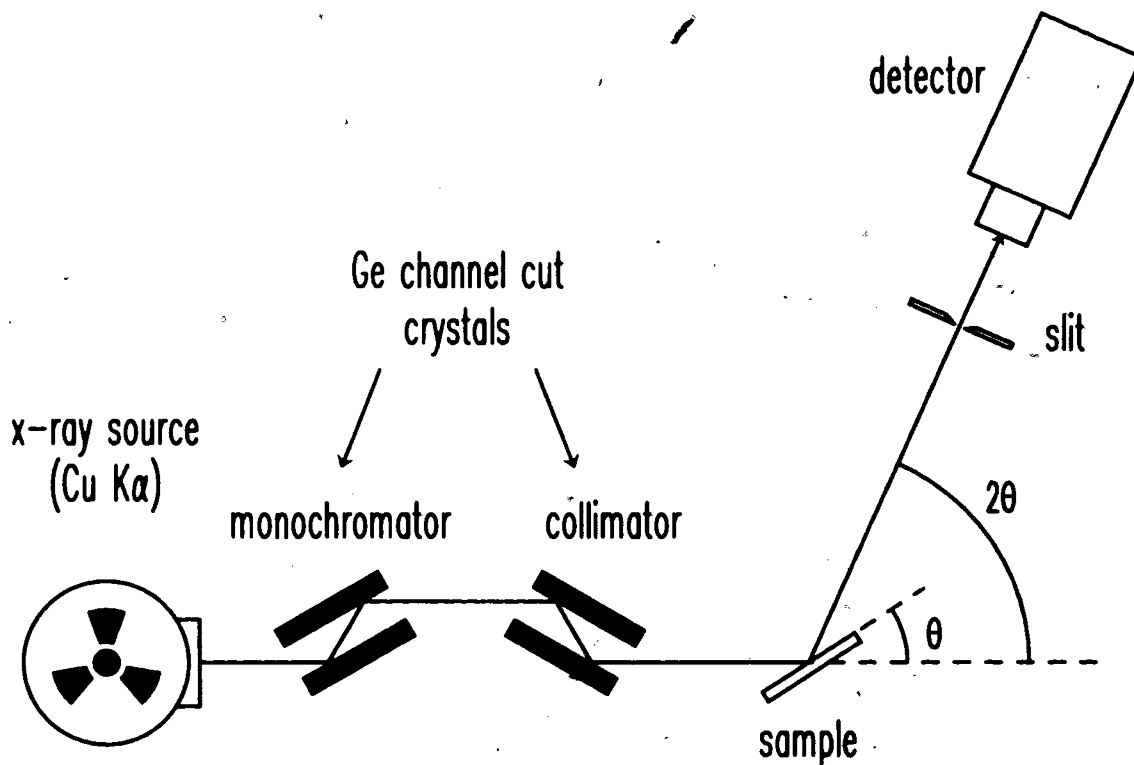

Fig. 4.6 Schematic view of the x-ray diffractometer. The sample and detector stages are rotated through angles of θ and 2θ respectively.

4.3.2 Growth rate measurements

Several techniques have been used to measure the thickness of epilayers. One of the most common consists of using a mask to cover part of the growing surface. After the removal of the mask the height of the step between the masked region and the epilayer is measured by surface profilometer. This technique has the advantage of being effective for any epilayer thickness but requires several pre– and post–growth treatment steps. The technique that we used is much simpler. It has been demonstrated that even a fraction of ML of a foreign material inserted inside a crystal greatly affects the rocking curve. [37, 38]

4.3.2.1 Kinematic description of the rocking curves

This section gives a simplified description of the effect of a thin inserted layer on the diffraction of x-rays. A more complete treatment can be achieved using the dynamical theory but for the sake of simplicity we will leave this interpretation to the reader. The details have been reported earlier. [38] The kinematic theory gives a justification for the presence of fringes in the rocking curves for a thin layer inserted in a crystal. According to that theory the reflectivity of a thin layer as a function of the angular deviation ω around the Bragg angle θ_B is given by:

$$R = |\Phi|^2 = \frac{\sin^2(AY)}{Y^2}, \quad (4\text{-}14)$$

where

$$A = \frac{\pi \chi_h \Delta}{\lambda} \left| \frac{\gamma_h}{\gamma_0} \right|^{1/2}, \quad (4\text{-}15)$$

and

$$Y = \frac{-|\gamma_0 \gamma_h|^{1/2} \sin(2\theta_B)\omega}{\chi_h}. \quad (4\text{-}16)$$

χ_h is the hth Fourier coefficient of the polarizability, λ the x-ray wavelength, Δ the layer thickness and γ_0 and γ_h the direction cosines of the incident and diffracted

waves. For a layer that is much thinner than the x-ray extinction length the reflectivity exhibits a series of fringes around the main peak which are commonly called Pendellösung fringes. The angular separation between adjacent fringes is given by $AY=\pi$ so it is related to the layer thickness through the equation:

$$\Delta\omega = \frac{|\gamma_h|\lambda}{\sin(2\theta_B)\Delta}. \qquad (4\text{-}17)$$

We consider now the reflection from a structure composed of 3 layers, namely the cap and inserted layers and finally the substrate that we label 0,1,and 2 respectively. The amplitude of the reflected wave field is given by the expression:

$$\Phi = i\left|\frac{\gamma_0}{\gamma_h}\right|^{1/2} \sum_{j=0}^{2} a_j \exp(-i\varphi_j)\Phi_j, \qquad (4\text{-}18)$$

where

$$\varphi_j = A_j Y_j + 2\sum_{i=1}^{j-1} A_i Y_i. \qquad (4\text{-}19)$$

In the last two expressions a_j represents the attenuation of the signal through absorption. The reflectivity of the 3 layer structure is equal to $|\Phi|^2$:

$$\begin{aligned} R_3 &= |\Phi|^2 \\ &= \Phi_0^2 + \Phi_1^2 + \Phi_2^2 \\ &\quad + 2[\Phi_0\Phi_1\cos(\varphi_0-\varphi_1) + \Phi_1\Phi_2\cos(\varphi_1-\varphi_2) + \Phi_0\Phi_2\cos(\varphi_0-\varphi_2)] \end{aligned} \qquad (4\text{-}20)$$

and using eq. 4-19 we obtain

$$\varphi_0 = A_0 Y_0 \qquad (4\text{-}21a)$$

$$\varphi_1 = A_1 Y_1 + 2A_0 Y_0 \qquad (4\text{-}21a)$$

$$\varphi_2 = A_2 Y_2 + 2A_0 Y_0 + 2A_1 Y_1 \qquad (4\text{-}21a)$$

On the other hand if we calculate the reflectivity for the same structure without the inserted layer or simply a monocrystal we get:

$$R_1 = \Phi_0^2 + \Phi_2^2 + 2\Phi_0\Phi_2\cos(\varphi_0-\varphi_2). \qquad (4\text{-}22)$$

with

$$\varphi_0 = A_0 Y_0 \qquad (4\text{-}23a)$$

$$\varphi_2 = A_2 Y_2 + 2A_0 Y_0. \qquad (4\text{-}23a)$$

For simplicity we assume that the cap layer and substrate have the same thickness and we make the approximation that the inserted layer is so thin that the intensity of the diffracted field coming from it can be neglected. Using these approximation, the difference between the reflectivity of the two structure is given by:

$$\begin{aligned} \Delta R &= R_3 - R_1, \\ &\cong 4\Phi_c^2\left[\sin(A_1Y_1 + 2A_cY_c)\sin(A_1Y_1)\right], \end{aligned} \tag{4-24}$$

where we have used

$$\Phi_0 = \Phi_2 \doteq \Phi_c, \tag{4-25a}$$

$$A_0Y_0 = A_2Y_2 = A_cY_c, \tag{4-25a}$$

$$\Phi_1 << \Phi_c. \tag{4-25a}$$

We can see that the difference in reflectivity is equal to the reflectivity of the thick layers modulated by two sinusoidal functions taking into account the phase shifts. The first function depends on the total thickness of the 3 layers and the second singles out the effect of the inserted layer. This result shows that the presence of a thin layer of material inserted in a crystal produces a modulation of the signal which depends on the thickness of the inserted layer. A simple representation of that effect is shown in Fig. 4.7. First consider the Bragg condition. The waves diffracted from planes in the

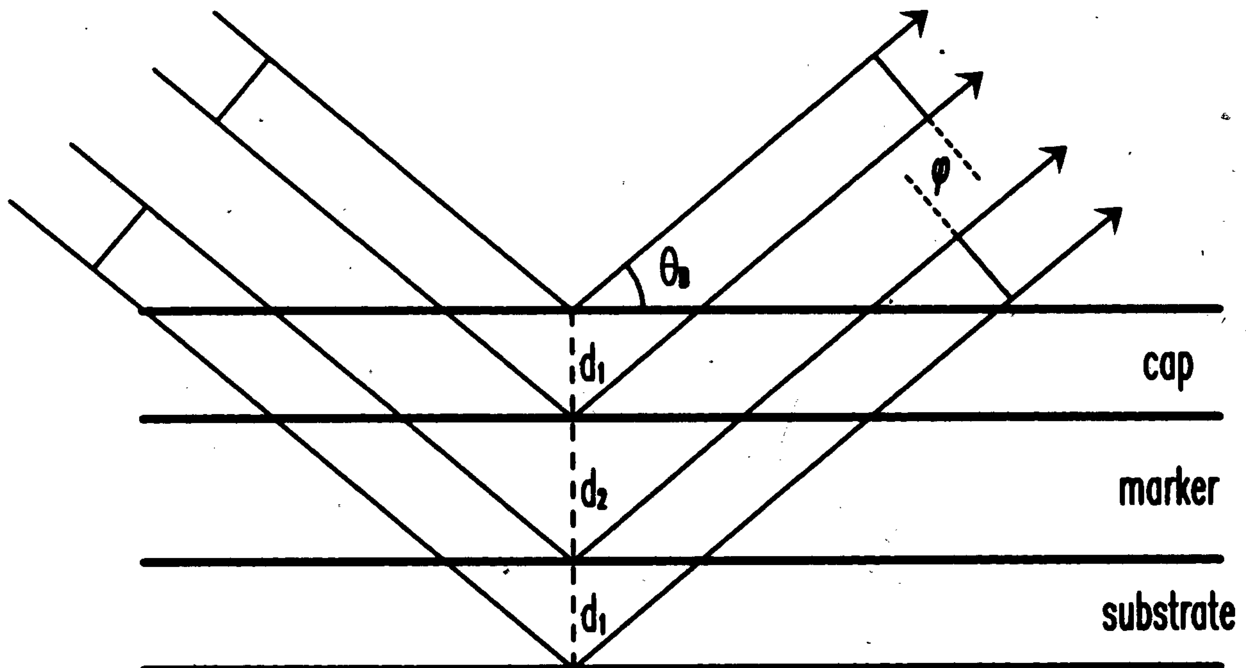

Fig. 4.7 Kinematic justification for the modulation of the diffracted beam when a thin marker layer is inserted in a single crystal. The wave fields diffracted from the cap and buffer layers interfere.

substrate are coherent with each other and interfere constructively. X-rays coming from the cap layer planes are also coherent among themselves. These two reconstructed wave fronts, however are not coherent because their respective phase is shifted by φ which depends on the thickness of the marker layer. They will therefore interfere with each other. When the angle is varied around the Bragg condition the interference between the two wave fields modulates the signal.

A closer look at the rocking curve of such structure shows that the position of the fringes around the Bragg peak varies with inserted layer thickness. The kinematic treatment we just outlined does not explain such a shift. The dynamical theory is needed for such a demonstration. This approach properly keeps track of the multiple reflections that can happen in a layered structure with a variation of the refractive index. With the dynamical theory the boundary conditions are preserved at each heterointerface. The shift in the position of the fringes relative to the main Bragg peaks is reproduced well with this treatment. The details have been reported in ref. 38. The

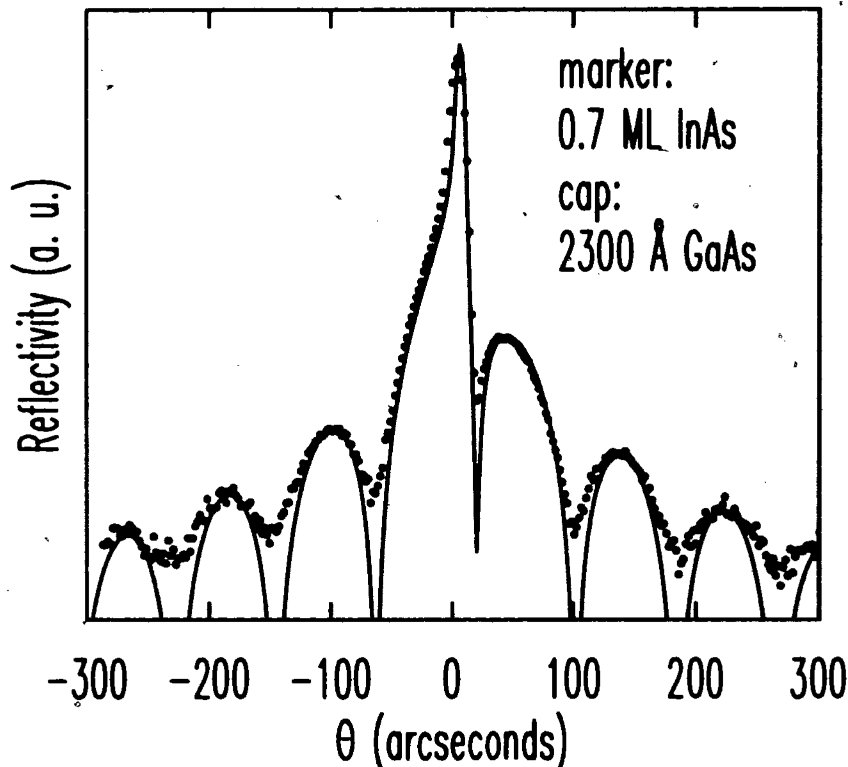

Fig. 4.8 Modulation of the diffracted x-ray intensity by the presence of a thin InAs layer in GaAs. The dots represent the experimental data and the solid line the simulation using the dynamical theory.

simulation program we have utilized to fit the rocking curves and obtain the growth rate values as well as the inserted layer thickness makes use of the dynamical theory. An example of a fit is shown in Fig. 4.8. The technique is sensitive to inserted layers with a thickness as low as 0.25 ML for InAs layers inserted in GaAs. However it does not give absolute information on the distribution of the InAs within the crystal.

4.4 Atomic force microscopy

This section gives a description of atomic force microscopy (AFM) with some details on the microscope that was used in our studies. A brief overview of the technique used to acquire the morphology information is outlined first and the section ends with technical information on the microscope.

4.4.1 Contact and non-contact modes

AFM uses the interactions between a sharp tip and the atoms on the surface of the material to obtain information on its morphology. As the tip is brought within a few angstroms of the surface different forces are exerted on it. Fig. 4.9 shows an illustration of the force applied on the tip as a function of distance from the surface.

At long distances the van der Waals interaction produces an attractive force (negative on graph) on the tip while for short distances the force becomes strongly repulsive (positive). When the microscope is used with the tip in the attractive force region it is considered in the non-contact mode. Similarly the strongly repulsive part of the curves corresponds to the contact mode where the tip is actually "touching" the surface. This is the mode that we used for this work. In this mode the gradient of force is extremely steep, meaning that the slight change in the distance between the tip and the sample surface results in a large variation in the repulsive force. Inversely if a given force is applied to the tip, its position relative to the surface will be well determined. This constitutes the main idea behind the contact mode of operation. The main components of the setup as well as the procedure to acquire the data are outlined in the next section.

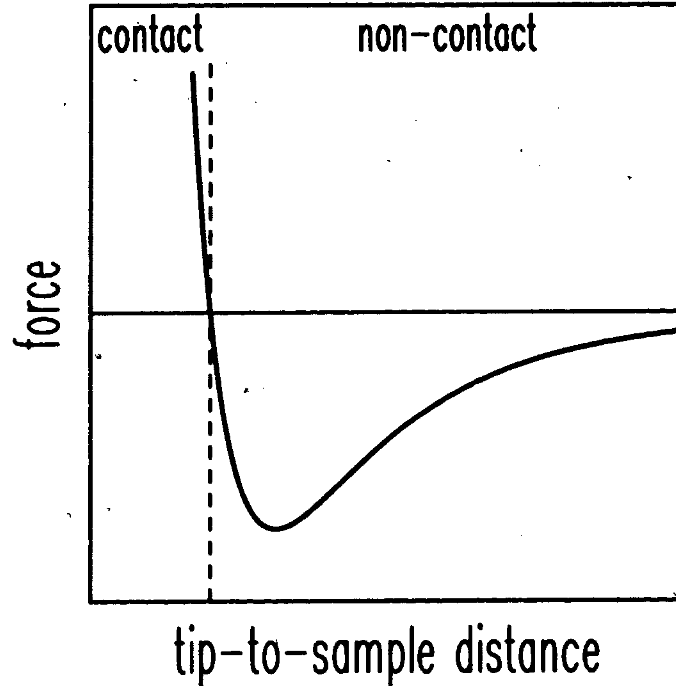

Fig. 4.9 Interatomic force acting on the cantilever as a function of the distance between the tip and the sample.

4.4.2 Description of the microscope and data acquisition

The position of the tip is detected by reflecting a laser beam from a mirror on the back of the cantilever and using a position sensitive photodetector (PSPD) to record the position of the reflected beam. The detector is made of two photosensitive cells mounted side by side. When the system is adjusted for a measurement the reflected spot is adjusted so it is located at the junction between the two cells and the signals coming from each detector are equal. Any small variation in the position of the spot can be recorded by monitoring the difference in the two detector signals. With such a configuration the detector can measure tip vertical movements of less than 1 Å. Fig. 4.10 shows a schematic illustration of the microscope.

Information on the surface morphology can be obtained in two different ways: using a constant stage height or a constant tip force. We have used the second technique. A given force is applied to the tip as the sample is moved laterally. Any change in the height of the surface is detected by the PSPD which relays the signal via a feedback loop to the piezoelectric cell controlling the vertical movement of the stage which corrects the height to maintain the PSPD signal constant. The morphology is then obtained by plotting the changes in the height of the stage. This way the entire sample is scanned with the same force applied to the tip.

The total range of the scanner stage is 100 μm × 100 μm laterally. The spatial resolution of the system depends on the tip size and is of 100 Å for our case. The samples are mounted in air on the stage with double sided adhesive tape. The formation of oxide with time has not been observed to affect the quality of our images. Most samples were measured minutes after they were taken out of the growth chamber

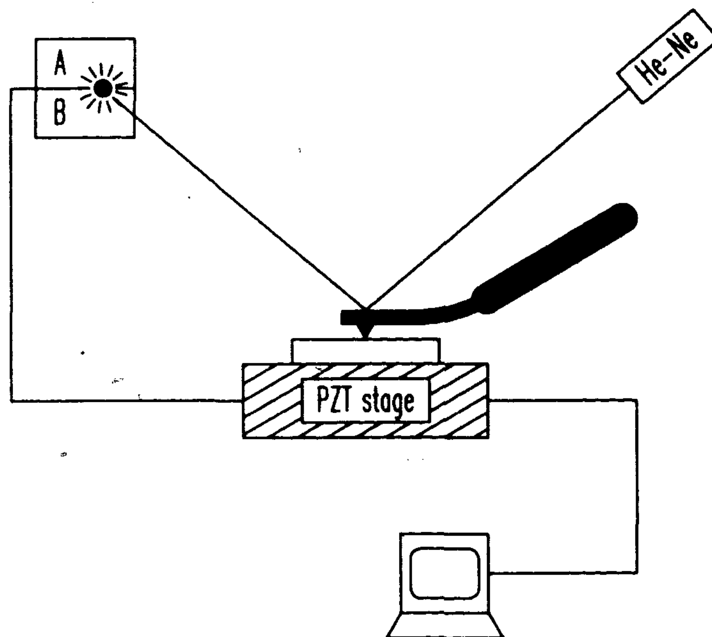

Fig. 4.10 Basic components of the atomic force microscope.

but images measured several weeks later did not show significant differences from the ones taken immediately following the growth.

Since the main crystalline axes on the surface are parallel to the sample edges, most of the features of the morphology have a preference for these direction. We mounted the samples at a 45° angle with the scanning direction in order to avoid any confusion between real features and systematic drifts of the microscope electronics.

5. Growth Mechanisms

Even if the ALE process takes place in an environment similar to MOCVD, the mechanisms governing the growth differ considerably. ALE is normally performed at lower temperatures than MOCVD growth. This has the effect of slowing down all thermally driven reactions such as precursor dissociation and surface reactions. ALE also supplies precursors from one group at a time to the surface. Any reaction between precursor molecules of different groups in the gas phase are supressed in ALE. The accumulated knowledge of these processes in MOCVD must therefore be renewed for ALE. The following chapter reports on our contribution to that endeavor.

During the ALE cycle the surface is submitted to two distinct types of conditions: hydrogen purge and precursor exposure. Under the first type of condition there is no net growth of the crystal. These are the steps in the cycle where the chamber is purged of any remaining precursor molecules from previous exposures. Desorption of chemical species that are weakly attached to the surface also occurs during that time. When the surface is exposed to precursor molecules of a given group (III or V), they react with the surface and new atoms are incorporated in the crystal. We will devote most of the coming chapter to this part of the cycle and more specifically to the exposure to the group III precursor.

The problem of group III incorporation will be investigated with the following questions in mind:

- What is the state of the surface when the first group III molecules react with it?
- How do the group III atoms enter the layer?

- How does the surface reconstruct as more group III atoms are incorporated?
- What keeps the incorporation within 1 ML even though none of the known adsorbate-free reconstructions has that coverage?
- What is the role of the methyl radicals in the self–limiting behavior of the growth?

We are going to treat each of the preceding problems individually. The first part of the study considers the surface during the time it is purged before being exposed to the group III. We then proceed to look at the surface state during the whole group III exposure using time resolved RDS. The absolute amount of group III atoms that enter the layer is then measured by XRD and we compare the results with RDS data. Using these results, we propose a model for the evolution of the surface as the group III atoms gradually cover it.

The mechanisms that preserve the morphology and inhibit the formation of Ga droplets are investigated with AFM and the role of methyl radicals is assessed. In the last section of the chapter RDS is used to extract some activation energies for the desorption of the alkyl species attached to the surface after the group III exposure.

5.1 Arsenic desorption

The state of the surface at the initial moments of the group III exposure and more specifically the amount of As covering it is very important in the elucidation of the stoichiometry problem. The goal is to understand why the surface collects exactly 1 ML of group III atoms during exposure. Two situations were investigated in previous work. The first situation has an As stabilized surface that is reconstructed in the (2×4) fashion with less than a single layer of As on top. In this case it is impossible to account for a growth rate of 1 ML/cycle. There is not enough As on the surface to generate 1 ML of material during group III exposure. In the other cases the surface was typically reconstructed in the c(4×4) symmetry which is terminated by more than 1 ML of As. In this case most authors simply stated that the "excess" left the surface during the purge cycle preceeding the group III exposure.

In order to verify this last claim we have performed *in situ* monitoring of the surface during As desorption for both GaAs and InAs. The results constitute an important element of our model for the incorporation of the group III element during the ALE cycle.

5.1.1 GaAs

We begin with the study of group V desorption with GaAs as it is the most documented III-V compound of all. Most of the known surface reconstructions have been investigated and their respective RDS energy spectra have been reported [39, 40]. A summary of the RDS spectra for the different surfaces from our data is given in Fig.3.2. We will use these spectra as the basis of our analysis. The experiment proceeds as follows: The surface of GaAs, initially stabilized under TBAs at 470°C, is then purged under hydrogen until the RDS signal shows signs of saturation, at which point the TBAs flow is resumed. The top panel of Fig. 5.1 shows the RDS signal taken at the energy of the As dimers, i.e. 2.6 eV, for that energy is expected to show the biggest changes during desorption of As from the surface. The labels represent time points at which the complete corresponding energy spectra are given in the lower panel of the same figure. For the sake of simplifying time interval reading, we have chosen the moment of the termination of the TBAs flow as the origin of the time axis.

The RDS signal is stable under TBAs and the corresponding energy spectrum indicates that the surface has the d(4×4)–like character (i) in Fig. 5.1. Almost immediately after the termination of the TBAs flow, the signal shows a rapid change. After 3.7 s of purge the rate of change in the signal decreases noticeably. At that point the spectrum resembles that of the c(4×4) (ii). This fast modification of the spectrum is generated by the quick desorption of excess As from the d(4×4) surface. An activation energy of 59 kcal/mol was obtained using SPA for this part of the desorption [41]. Sakamoto *et al.* have also reported a two step As desorption on GaAs (001) and their value of the energy of activation of the first process was 50.5 kcal/mol [42]. The shape of the RDS signal during the desorption does not allow us to obtain kinetic information and compare with these results. The RDS signal does not exhibit the required

exponential shape that is observed in SPA suggesting that the signal is not directly proportional to the concentration of As on the surface.

Between 3.7 s and 30 s the spectrum slowly shifts as a whole towards a more positive response but remains with an essentially c(4×4)–like shape. This can be seen

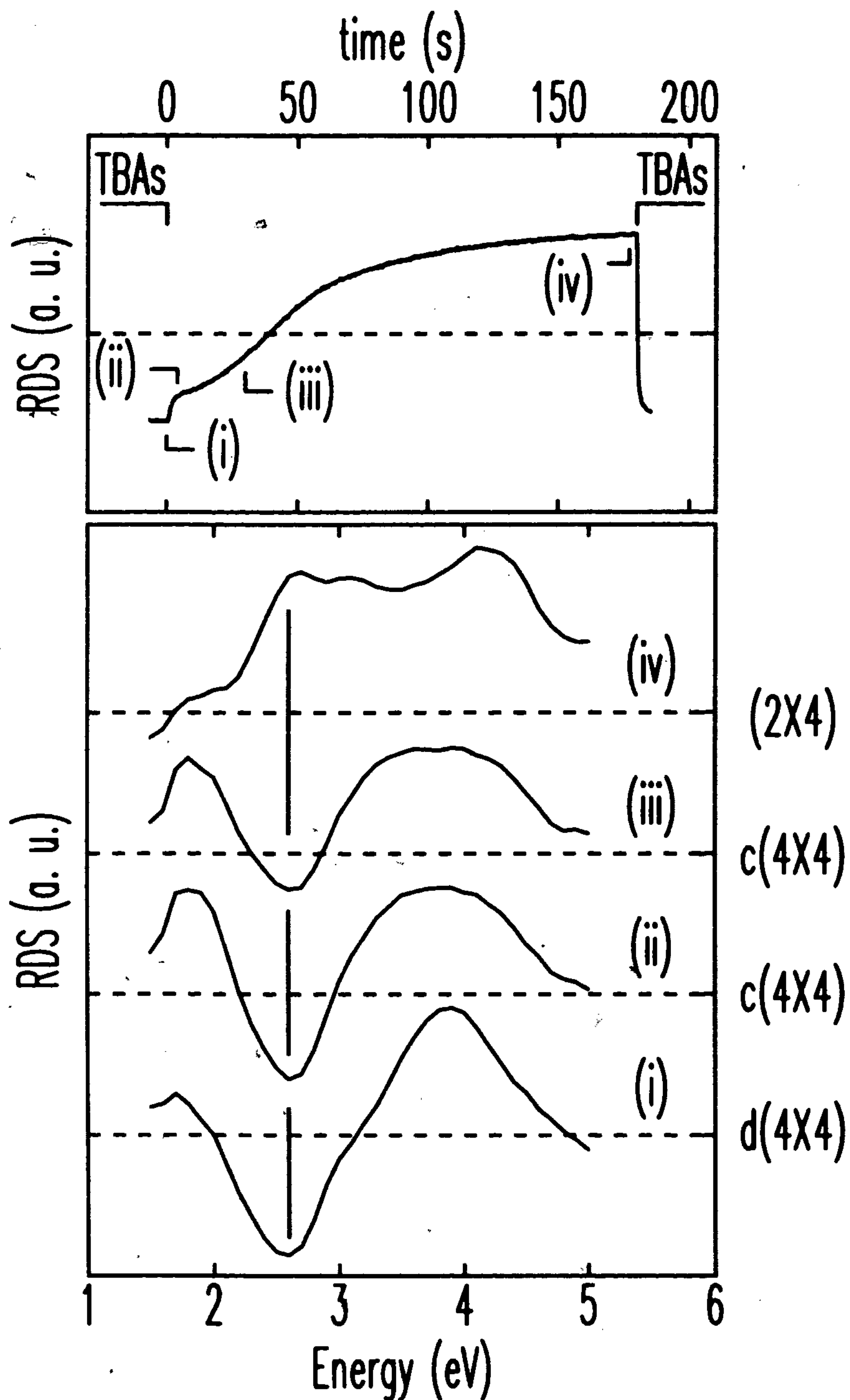

Fig. 5.1 *In situ* RDS monitoring of the desorption of As from the GaAs surface. The top panel shows the time transient at 2.6 eV. The specific instants during the transients are: (i) 0 s, (ii) 3.7 s, (iii) 30 s, and (iv) 180 s. The corresponding energy spectra are shown in the lower panel.

by comparing spectra (ii) and (iii) with Fig. 3.2. After more than 30 s of purge, the spectrum starts to go through a complete change in shape where the 2.6 eV negative feature, attributed to second layer As dimers, starts to disappear, being replaced by a new positive feature at the same energy. This trend persists until the RDS spectrum takes a clear (2×4)–like shape after more than 3 min. of purge (iv). A very similar set of energy spectra could be observed by cooling down the GaAs surface from 600°C to 200°C under a constant As flow in UHV [30]. The main conclusion we draw from such an experiment is that the c(4×4) reconstruction remains for more than 30 s under an As free environment at 470°C. Any attempt at explaining the stoichiometry of ALE growth must account for the fact that the As stabilized surface is always terminated by more than one layer of As. This surface is sufficiently long lived to remain in effect under most ALE conditions.

5.1.2 InAs

The only reported comparison of InAs surface reconstructions with RHEED and RDS measurements showed both an As terminated (2×4) and an In rich (4×2) reconstruction [43, 44]. In addition to those RDS spectra we observe a different spectrum when the surface is stabilized under a TBAs flow at regular ALE temperatures. Fig. 5.2 shows such a spectrum taken with a TBAs partial pressure of 22 Pa at 390°C. It is characterized by the two dominating features at 2.3 eV and 3.5 eV respectively. It differs considerably from the (2×4)–like spectrum which also has two main features but they are much broader and are located at slightly different energies (2.1 eV and 3.6 eV). The exact atomic structure of such a reconstruction is not known but by analogy with the GaAs case, it can be expected that the TBAs stabilized surface has a larger As coverage. The As dimers in the TBAs stabilized surface do not seem to be in a direction opposite to the dimers on the (2×4) surface as is the case for the GaAs c(4×4) surface. Proper RHEED studies would need to be done to verify this assessment. For the sake of clarity in this work we will use the label "As super rich" (ASR) for the surface under TBAs.

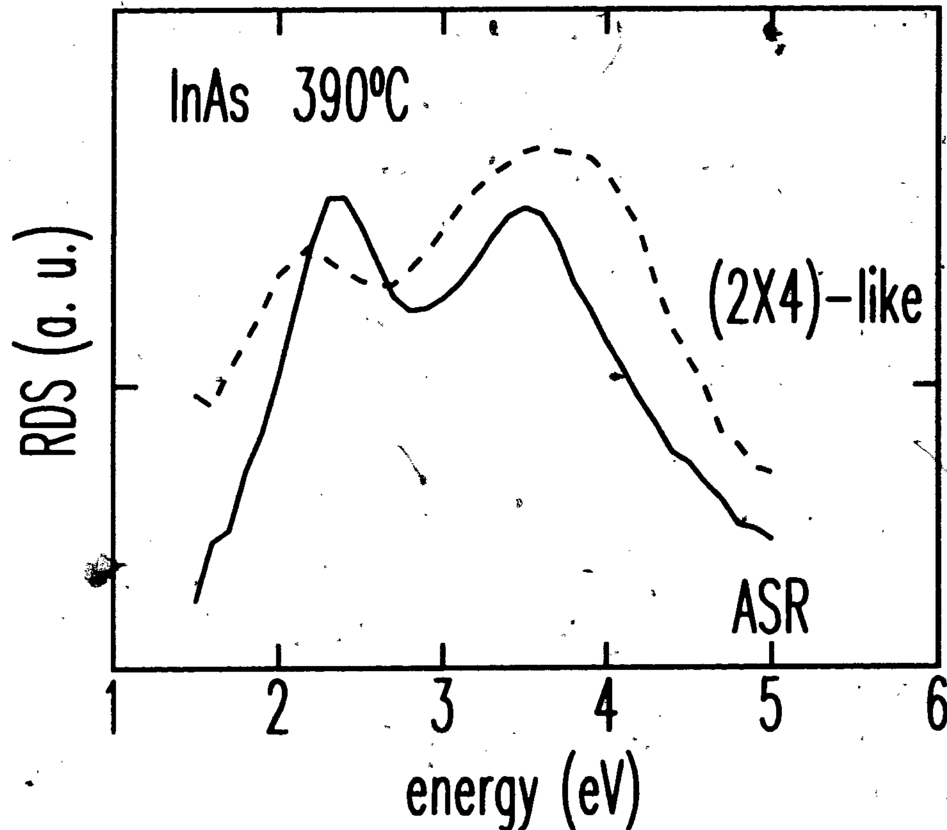

Fig. 5.2 RDS energy spectra of the InAs surface with (solid) and without (dotted) TBAs overpressure. The corresponding recontruction for the purged surface has been identified as (4×2). The other spectrum is called "As super rich" (ASR) in this work.

The time resolved RDS signal of the purged InAs surface taken at 2.3 eV is shown in the top panel of Fig. 5.3. Key instants during the purge are labeled in a fashion similar to the GaAs case and the corresponding spectra are given in the lower panel. The initial spectrum represents the surface when it is stabilized under TBAs and is a good example of the ASR surface. When the TBAs is interrupted the signal drops almost instantly to a near zero level. A spectrum taken half way through this drop at 0.25 s shows the same two features of the ASR surface but slightly modified towards the (2×4)–like characteristics.

One point is important though; the low energy feature for InAs is not shifted compared to the ASR surface like it is for the (2×4) surface. That fact remains true until the signal reaches a minimum near zero at 0.75 s where all that remains in the RDS spectrum is the higher energy feature. What happens afterwards is simply the

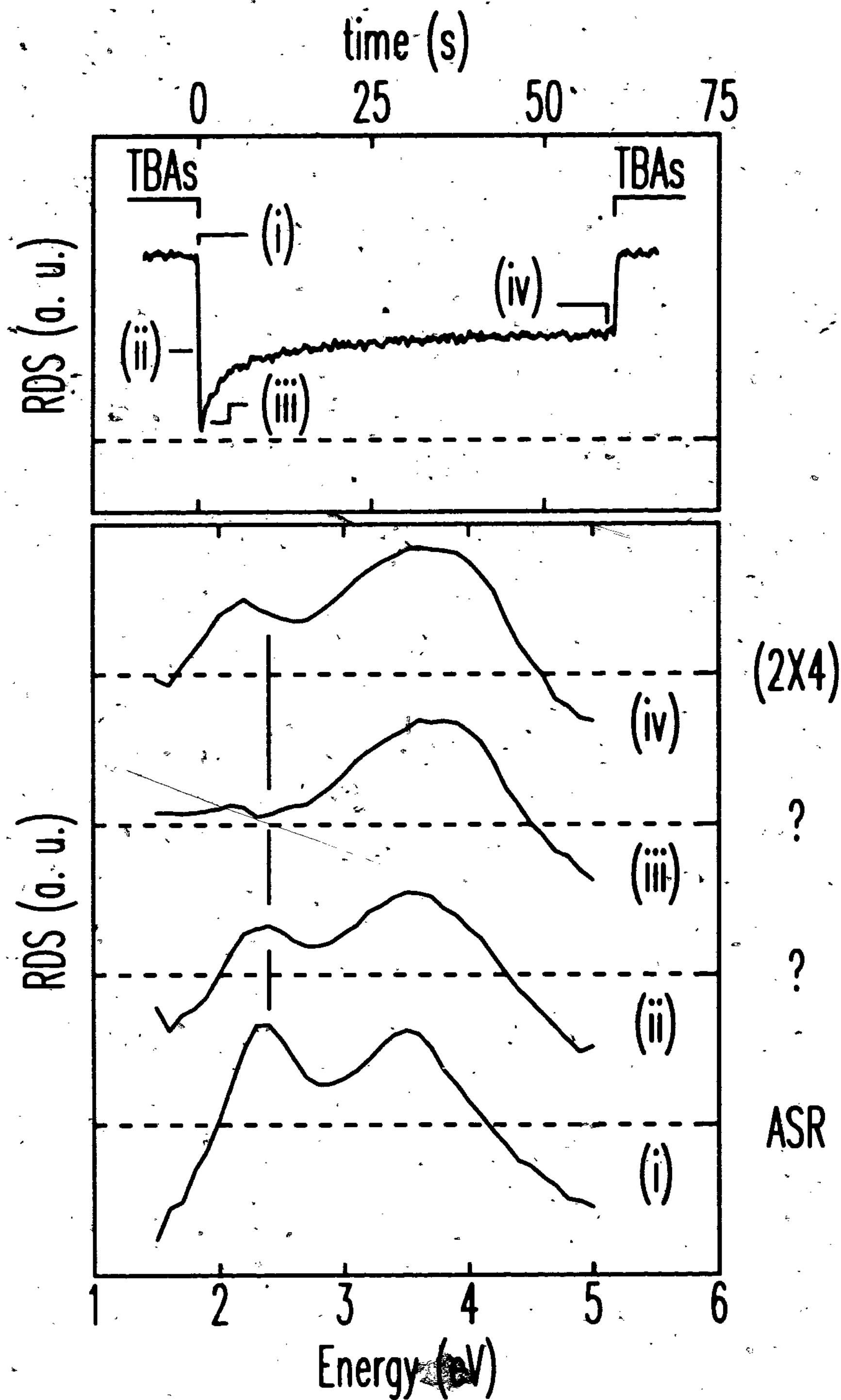

Fig. 5.3 *In situ* RDS monitoring of the desorption of As from the InAs surface. The roman numerals correspond to specific instants and their energy spectra are displayed in the lower panel.

slow growth of another low energy feature now located at the right energy (2.1 eV) until the signal becomes stable after roughly a minute. At that point the surface has the standard (2×4)–like RDS spectrum.

This two step desorption process gives evidence that the ASR surface has a somewhat different dimer structure than the (2×4). The fast transient is due to the rapid desorption of loosely bound As that constitutes part of the ASR surface. Presumably, in contrast to the GaAs c(4×4) surface, the dimers on the second layer of the InAs ASR reconstruction are aligned in the same direction as the (2×4) dimers, i.e. there is no rotation of the dimer. At present we have no detailed model of such a structure. The desorption of the second layer As breaks the dimers and seems to proceed much faster than the following process which should be the formation of the dimers on the (2×4) reconstruction. The spectrum taken after 0.75 s of purge represents the surface when no significant dimer structure is present at the surface, which explains the flat shape of the spectrum around 2.3 eV. From that point on a new structure slowly develops at 2.1 eV indicating that the dimers being formed have a different local environment than the ones present in the ASR surface.

We have recorded the evolution of those two processes as a function of temperature to obtain information on the energetics involved. The first part of the transient is almost linear and can be characterized by a straight line. The second portion of the desorption signal has a shape that is very close to an exponential decay. The rate constant of that exponential can be measured as well from simple fitting of the RDS signal. The functions that were fitted are:

$$RDS_{fast} = A - B(T)t \tag{5-1}$$

for the "fast" first part and

$$\mathrm{RDS}_{\mathrm{slow}} = \mathrm{A} - \mathrm{Ce}^{-\mathrm{kt}} \tag{5-2}$$

for the "slow" portion of the signal. In order to compare the values of the parameters found in this way, we have plotted the logarithm of the values of B and (Ck) versus T for the fast and slow process respectively. The resulting Arrhenius plot is given Fig. 5.4. Both parameters exhibit strong linear behavior to produce values of activation

energy of 49.6 kcal/mol and 58.5 kcal/mol for the fast and slow processes. It is interesting to note that the activation energy of the fast process is close to the reported value for the heat of formation of As_2 of 52.5 kcal/mol [45] and the slow process lies close to the heat of formation of As_4 at 54.2 kcal/mol [46]. This similarity might be coincidental but if we compare these results with the energy reported for the same two processes on GaAs we observe the same trend.

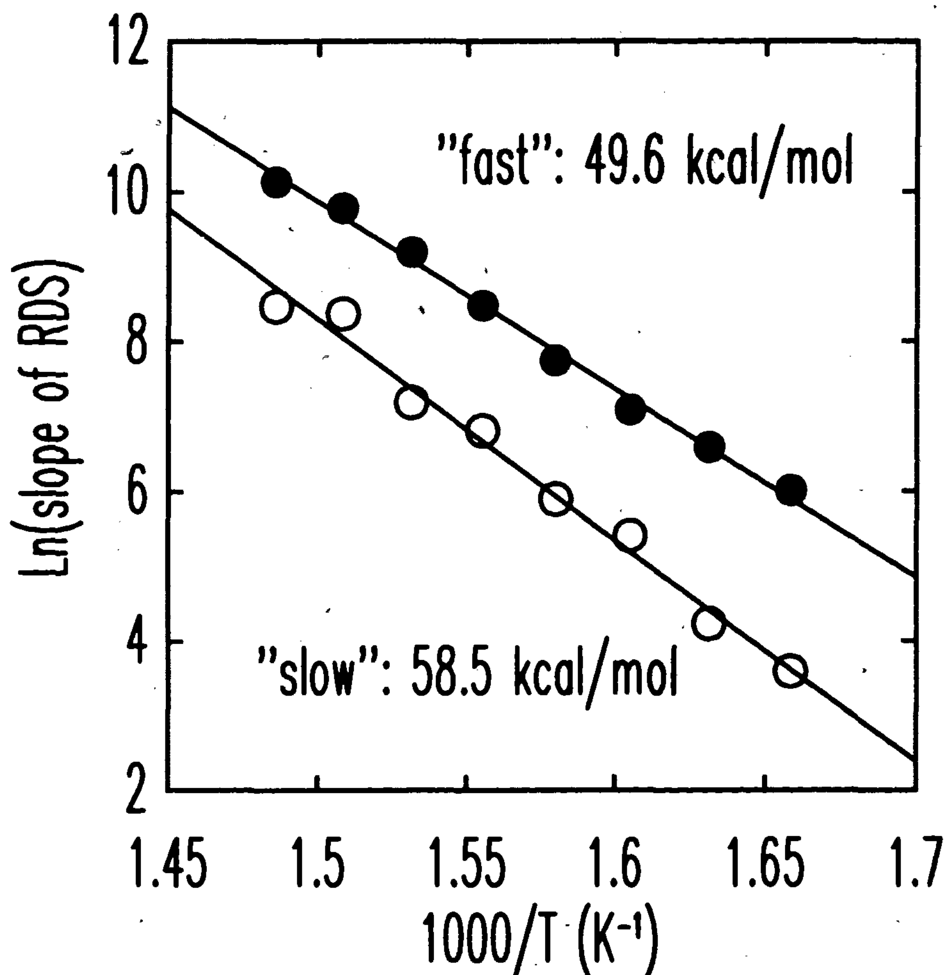

Fig. 5.4 Arrhenius plot of the two parts of the RDS transient for the desorption of As from the InAs surface.

For GaAs the excess As desorbs much faster with an activation energy of 59 kcal/mol and thereafter the As leaves the c(4×4) surface at a slower rate with an energy barrier of 63 kcal/mol [41]. In both cases the faster process has the lower energy of activation. Both values are lower for the InAs case as can be expected from the weaker crystal bonds. The relation to the heat of formation of the As_x molecules could be valid if the activation energy was the same for both compounds. Then it could

argued the energy barrier is the formation of the molecule in the gas phase. Since the activation energy is not only dependent on the compound but also exhibits the proper behavior based on bond strenght arguments, it is likely that the measured activation energy is related to the local environment of the desorbing As atoms at the surface.

The two processes in GaAs have been attributed to a fast transition from the d(4×4) to the c(4×4) reconstruction and a slow change from a c(4×4) to a (2×4) symmetry. For the case of InAs the sequence consists of a fast transition from ASR to an unidentified structure presumably without dimers and a slow transition to the stable (2×4) reconstruction. Both systems show a double step process of As desorption but there seems to be some difference in the structure of the surface.

5.2 Group III incorporation

Now that the state of the surface upon the arrival of the first group III species is known the next section deals with the reactions between the group III precursor molecule and the surface. The interactions of the molecules with the second layer of As and the role played by the latter in the growth will be investigated. The particular characteristics of the surface under self-limiting conditions and the evolution of the surface reconstructions during group III exposure give further insight in the microscopic mechanisms at play.

5.2.1 GaAs

TMGa is the most common precursor used in the ALE of GaAs but because of the high levels of residual carbon left in the layer it has been hindered in its way to commercial applications. Typical residual hole concentrations in the 10^{16} – 10^{18} cm^{-3} have been obtained with TMGa [47]. Adsorbed methyl groups are responsible for the high carbon incorporation. In conventional MOCVD the carrier gas removes the major portion of the methyl radicals and further reaction with TBAs at the growth interface makes the growth of high purity layers possible. Using fast gas streams in a technique called pulsed jet epitaxy (PJE) at temperatures closer to normal MOCVD conditions low carbon concentrations could be achieved [48] but in general the conditions

required for such low concentrations, namely very short pulses, short or even non existent purges, and high temperature make ALE doubtful at best [15]. In fact the samples displaying the best purity have been obtained with a growth rate of less than 1 ML/cycle. The problem of residual carbon remains a major concern with ALE at this point and one way to explore some of the solutions is to look for alternate sources which would exhibit the proper self–limiting behavior but with a much lower residual carbon contamination of the layers. We have investigated TNPGa as a possible candidate for low carbon GaAs grown by ALE. The details of the study have been reported previously [49] and will be detailed as part of Mr. Phillip Yeo's Master's thesis.

Fig. 5.5 shows a comparison of growth rate data for TEGa, TMGa and TNPGa at 470°C. The ALE cycle was (V:H_2:III:H_2): 6s:2s:Xs:2s. It is clear from these results

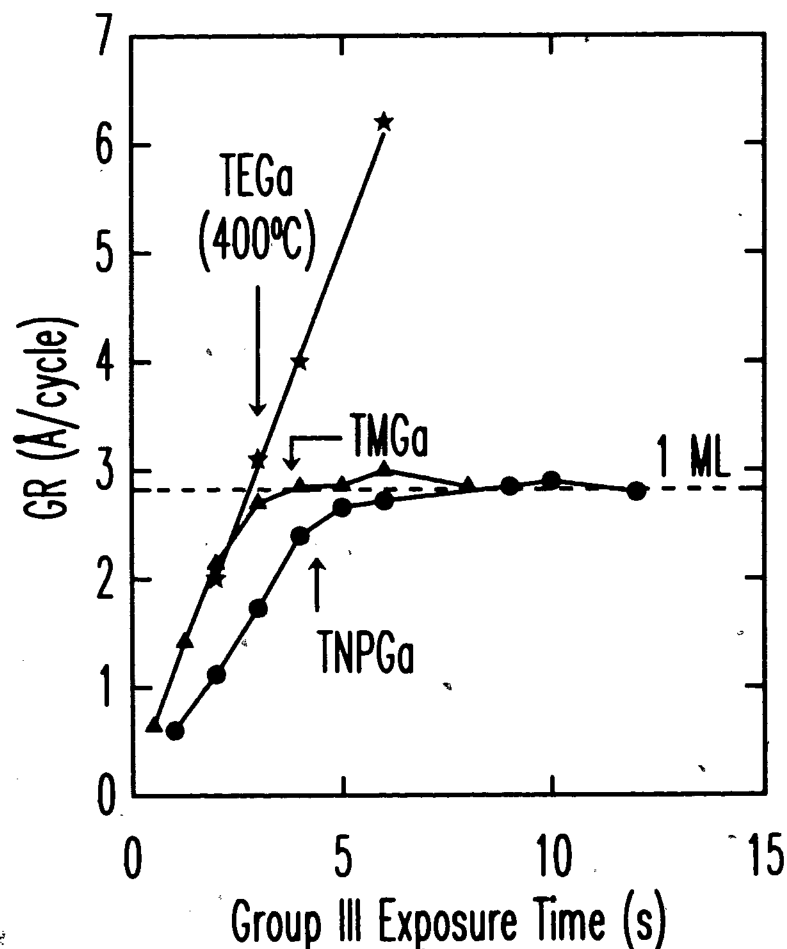

Fig. 5.5 Growth rate as a function of exposure time to the group III exposure at 470°C. The arrows are positioned at the time needed for the RDS transient to saturate.

that TEGa does not exhibit self-limiting behavior. This is a well known fact and it has been proposed that the dissociation of TEGa through a β-methyl elimination process produces a surface where the Ga atoms are exposed and the formation of droplets is possible. Our morphology studies using AFM give the first direct confirmation of such a claim and will be detailed in section 5.5. For the other two sources however, self-limiting growth is observed. The observed Ga incorporation from TNPGa is very similar to Ga incorporation from TMGa for the conditions we have used. This demonstrates the capability of the former precursor to produce good self–limiting growth. Under the proper flow conditions we have verified that self–limiting growth was possible over a range of temperatures comparable to the one for TMGa (400-500°C). This is consistent with the dissociation pathways which is expected to involve homolytic fission for both molecules.

The Ga incorporates more or less linearly for the first 80% of the coverage before slowly saturating at exactly 1 ML coverage and maintaining that coverage for several seconds. The long linear portion of the incorporation is a departure from the standard kinetic theory and requires further consideration that will be discussed in the next chapter. The fact that the amount of material grown during a single ALE cycle saturates at exactly 1 ML is somewhat intriguing since at no point is the surface terminated by only one ML of an atomic species, at least from the known reconstructions.

Another point that must be noted is the fact that for all precursors the Ga is observed to start incorporating immediately upon the arrival of the precursor molecules. It seems that the presence of a second layer of As on the surface does not affect the incorporation of Ga. We will show in the next few sections that the Ga does not insert itself between the two As planes but simply ejects the second layer As as it reacts with the surface.

We have used RDS in a real time mode to characterize the three sources available to us to grow GaAs by ALE. TMGa and TNPGa as self–limiting sources, decomposing via homolytic fission and TEGa as an example of a non self–limiting precursor, dissociating by β-methyl elimination. By choosing a specific RDS energy

we can highlight certain instants during the cycle where interesting changes are occurring. The natural choice is 2.6 eV, the energy sensitive to As dimers on the surface. Fig. 5.6 shows the RDS signal monitored at 2.6 eV for a specifically tailored ALE cycle with a long purge after the group III exposure to allow the surface to stabilize. The origin of the time axis is chosen to be when the TBAs is turned off. The signal is recorded for the three precursors used at 470°C. In all case the signal is initially stable under TBAs. Just as we observed in the desorption experiment, upon termination of the TBAs flow the signal first rises sharply while "excess" As is desorbed and the surface reaches the c(4×4) state. When the group III precursor is introduced in the chamber the signal first rises quickly until it reaches some positive maximum value and then starts going down again. The subsequent nature of the transient depends on whether the source is self-limiting or not.

For the two self-limiting precursors (TMGa and TNPGa) the signal reaches a certain value and then exhibits a slow rise until the exposure ends. The situation is different for a non self-limiting source (TEGa) where the signal continues to decrease before saturating and remaining at that value without change for the remainder of the exposure. The reason for such a difference will become more obvious with the spectral study of the surface but by looking at the effect of the subsequent purge, some clues as to what is happening can be inferred. When the surface is purged after having been exposed to a group III precursor there is a slow decay to a stable state for a self-limiting source which is absent in the non self-limiting case, suggesting the presence of some kind of adsorbate on the surface when a self-limiting source is used.

When TBAs is reintroduced in the chamber the signal recovers quickly to the original level for a stable surface. It should be noted that the formation of droplets during TEGa exposure is not detected by the RDS signal since they are essentially isotropic in nature. In Fig. 5.6 the labels (a) to (f) identify the instants at which we have recorded the energy spectra shown in Fig. 5.7

Those instants are:

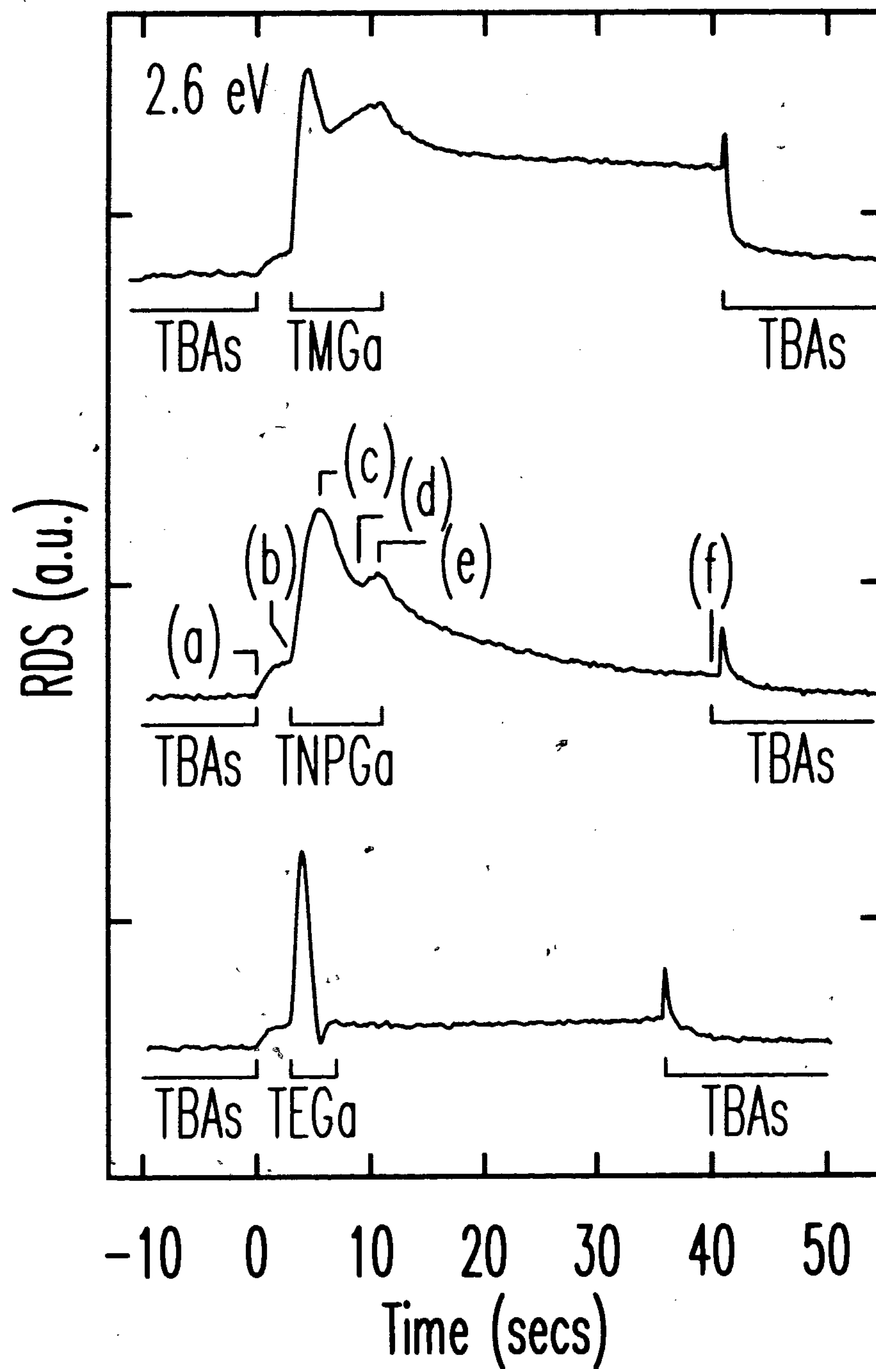

Fig. 5.6 RDS signal monitored at 2.6 eV during an ALE cycle for the three precursors. The energy spectra of the different instants of interest are compared in Fig. 5.7.

a) Termination of TBAs.

b) End of purge and onset of group III exposure.

c) Maximum of transient during group III exposure.

d) Saturation of transient during group III exposure.

e) End of group III exposure.

f) Stable surface during purge following group III exposure.

Fig. 5.7 is composed of two panels where we compare both TNPGa and TEGa to TMGa, represented by a dotted line. The labels explained above are given in the center column between the panels.

The surface under TBAs (a) has the familiar shape of the d(4×4) surface typical of MOCVD growth conditions at 470°C. The behavior during the subsequent purge is also identical, the surface reverting to a c(4×4) spectrum before the group III precursor is introduced (b). Even during that exposure the sequence of surface states is almost identical for the best part. The spectrum slowly evolves towards a (2×4)–like shape as shown in (c), in agreement with results from the same experiment previously reported [35, 36]. At signal saturation (d) the spectrum for a self–limiting source (TMGa and TNPGa) have an undetermined shape unlike the surface for the TEGa exposure which has a spectrum resembling the one attributed to the (4×2) surface. This strongly suggests that the surface exposed to TEGa does not collect other chemical species perturbing its reconstruction. The surface immediately forms Ga dimers which are then exposed to the incoming partially or completely decomposed TEGa molecules without the protection they need to prevent the formation of droplets. This will be further supported by AFM studies in section 5.5.

The lack of a transient following TEGa exposure also suggests the absence of ethyl groups because the surface being already in its stable configuration, a hydrogen purge has little effect on its state. The spectra for the beginning (e) and the end (f) of the purge cycle are basically identical. On the contrary the surface exposed to the other two sources, having a mixed state after the group III exposure (e), eventually relaxes to a Ga rich state which has a RDS spectrum close to the one reported in the literature for the (4×6) Ga-terminated reconstruction [40].

The main difference between self–limiting and non self–limiting conditions is therefore only the way the surface reconstructs during the Ga incorporation. In fact a "clean" process where the surface is smoothly transformed from an As terminated reconstruction to a Ga terminated one is not ideal for self–limiting growth. Since the RDS signal is a measurement of the local arrangement of atoms the difference could be either in the surface reconstruction, the presence of adsorbates or both.

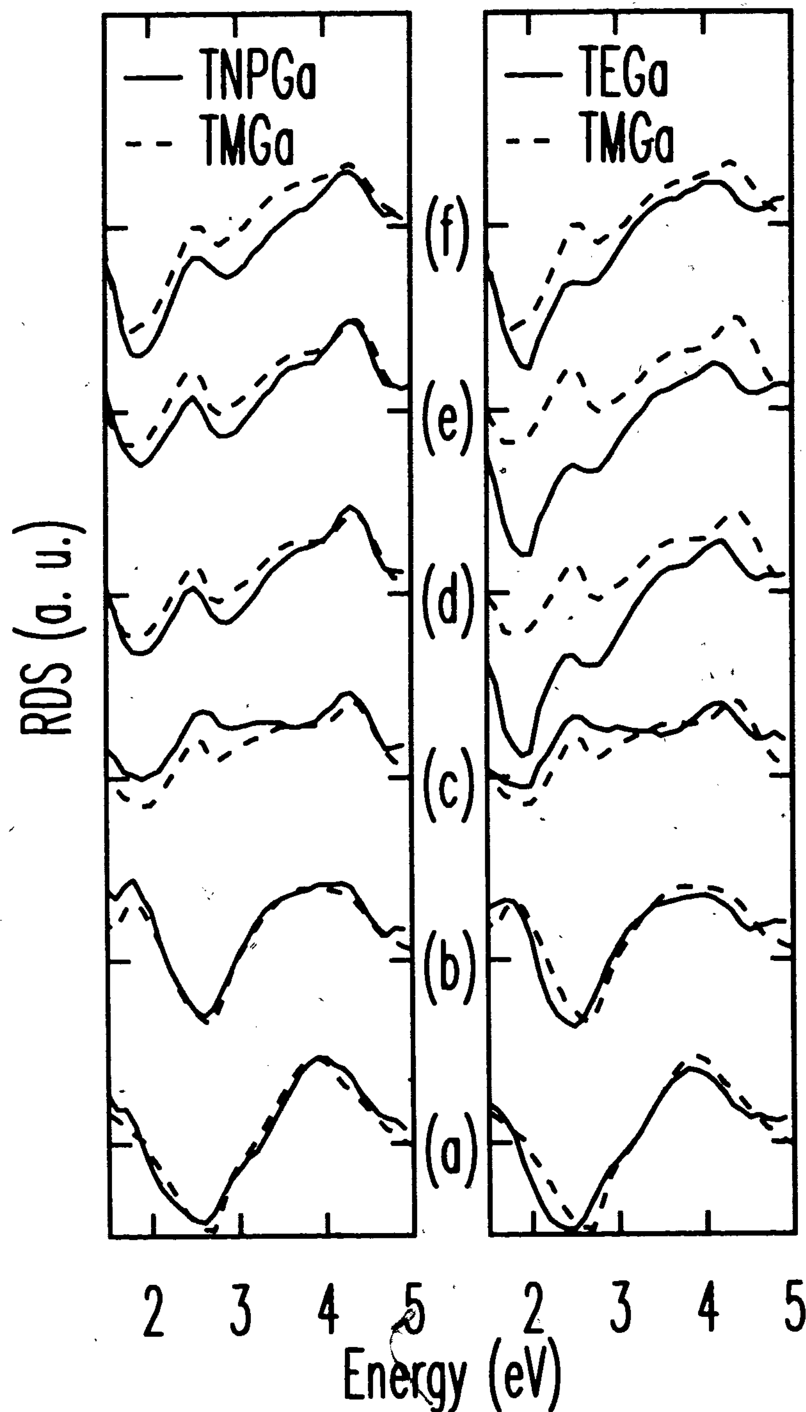

Fig. 5.7 RDS energy spectra of the surface during the ALE cycles illustrated in Fig. 5.6. The letters identify the specific instants.

5.2.2 InAs

In situ monitoring of the surface for InAs gives the same kind of information as that obtained for GaAs. We used TMIn as the In source to grow InAs by ALE and obtained self–limiting behavior between 350°C and 430°C with an optimal temperature of 390°C [50]. We have already pointed out that the only reported RDS energy spectra for InAs are the (2×4) As–terminated reconstruction and the (4×2) In-rich reconstruction. [43, 44] The ASR surface we observe under TBAs is given in Fig. 5.2 as well. The In-terminated surface which has a (4×2) symmetry is very similar to the Ga–rich surface of GaAs with the main feature at low energy (≈1.6 eV).

With these three surfaces as a background for data analysis we have performed *in–situ* monitoring of the surface during ALE and the results are summarized in Fig. 5.8. The top panel shows the RDS signal measured at meaningful energies namely 1.8 eV (dotted line) and 2.4 eV (solid line) as we expected them to be related to transitions in the In and As dimers respectively by analogy to the GaAs case. In a fashion reminiscent of Fig. 5.7 the same interesting instants of the ALE cycle are labeled and their energy spectra are presented in the lower panel of the figure.

The surface under a flow of TBAs (a) has the ASR configuration and it is stable until the TBAs supply is terminated. At this point the surface starts to go through the different transitions that were studied in detail earlier in this work (see section 5.1.2) and the surface state just prior to the exposure to TMIn is given in (b). The signal transient observed at 2.4 eV is very similar to the GaAs case where a peak is reached, followed by a decrease to eventually lead to saturation. The surface at the peak of the signal (c) has an RDS signature that is almost identical to the (2×4) surface from Fig. 5.2. This also is in perfect correlation with GaAs where the surface has a (2×4)–like character after a few seconds of TMGa exposure.

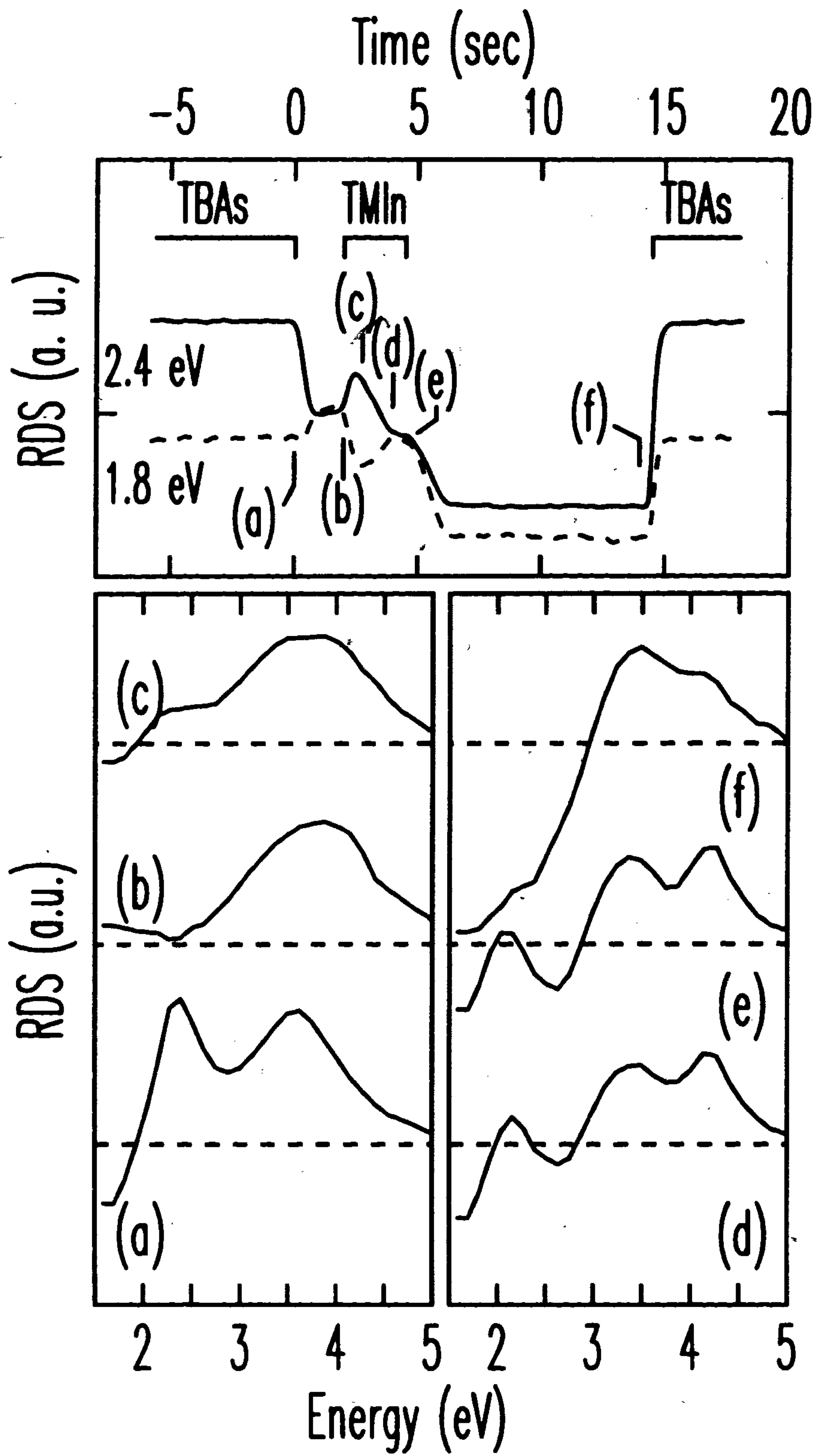

Fig. 5.8 *In situ* RDS monitoring of the InAs surface during ALE.

The spectra at saturation and at the end of the TMIn pulse ((d), and (e)) have new features at 2.2 and 4.25 eV respectively. The origin of these peaks is unknown at this point but the general trend is the same as with GaAs where the spectrum takes a hybrid–like shape after saturation until the end of the group III exposure. The state of the surface after the hydrogen purge is of an In–terminated (4×2)–like nature also in line with GaAs. This result demonstrates that InAs ALE with TMIn as the group III precursor proceeds according to the same processes as GaAs ALE with TMGa. This strongly suggests that methyl radicals also play a role in the self-limiting mechanism for this system. We have shown earlier that the ASR surface contains more As than the (2×4) reconstruction just like the GaAs c(4×4) surface has considerably more As than the (2×4) surface. The only differences between the two systems are the energies involved. TMIn decomposes at lower temperature than TMGa because of the weaker CH_3–In bond. The features appearing in the RDS spectrum when the surface is saturated with In at 2.2 and 4.25 eV are similar and at lower energy than those observed for GaAs at 2.6 and 4.5 eV in agreement with the difference in bond energy.

5.3 Preservation of the stoichiometry

At this point we have demonstrated that the surface of the crystal is terminated by more than 1 ML of As when the first group III precursor molecule arrive at the growth front. We also showed from our time resolved RDS that the surface seems to remain As terminated for a good part of the group III exposure (see Fig. 5.7b-c for example). This can be explained in three different ways. In one interpretation the first group III atoms to arrive at the surface are kept from incorporating in the crystal by the presence of As in the second plane where they should sit. There would then be a time delay between the onset of the group III exposure and the actual incorporation of atoms in the layer, while the second layer As leave the surface. Alternatively the group III atoms might intitially insert themselves between the two planes of As and remain hidden from the RDS measurements. Such a situation would probably generate more than 1 ML of growth per cycle since once the group III have filled the first plane by being inserted between the As atoms there would still be plenty of As available on the

surface to grow a second plane of group III atoms. Finally the third explanation is that the group III precursor dislodges the second layer As as it is incorporated but oonfigures itself in such a way that no dimers are formed, making the incorporated group III atoms invisible to the RDS measurements. The following sections investigate such a problem and propose a model for the incorporation of group III atoms during ALE.

5.3.1 GaAs

During the group III exposure the state of the surface continuously changes. From the time resolved RDS it is difficult to determine exactly the amount of Ga in the layer because the spectra are often of a hybrid form which does not correspond to any known reconstruction. In order to avoid that problem we have designed an experiment where we obtain a stabilized RDS energy spectrum for different exposure times. The experiment consisted of the following sequence of operations for the whole range of TMGa exposure times.

1) Stabilize the surface under TBAs.
2) Purge the surface for 2 s.
3) Supply TMGa for a given time.
4) Purge the surface until the RDS is stable.
5) Measure the energy spectrum of the surface.

The energy spectra we obtained in this fashion can be sorted into three different categories which are illustrated in Fig. 5.9. The first category corresponds to TMGa pulses that stop before the RDS signal reaches the maximum of its transient (between b and c in Fig. 5.7). We observe in this case that the purged surface is close to the (2×4) As-rich reconstruction. The second set of spectra correspond to TMGa pulses that are shorter than the saturation time but longer than the first category (between c and d in Fig. 5.7). In this set the spectra do not correspond to any known reconstruction but are close to a simple linear combination of the As-terminated (2×4) and Ga-terminated (4×6) reconstructions. An example of such a combination is given as a dotted line in

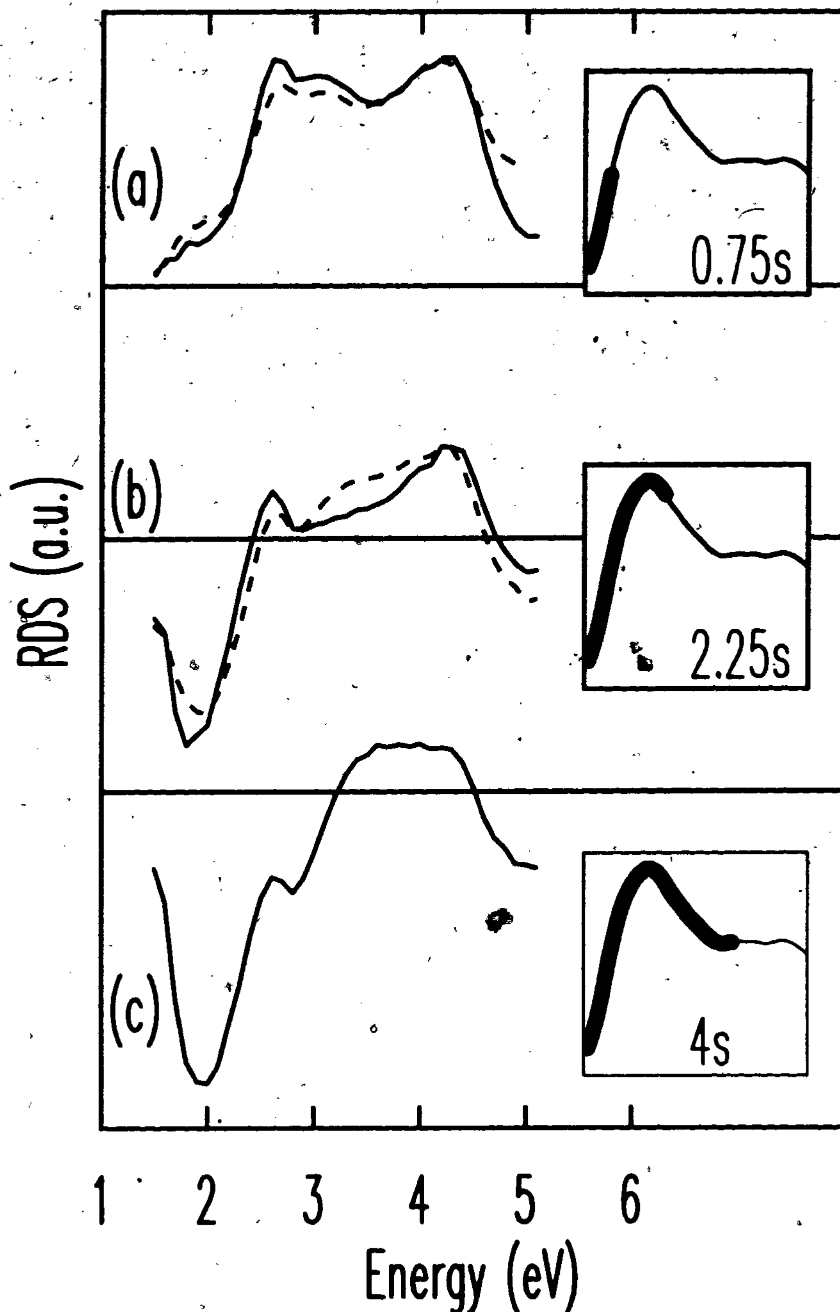

Fig. 5.9 RDS spectra of the surface of GaAs after a long purge with different TMGa pulse durations (given in the insets with the RDS transient).

Fig 5.9b. The agreement is not perfect but still quite satisfactory. Lastly all the spectra corresponding to TMGa pulses longer than the saturation time resemble the (4×6) given in Fig. 5.9c. The function we have used to fit the data is as follows:

$$S_{total} = \alpha S_{(4\times 6)} + (1-\alpha) S_{(2\times 4)}, \qquad 0 \le \alpha \le 1. \tag{5-3}$$

A detailed report of the results of the fits is given in Fig. 5.10. The RDS data are represented by solid lines and the fitted spectrum is shown by a dotted line. The TMGa pulse duration is labeled on the right of the graph. The agreement is satisfactory

even for the spectra with TMGa pulses between 1.75 and 2.75 s where the shape of the spectrum changes rapidly and takes highly mixed configurations.

It is interesting to compare the results of the fits with both the RDS signal and the measured growth rates. Fig. 5.11 overlays the fraction α of (4×6) reconstruction (dots), the RDS signal (dashed line) and a smooth interpolation of the XRD results (solid line) for comparison. As we already have pointed out the RDS spectrum does not seem to be modified during the first phase of TMGa exposure that includes the first 1.5 seconds. The XRD results tell us that more than 0.5 ML of Ga is included in the layer during that period. This result indicates that the first hypothesis that we considered must be discarded. The Ga atoms enter the layer from the first instant and no delay is oberved in the incorporation. Also since the XRD data demonstrate that no more than 1 ML of Ga is incorporated in the layer, the second hypothesis must be wrong as well. The Ga atoms are not inserted between the two As planes. They are entering the layer by dislodging As atoms from the top layer. We must now consider where they go to explain the fact that they are invisible to RDS.

The key to the explanation comes from the fact that RDS is only sensitive to dimers on the surface and not directly to relative concentration of atoms. The Ga atoms are incorporating in the crystal but they do not form dimers. If the Ga atoms were forming regions with a surface coverage close to the Ga rich surface, the dimers they would form would affect the RDS spectrum by generating a negative signal in the 1.8 eV region. The extra As occupying the Ga sites are most probably responsible for perturbing the dimer formation. The nature of the Ga incorporation sites can influence the formation of dimers. If the Ga atoms are incorporated at the step edges for example, the As from the adjacent terrace can then move laterally to cover them, inhibiting the formation of dimers and preserving the effective As termination. More details on such an approach will be given when we discuss a model for the entire process.

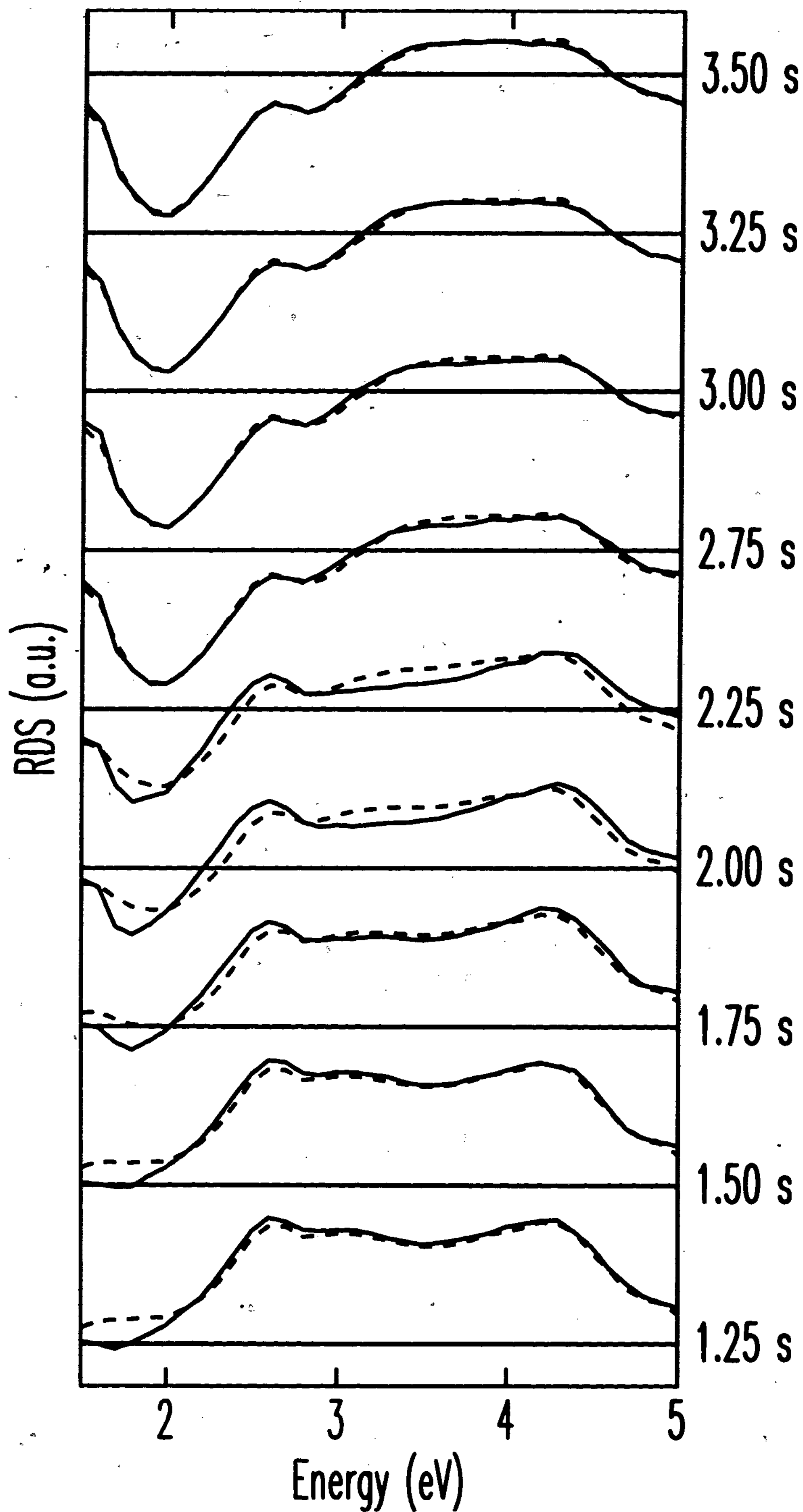

Fig. 5.10 RDS spectra of the purged GaAs surface as a function of TMGa exposure length at 470°C. The dotted lines are fits according to the ratio discussed in the text. The values of the ratio are plotted in Fig. 5.11.

In the second phase, with a Ga coverage of 0.5 to 1 ML, the purged spectrum gradually changes from a pure (2×4)–like shape to the saturated (4×6)–like reconstruction. The change proceeds linearly in time suggesting that each new Ga added to the surface forms a dimer with the neighboring atoms when the surface is purged. It should be noted here that the dimers are not necessarily formed immediately because the RDS spectrum does not have the exact (4×6) shape before the surface is purged (see Fig. 5.7c and d).

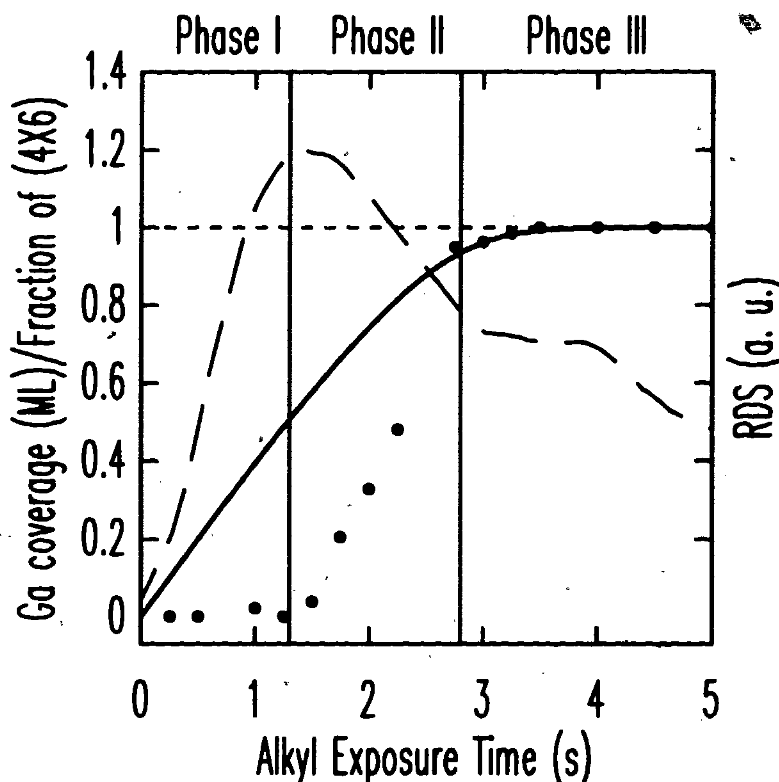

Fig. 5.11 Overlay of the Ga incorporated in the layer as measured by XRD (solid line) with the fitted ratio (dots). The RDS transient at 2.6 eV (dashed line) is included for comparison.

The RDS spectrum of the surface during the second phase of the incorporation has a generally negative response in the low energy end even though there is still a peak at the As dimer position (Fig. 5.7c and d). It is probably due to the fact that the surface is composed of dimerized regions of both kinds. With the addition of methyl radicals that further perturb the reconstruction of the surface the resulting RDS spectrum is different from any "pure" reconstruction as compiled by RHEED studies.

Once the surface has been covered with 1 ML of Ga, the spectrum of the purged surface stops changing and remains of the (4×6) nature. The RDS spectrum taken during the ALE cycle does not have the typical (4×6) shape however. We have already argued that it must be modified by the presence of adsorbates on the surface. Previous RDS studies have shown that when the stable (4×6) surface is exposed to TMGa at 450°C the signal decreases rapidly and returns to the original level when the TMGa flow is stopped.[51] This was attributed to adsorption and partial dissociation of TMGa molecules on the surface, liberating methyl radicals which in turn attach themselves to adjacent Ga atoms, breaking the dimer formation. The situation is identical in our case and a similar argument can be used to explain the modified spectrum during the saturated part of the incorporation. When the surface becomes saturated with Ga the TMGa molecule still dissociate at the surface but the Ga atoms do not attach to the surface. The methyl radicals produced by this dissociation completely coat the surface. This coating layer of methyl radicals probably plays a role in preventing more Ga from entering the crystal. We will investigate this hypothesis in section 5.5.

We know now that in the first phase the Ga that enters the layer does not form dimers. We know also that even if the initial As coverage of the surface is more than 1.75 ML the net amount of material grown during one complete cycle is exactly 1 ML. Where or more importantly when did the extra As go? It is reasonable to assume that the early Ga to enter the layer will disrupt the second layer As since it sits on natural Ga sites. The opposite is also true: the presence of second layer As intermixed with the Ga will likely hinder the formation of dimers. At this point our results suggest that the second layer of As does not participate in the stoichiometry of ALE. The As atoms are displaced by the incoming Ga and desorb without generating any growth. Another question arises then: Is the presence of Ga on the surface influencing the desorption of the second layer As?

To verify the effect of Ga on the surface on the second layer As we have compared the RDS transient at 2.6 eV for different TMGa pulses in the first moments following the exposure. Fig. 5.12 is an example of such a comparison. The dashed-

dotted line represents the RDS signal when TBAs is terminated and the surface is allowed to purge. We know already that the surface remains in the c(4×4) for several minutes from the desorption experiments.

When a very small amount (0.25 ML) of TMGa is supplied to the surface, the RDS signal quickly increases and stabilizes as shown by the solid line. The thick part of the signal shows the evolution of the RDS during the TMGa exposure. Immediately after the termination of the TMGa flow the signal rises to the level characteristic of the (2×4) reconstruction. The layer is then is terminated with a single layer of As. Also shown as a dotted line is the RDS transient for a TMGa supply larger than 1 ML. It is clear that the addition of even a small amount of Ga to the surface greatly decreases the time it needed to desorb the remaining second layer As. This means that the Ga atoms on that layer are either replacing As atoms, helping neighboring As atoms to desorb or both. This can easily be expected since the top layer As bonds to the surface are much weaker than the Ga bonds and probably are further weakened by the presence of a Ga atom nearby.

Furthermore the methyl radicals liberated by the reaction of TMGa or its byproducts with the surface will attach to neighboring As and likely help them desorb due to the stronger MeAs bond compared to MeGa as evidenced by the difference in dissociation energy between TMGa (59 kcal/mol) [52] and TMAs (68 kcal/mol) [53]. Recent work on the (2×4) surface in UHV has shown that upon adsorption of TMGa at least one methyl group is transferred to a nearby As [54]. This argument forms one of the cornerstones of our model to explain the stoichiometry problem in ALE.

5.3.2 InAs

The desorption experiment we have performed on InAs suggested that the As–terminated surfaces effective in ALE are very similar to the GaAs case. The so–called ASR surface has a higher coverage of As than the (2×4) surface and probably more than 1 ML. We now attempt to verify if the similarity extends to another part of the ALE cycle namely the group III exposure. The results from the same purge experiment are given in Fig. 5.13 for part of the range of TMIn exposure time. Here again the

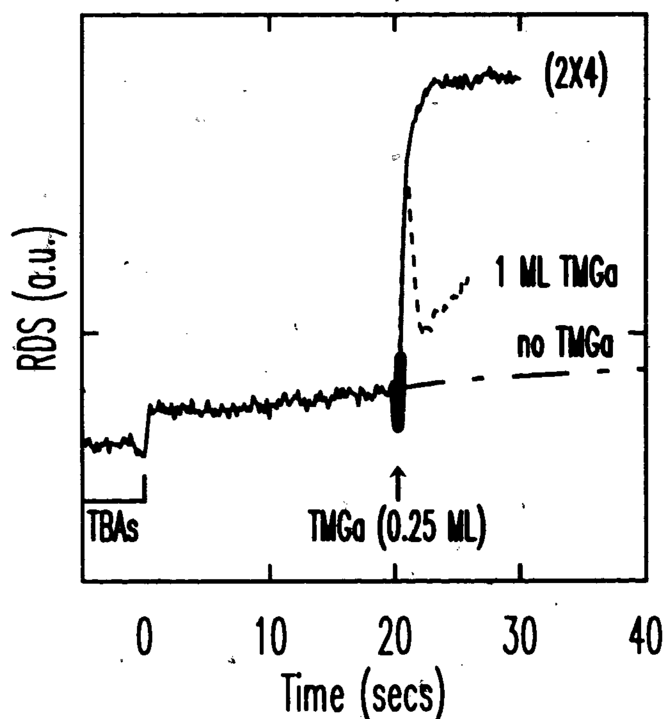

Fig. 5.12 RDS transient for the desorption of As from the GaAs surface with no TMGa (dot-dashed line), 0.25 ML TMGa (solid line) and > 1 ML (dotted line).

quality of the fits is satisfactory with only a slight disagreement in the 0.75 to 1.5 s range where the spectrum changes rapidly. The value of the fraction of (4×2) contributions (triangles) is plotted in Fig. 5.14 to compare with both XRD (thick line) and RDS (thin line) results. The same general features can be observed in the evolution of the purged spectrum with In coverage. The first half of the full exposure time does not produce any noticeable change in the shape of the purged surface which is essentially a (2×4) reconstruction.

At a surface In coverage of about 0.45 ML the spectrum abruptly starts changing towards the (4×2) reconstruction up to a coverage of about 0.9 ML when the RDS shows a pure In terminated surface. Any longer TMIn exposure generates a (4×2) reconstruction after the hydrogen purge. The same sequence of three phases is therefore observed for both GaAs and InAs confirming the extended similarity between the ALE of these compounds.

In this case however the XRD measurements do not indicate a saturation at 1 ML exactly. The surface In coverage seems to stabilize at 1.1 ML. This might indicate that the TMIn molecules are less effective in removing the top layer As while they incorporate. Another reason could be related to the different As configuration of the InAs ASR reconstruction. The bond structure of the top layer As in this case might prevent the desorption of some of them. The incorporating In can then insert itself between the two As planes and more than 1 ML is accumulated on the surface.

Using all the information we have collected for the two materials we can suggest a possible model for the incorporation of the group III atom in GaAs and InAs. Special attention will be devoted to the stoichiometry issue. The model is detailed in the next section.

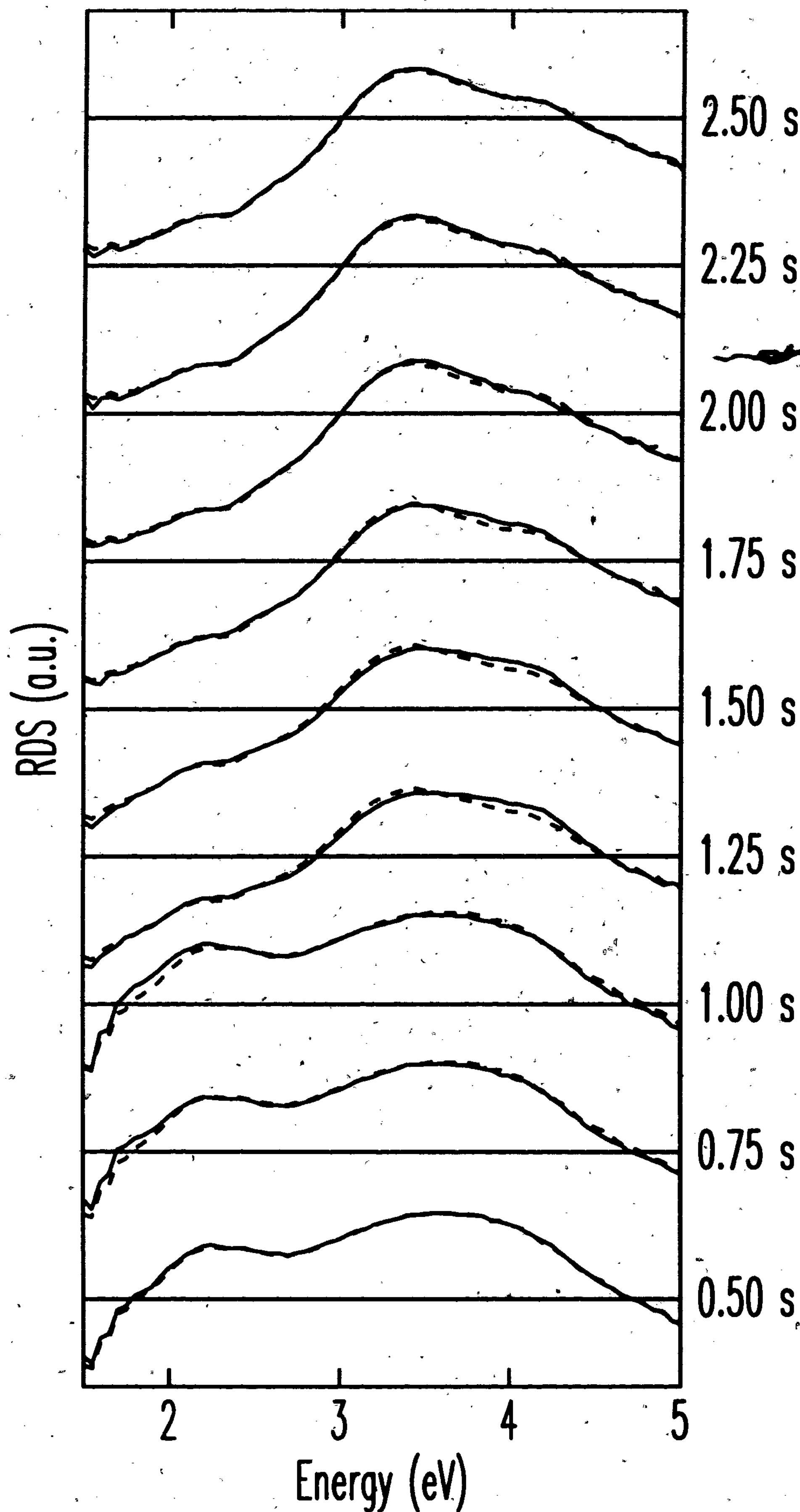

Fig. 5.13 RDS spectra of the purged InAs surface as a function of TMIn exposure length at 390°C. The dotted lines are fits according to the ratio discussed in the text. The values of the ratios are plotted in Fig. 5.14.

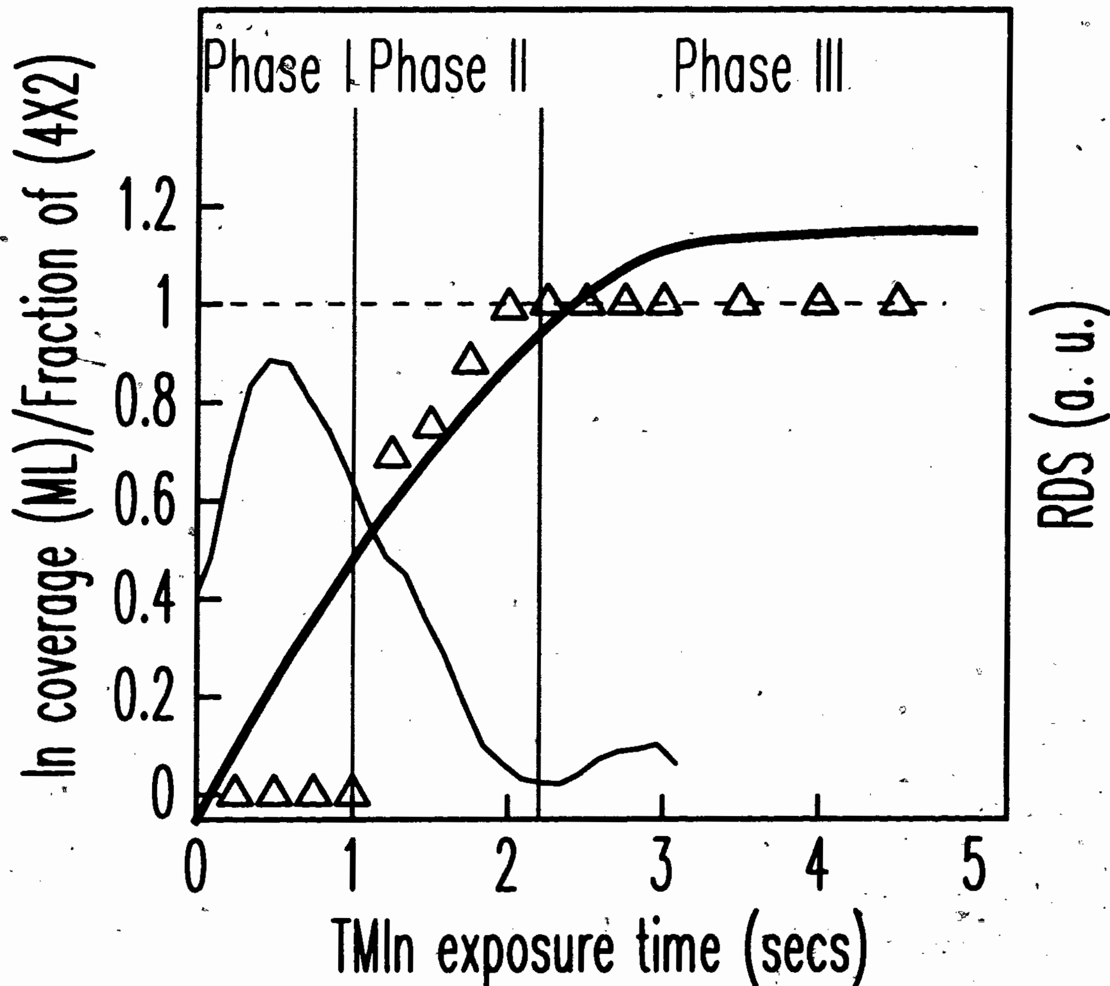

Fig. 5.14 Overlay of the In incorporated in the layer as measured by XRD (thick line) with the fitted ratio (triangles). The RDS transient (thin line) is included for comparison

5.4 Model for the chemisorption of the group III atoms

We can now assemble the evidence gathered in the last sections and combine it with previously reported results and try to build a credible model for the incorporation of the group III atom in ALE of GaAs or InAs. Here is a summary of the facts that our model will need to include to explain the ALE under our growth conditions. The reader should note that the model is fashioned mainly after the GaAs results so will use Ga and As as components but because of the many common characteristics in our results with InAs a very similar sequence of events is expected for this material as well:

- The initial surface has a c(4×4) reconstruction with a surface coverage of 1.50 to 1.75 ML of As. (ASR for InAs)
- The c(4×4) reconstruction has a relatively long lifetime under hydrogen at 470°C (>30s).
- This lifetime is reduced to only a few seconds when a very small amount of Ga (0.25 ML) is supplied to the surface.
- The Ga enters the layer from the very first instant of exposure and accumulates linearly for most of the process and eventually saturates at 1 ML coverage.
- The first 0.45–0.5 ML of Ga does not form dimers when the surface is purged.
- Exposure times that extend further than the time needed for surface saturation do not generate growth but the surface does not reconstruct in the usual Ga rich way until it has been purged.

Some important configurations of our model are illustrated in Fig. 5.15. On the left of the figure we show schematically the state of the surface immediately after the TMGa pulse ends, if there is one. The right side gives the configuration of the surface once it has been purged long enough to stabilize the RDS signal and should therefore provide information of the location of the incorporated Ga. Beside each configuration the respective surface coverages are given. In some cases the total of the two coverages does not add up to 1 ML. This is because we have included in the values of surface coverage all the atoms that are in the last two atomic planes of the surface so in principle the total should remain under 2 ML. These two planes are the ones that are constantly reconfigured as the surface stoichiometry is modified and it is more convenient to use a modified coverage in this case. An example of this is the c(4×4) surface. The top layer As is located in a crystal plane where Ga atoms normally sit. Under the conventional notation, where the sum of the coverage of Ga and As should be equal to 1 ML, it is difficult to characterize this surface because the total As coverage alone is more than 1 ML. On the other hand, if we compute the last two

atomic planes of the surface and expect a total coverage for both species that is less than 2 ML, we get 1.75 ML for As and 0 ML for Ga. When we purge the surface and reach the (2×4) reconstruction which has 0.75 ML of As and still no Ga. Then it is easy to see that the surface has simply lost 1 ML of As in the process.

The top two surfaces represent the situation where no TMGa is supplied to the surface at all before and after the long purge. The c(4×4) is purged until it stabilizes to a (2×4) state. We assume here that the reconstruction it reaches is the β(2×4) even though it could be another state of the (2×4) family. We have no way to verify this from our results but experiments using long purge times following AsH_3 exposure have

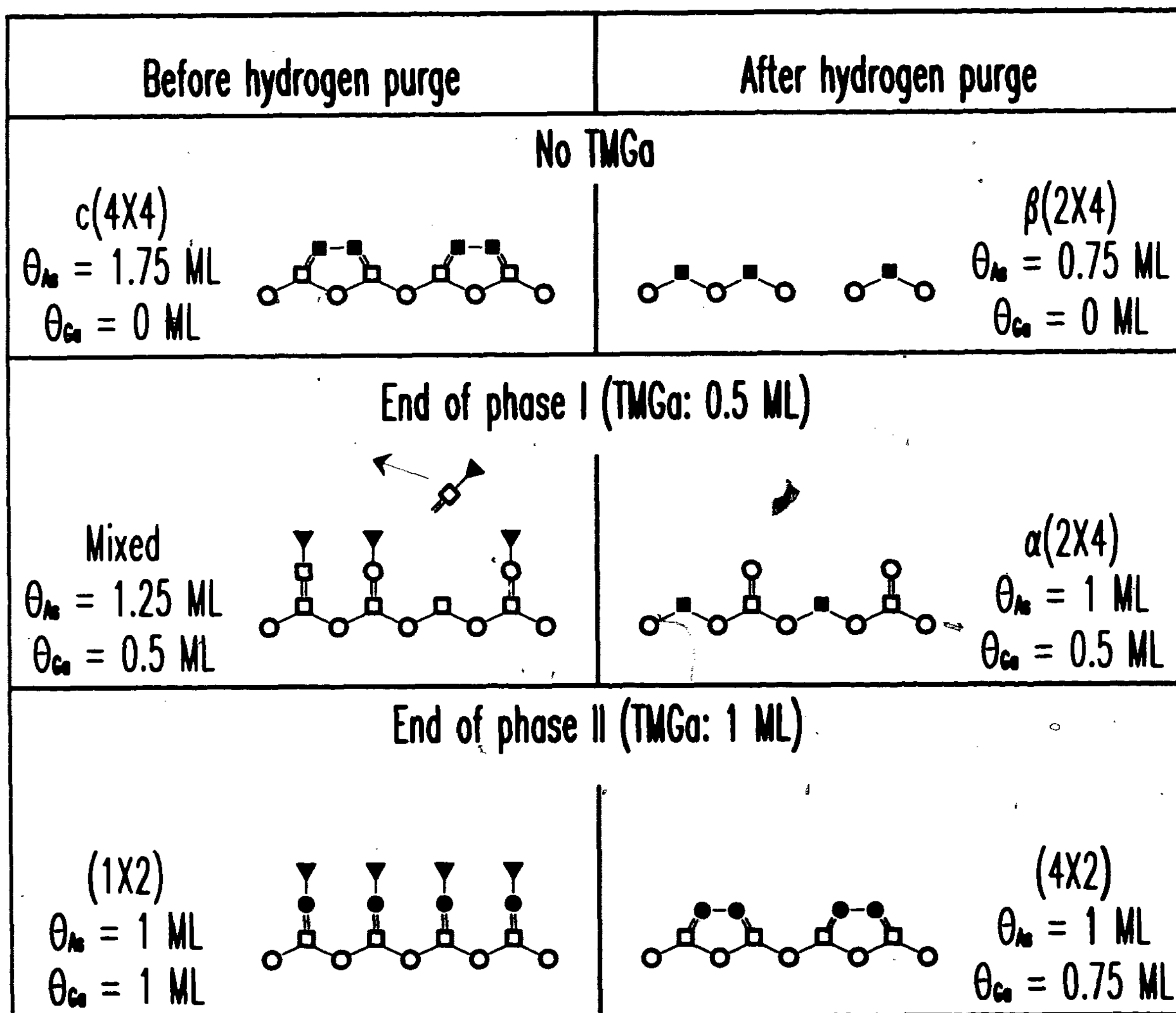

Fig. 5.15 Schematic illustration of our model for the incorporation of Ga during ALE of GaAs.

shown that the growth rate decreases and stabilizes at around 0.75 ML suggesting that the surface reconstruction must have the same As coverage [55]. Any second layer As and part of the first are desorbed during the long purge segment and do not participate in the growth. This is important since the initial As coverage is 1.75 ML with 0.75 ML of these on the second layer. As long as the TMGa exposure attaches one Ga to every As on the first layer, the 1 ML/cycle condition will be respected.

During the first half of the Ga accumulation on the surface (phase I) the TMGa molecules, decomposed to different degrees, attach themselves to the crystal, dislodging an As atom each time, and releasing one or more methyl radicals. These methyl radicals can then react with neighboring As dimers, breaking them and forming a methyl–As bond on the surface. Since this bond is relatively strong, it is much easier to desorb the MeAs group than the second layer As from a dimer. This explains the observed decrease in purge time needed to reach the (2×4) state when a small quantity of Ga is added to the surface. When such the surface is purged at this point the second layer desorbs as before, leaving the incorporated Ga on the surface. The presence of these Ga atoms will likely keep any first layer As from leaving the surface keeping the As coverage at 1 ML.

We know that the first 0.5 ML of Ga do not dimerize. The most likely reason for such a behavior has been explained by Creighton. [56] According to his picture the atoms on the surface of a semiconductor can move within their respective planes on the surface and rearrange themselves. Using such an argument, Creighton shows that a surface can be transformed from an As-terminated to a Ga-terminated structure without adding or removing any atoms. Using the argument of this model we propose an explanation for the inhibition of the Ga dimer formation during the first 0.5 ML of coverage. The process is illustrated in Fig. 5.16.

Fig. 5.16a shows a stable As-terminated surface with steps on it. We have represented here only the first layer of As, which has a 1 ML coverage, because only those atoms actually participate in the growth. As we have already discussed, the second layer As desorbs during Ga incorporation. The presence of second layer As

(a) Bare

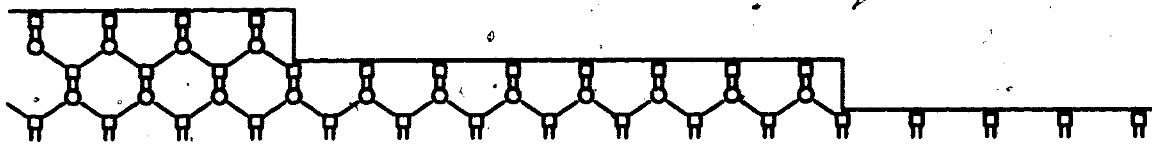

(b) Ga deposition

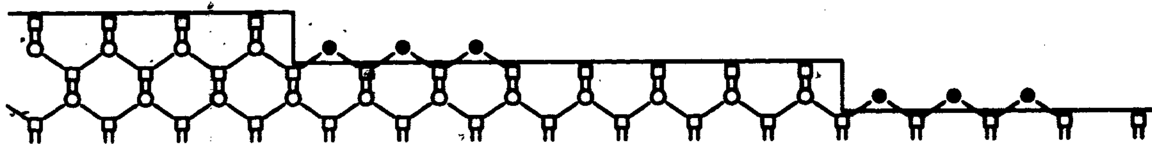

(c) As redistribution

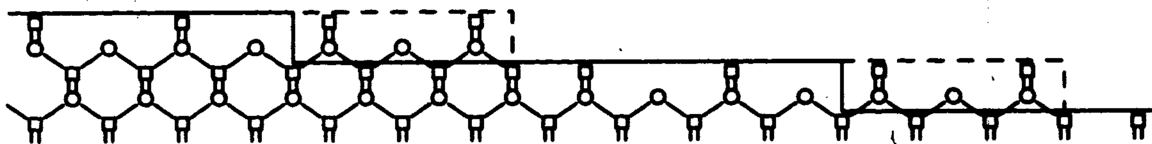

Legend: As/squares
Ga/circles

Fig. 5.16 Mechanism inhibiting the formation of Ga dimers through the redistribution of As atoms from the step edges.

however keeps the first layer coverage at 1 ML. If there was no As on the second layer, the surface would relax to a (2×4) reconstruction which has only 0.75 ML of As.

We assume that the first Ga atoms are incorporated at the step edges (b). We performed AFM measurements on GaAs layers grown by ALE under similar conditions

and they exhibit atomic terraces which is an indication that the growth proceeds by nucleation at steps on the surface. Once the Ga atoms are attached to the edge of a terrace they effectively extend its surface. The As atoms covering the terrace can then redistribute themselves so the coverage is more uniform. Some atoms then move to cover the incorporated Ga and prevent the formation of dimers (c).

This process can be sustained until the available As is insufficient to cover enough Ga atoms and dimers start to appear. There has been (2×4) surface reconstructions observed that had surface Ga concentrations of up to 0.5 ML as in the case of the $\alpha(2\times4)$. No stable As rich surface has been observed with less than 0.5 ML of As on the surface.

When a full ML of Ga has entered the layer no second layer As remains and the coverage of both species is effectively 1 ML which is the situation we were looking for to explain the 1 ML/cycle growth mode. Some supplemental information is needed though to explain how it is possible to accumulate more than 0.75 ML of Ga on a surface in spite of the fact that no adsorbate free reconstruction has that surface coverage. Creighton *et al.* [57] have studied the problem and demonstrated that the presence of methyls on the surface changes the reconstruction to a (1×2) and contained about 1 ML of Ga. When that surface is purged all the methyl radicals leave the surface and most probably part of the Ga as well. The process is illustrated in the lower part of Fig. 5.15. The stable surface reconstruction is the Ga–terminated $\beta(4\times2)$ or another Ga rich configuration such as the (4×6). This is in agreement with our observations for GaAs and sufficiently close in the case of InAs to attribute the same process to ALE in this case as well.

5.5 Morphology study of the self–limiting process

This section deals with the last part of the Ga incorporation, namely the evolution of the exposed surface after is has acquired a full ML of Ga. In section 5.4 we have argued that methyl groups attached to the surface change the surface reconstruction

and disturb the system enough to allow one complete ML of Ga to chemisorb. The attribution of such a key role for the methyl radicals constitutes a definite position in a much debated topic, that is, the mechanism underlying the self–limiting growth of GaAs, and for the first time InAs. In chapter 2 we have given a brief review of the different schools of thought on the matter. One of these schools, the selective adsorption (SA) model, discards the role of methyls totally and relies entirely on the selective affinity of the group III molecules. The other two models attribute a significant role for the methyls but differ in their interpretation of the mechanism governing the adsorption of the group III precursor. The adsorbate inhibition (AI) approach states that methyls attached to the surface physically block the way for other group III molecules to react with the surface. It states that molecules arriving at the interface are just repulsed by the methyl radicals and do not react at all. The flux balance (FB) model on the other hand says that TMGa molecules still react with a methyl covered surface but the products contain one Ga atom so there is no net gain of Ga during the reaction. In the last two models, a significant number of free methyl radicals are produced by the decomposition of TMGa on the surface and they play a central role in the self-limiting behavior.

The only morphology study of ALE that we are aware of was done under self–limiting conditions [58]. It is widely believed that when the incorporation of Ga is not self–limiting the extra Ga gathers to form liquid Ga droplets on the surface. In our case, these droplets should then react with TBAs to form GaAs structures and the controlled growth conditions preserving the smoothness of the surface are jeopardized. The extreme sensitivity of AFM to surface irregularities and its non destructiveness make it a method of choice to study a problem such as the formation of droplets during ALE. We have used this technique for the first time to probe the surface *ex situ* after a single ALE cycle had been performed. The first part of the study was to ascertain the capability of AFM to show the difference between a self–limiting growth and one that is not. For such an experiment we have used 2° off miscut substrates that were exposed to a group III dose equal to 2 ML of Ga. The surface was then purged and cooled down to room temperature under a flow of TBAs.

5.5.1 Droplet formation

Fig. 5.17 is a composite of the results for the three sources studied in section 5.2. All pictures have been normalized to the same gray scale given on the left. A picture of the substrate simply annealed in TBAs with no growth is given in Fig. 5.17a. The main crystalline axes are oriented at 45° on all the pictures.

We observe some measure of step bunching from the growth of the buffer layer. The average terrace width for a 2° miscut surface is 75Å which is smaller than the lateral resolution of the AFM of about 100Å meaning that individual terraces should be virtually invisible to the microscope. We observe nonetheless horizontally oriented step edges uniformly distributed over the surface. Since the miscut is towards the (111) direction, the initial terraces are at 45° from the picture's edges. The same type of step bunching was observed on all the miscut samples and was assumed to play no significant role in the morphology of ALE. This could be confirmed by comparing the results from miscut substrates with the ones obtained from exactly cut samples. All morphologies coming from identical conditions were within experimental error from each other.

Fig. 5.17 AFM pictures of the GaAs surface after 1 ALE cycle with a group III exposure equivalent to 2 ML. Picture (a) shows the buffer layer only. The group III precursors are TEGa (b), TMGa (c), and TNPGa (c).

The pictures shown in Fig. 5.17b, c, and d show the surface after an ALE cycle where the surface was exposed to 2 ML of TEGa, TMGa, and TNPGa respectively. It is obvious that for self–limiting precursors the surface remains smooth with only some irregularities that could be due to the rather long exposure (double the saturation time). In the case of TEGa several clusters resulting from the solidification of Ga droplets are observed, randomly distributed on the surface. We do not detect a correlation between the droplet distribution and the step orientation. We also observed very similar morphologies with exactly cut substrates as will be discussed below.

These two results show that the formation of Ga droplets is not triggered at step edges. When the gray scale of the image is extended (not shown) the shape of the droplets is observed to be a hollow conical shape, somewhat reminiscent of a volcano with a wide chimney.The size distribution of the droplet is very narrow as well. They are on average 3500Å at the base and 250Å high. The "chimney" has an inverted conical shape and is 1000Å at the top and is 200Å deep. the average volume of a droplet is then approximately 4×10^{8} Å^{3}. There is 19 droplets showing on the picture which corresponds to a total volume of 7.6×10^{9} Å^{3} or 1.1 ML of GaAs.

When a sample is grown under these conditions and 200 cycles are executed using TEGa with 2 ML pulses (6 s), the XRD measurement shows weak fringes that correspond to a growth rate of 1 ML/cycle but AFM investigation shows tall droplets as shown in Fig. 5.17b. XRD is only sensitive to the crystalline planar regions of the sample so the fringes correspond to the thickness that was grown between the droplets and it is measured at 1 ML during every cycle. This means that a ML of material is grown between the droplets as well, bringing the total material to 2.1 ML which is close to the nominal value of 2 ML. The droplets therefore are efficient nucleation centers and all the Ga in excess of the 1 ML/cycle regime gathers at these sites. The growth seems to be self–limiting between the droplets though and a distance of the order of 1 μm show that there is some sort of adsorption selectivity in the process even for TEGa.

5.5.2 Effect of methyl radicals

In order to verify the effect of methyls on the surface we have used exactly cut substrates since they show wide terraces which facilitates the analysis of the data. We first looked at the surface morphology for a self–limiting source and TEGa as the non self–limiting precursor. Fig. 5.18 gives a comparison of the buffer layer only (a) with TMGa (b) and TEGa (c). In each case here the total group III supplied to the surface was 1 ML according to our RDS and XRD characterization. After the group III exposure, the surface was purged for 10 s before being cooled to room temperature under TBAs. The buffer layer shows very regular terraces roughly 2500Å wide giving a value for the residual miscut of 0.13° towards one of the crystalline main axis since in this case as well the samples are positioned so the main axes are 45° to the picture's edges. This is evidence that the buffer layer grows in a step–flow growth mode. Substrates cut from the same wafer were used so this picture can be used as reference for comparison. The surface exposed to TMGa shows a terraced structure as well although the width is not as regular. The fact that we recover the same structure as the buffer layer is not necessarily an indication of step–flow growth for the ALE as was deduced in reference 58 since in this case we simply covered the entire surface with an extra ML of material. After the surface has been completely covered it should mimic whatever morphology the underlying layer had regardless of the growth mode.

The TEGa exposed surface has a very different morphology. The step structure of the buffer layer is still visible but there is formation of islands and noticeable disruption of the step edges. The large islands, which spatial distribution resembles that

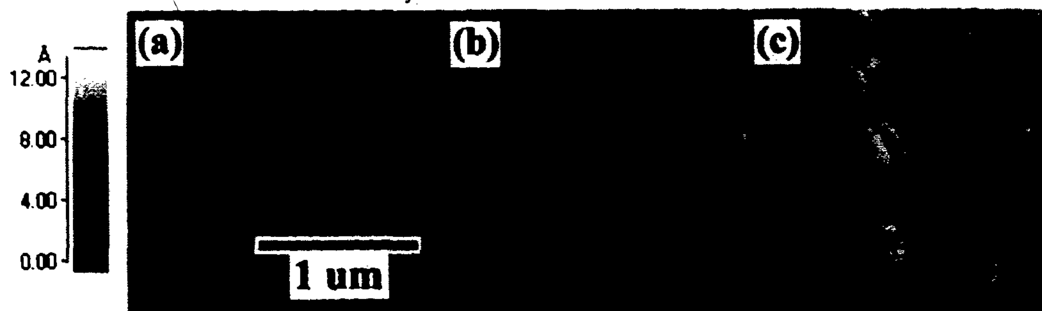

Fig. 5.18 AFM pictures of the GaAs surface for a 1ML exposure to TMGa (b) and TEGa (c). Picture (a) shows only the buffer layer.

of the droplets in Fig. 5.17b, will act as nucleating sites for further Ga incorporation. The height of the islands is still at the ML level even if the amount of deposited Ga is half of what it was for the figure 5.17b. The droplets are therefore formed mainly after the surface has already been covered with Ga. There is some measure of self–regulating of the growth even for a precursor which does not produce adsorbates providing some credit for the SA model.

The next step in the investigation is to focus on the methyl radicals themselves. We know that TMGa provides methyl radicals during the exposure and we have shown earlier RDS evidence that they can be desorbed by a hydrogen purge of several seconds. We have verified already that TEGa arriving at a surface devoid of methyl radicals will generate droplets very efficiently. We first saturate the surface by exposing it to 1 ML of TMGa and we purge the surface for various intervals. The surface is then exposed to 1 ML of TEGa before being cooled to room temperature under TBAs. Fig. 5.19 is a summary of the different morphologies as a function of purge time. The hydrogen purge times between the two pulses are 0s (a), 2s (b), and 10s (c) respectively. When no purge is allowed before the TEGa exposure the surface is covered with methyls and the morphology remains atomically smooth even though there is formation of small islands. The formation of droplets has been almost totally prevented. If the surface is purged for 2s, several droplets are observed with an average height of 40 Å. Lastly for a long purge where all the methyls have been removed, the droplet structure is similar to the normal 2 ML exposure. We can deduce from these results that the methyls are very efficient in preventing the formation of droplets during ALE. They must therefore play a critical role in the self–limiting growth in ALE. We have observed site selecfivity with TEGa to some extent but the effect of the presence of methyl group on the surface is more pronounced.

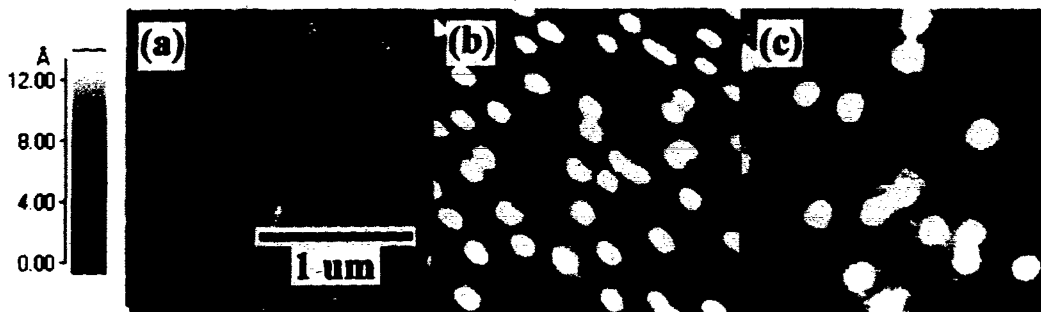

Fig. 5.19 AFM picture of the GaAs surface after the exposure to 1 ML of TMGa and 1 ML of TEGa separated by 0 s (a), 2 s (b), and 10 s (c) of hydrogen purge.

It seems that there is some degree of selectivity in the ALE process, supporting the SA model. It is a difficult task to analyze our data in the framework of the other two models. It seems that methyl groups act as a shield for the surface so that the TMGa cannot reach the chemisorption site and decompose. When a region of the surface has lost its methyls, the TMGa molecule can then act as a supply for methyl radicals by decomposing on a site in that region and according to the FB model return a Ga to the gas phase but also generate one or more free methyl radicals that can then attach themselves in the vicinity of the decomposition site and regenerate the methyl coverage. It seems that all three models participate to the self–limiting growth regime to different degrees. Our experiments show that methyl radicals are present and play a central role in preserving the stoichiometry of the surface.

5.6 Alkyl desorption

5.6.1 GaAs

If we follow the assumption that the presence of alkyl radicals of some sort on the surface after the exposure to the group III precursor is responsible for the modified RDS response, we can expect to obtain kinetic information by studying the signal during the following purge. In this regard TNPGa can be expected to leave neopentyl radicals at the surface, producing effects useful for the understanding of the growth process. For instance if site blocking by adsorbed alkyls is important then this effect should be more pronounced for TNPGa as the radicals would be larger in size.

The effect of desorbing the radicals from the surface is to allow the formation of Ga dimers so the best energy to monitor for the modeling of the desorption is 1.8 eV corresponding to the position of the structure attributed to those dimers. Since the dimer structure is seen to be stable immediately after the surface has been saturated during TEGa exposure, we assume that the rate of formation of the Ga dimers is fast compared to the rate of desorption of the alkyls. Therefore the signal response can be expected to be limited by the desorption and not by the formation of dimers even though it is the dimers that create the anisotropy.

We have proceeded to model the decaying RDS signal after the exposure to the group III precursor over the same temperature range for both TMGa and TNPGa. Fig. 5.20 show an Arrhenius plot of the fitted data. An example of one of the fits is given in the inset. We observe a deviation from the linear behavior at higher temperature. This is due to the fact that the Ga rich surface is not stable at those temperatures under a hydrogen flux. This has been previously reported and attributed to the chemisorption of residual As coming from the reactor walls or the susceptor [35]. The accumulation of As on the surface modifies the surface affecting the RDS signal and keeping it from saturating and having a true exponential shape. At lower temperature this incorporation of As is slow enough to be neglected at least for the early part of the signal.

The first striking result of such a measurement is that both sources have an identical profile. The rate constants obtained from the fits coincide completely for all temperatures. This is surprising because of the very different nature of the desorbing species that we expected to observe. The adsorbed alkyl for TNPGa exposures is therefore the same as for TMGa: methyls. How can this be possible? What reaction path would leave methyl radicals instead of neopentyls? As it turns out there is a possible β–type reaction that could be applied to the surface reaction of TNPGa and that could explain the presence of methyls at the surface It has been demonstrated that the first step of the decomposition of TNPGa proceeds by homolytic fission, by breaking the neopentyl bond to the Ga. [49] However, the subsequent steps of the decomposition can be proceeding differently. When a partially decomposed TNPGa

Fig. 5.20 Arrhenius plot of the time constant of the RDS transient during the surface purge following the group III exposure for TMGa (empty) and TNPGa (solid). The solid line is a least square fit. The inset shows a typical RDS transient with the fit given by the solid line.

molecule, let's say mono–neopentylgallium, reacts with the surface, there can be a rearrangement of the neopentyl radical which leaves behind a methyl radical and produces an isopropylene molecule in the gas phase. The reaction path is as follows:

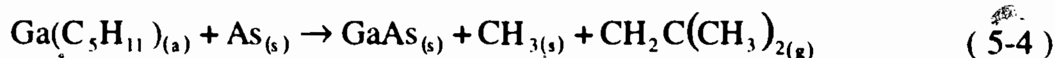

$$Ga(C_5H_{11})_{(a)} + As_{(s)} \rightarrow GaAs_{(s)} + CH_{3(s)} + CH_2C(CH_3)_{2(g)} \qquad (5\text{-}4)$$

In this equation we have left the methyl radical term separate to account for the fact that it can attach itself to either the Ga atom from the originally reacting molecule or any other atoms from the surface in the vicinity of the reaction site. Fig. 5.21 gives a

schematic representation of the reaction. The same type of β–methyl reaction has been observed with tri–isobutylgallium for the growth of GaAs by chemical beam epitaxy (CBE) [59]. The almost identical kinetic behavior of TMGa and TNPGa suggests that the latter decomposes via a β–methyl reaction path.

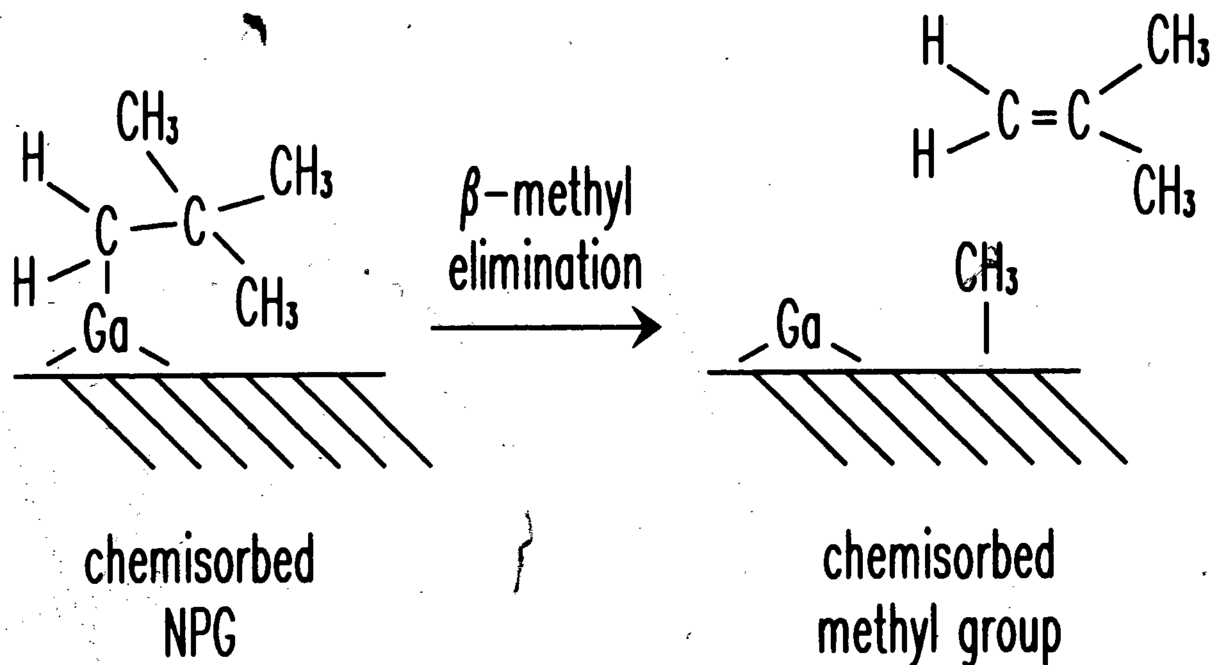

Fig. 5.21 Decomposition of the mononeopentylgallium via the β-methyl elimination process.

In order to further investigate this claim we have measured the carbon incorporation during growth with both TMGa and TNPGa and compared their level for similar growth conditions. The hole concentration was of the same order giving more support to our interpretation of the reaction path. This is a significant setback in the development of TNPGa for the growth of high purity GaAs. The idea of using heavier alkyl radicals to lower the carbon incorporation has to account for all the decomposition pathways possible for the precursor and for simple tri–alkyl type of molecules, the heavier the molecule, the more likely it is to decompose through β–methyl elimination, defeating the purpose altogether. This is true at least for the tri–alkyl family of molecules. Other configurations could be considered as candidates for low carbon ALE but no viable alternative as yet been reported.

The energy we calculate from the plot is 59 kcal/mol a value considerably higher then the ones given in most previous reported values which range from 38 to 45

kcal/mol [11, Fig. 5]. The reason for that is not clear to us. RDS single energy monitor is not simply related to the number of Ga dimers on the surface making the direct interpretation of the signal difficult. The surprising similarity between the two sources remains valid though.

5.6.2 InAs

The same type of experiment can be applied to the desorption of the radicals from the InAs surface after the TMIn exposure. By investigating the shape of the RDS transient in Fig. 5.8 we can see that the signal starts to drop when TMIn is turned off and changes linearly until it reaches a stable level. By calculating the slope of this transient for a range of temperatures we obtained the Arrhenius plot shown in Fig. 5.22. The time constant shows good linear dependence and the calculated activation energy is 51.1 kcal/mol. It is again much higher than the values measured in GaAs. Since the methyl-In bond is weaker than the Ga-methyl bond, this result is also surprising. It does show the right trend with respect to our measurement for GaAs though. Again the reason for such a discrepancy is not clear. The theoretical energy for the formation of dimers on a semiconductor surface is expected to be around 46 kcal/mol. It is possible that the assumption that the dimer formation is fast enough to be negligible may be incorrect.

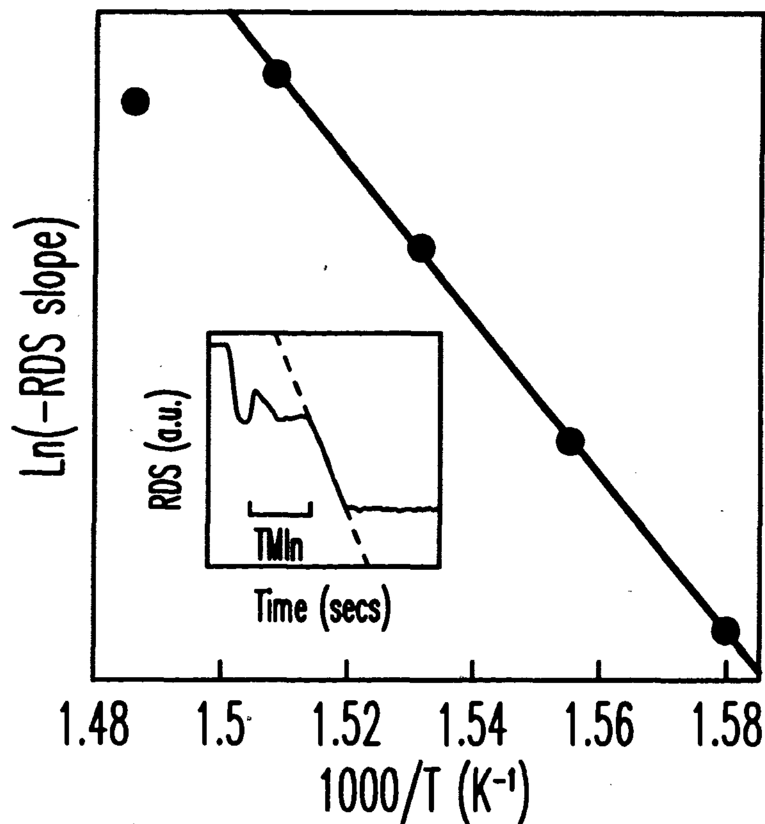

Fig. 5.22 Arrhenius plot of the slope of the RDS signal during the hydrogen purge following TMIn exposure in ALE of InAs.

5.7 Conclusions

In summary we have applied RDS and AFM in different ways to probe the surface during ALE of GaAs and InAs to obtain information on the incorporation of the group III element in the crystal. We have found that during the group III exposure the surface is initially covered with more than 1 ML of As. The second layer As does not participate in the growth by generating more Ga incorporation but does play a role in the preservation of the first layer at full coverage. The Ga atoms are incorporated continuously from the first instant until the surface is entirely covered. The methyl radicals play several roles in the growth by attaching themselves to As atoms in the second layer and helping in their desorption. They also stay with the incorporated Ga to generate a different reconstruction that allows 1 ML of Ga to be on the surface. We also have shown that the presence of methyl radicals at the surface prevents the formation of Ga droplets.

6. Kinetic study of the growth process

6.1 Introduction

Since the early days of ALE, relatively few efforts have been devoted to the different processes taking effect during group III incorporation. This is especially true for the early moments of the group III exposure but it can be explained by the fact that when one is optimizing the ALE cycle, the ultimate aim is to find conditions that will produce a complete ML of growth per cycle. Because of that the chosen conditions were almost always in a regime of full coverage. The models that were then developed to simulate the incorporation could easily be misled by the scarcity of data in the partially covered part of the growth. Most models assumed that the incorporation was proceeding with a simple, Langmuir type adsorption scheme. Under this assumption the atoms or molecules from the gas phase contact the surface on a given site and incorporate only if the site is favorable. Under this approach the rate of incorporation is directly proportional to the fraction of favorable sites on the surface.

Some experiments, including ours, have looked closely at the early moments of group III exposure and found that the rate of incorporation is not continuously changing with coverage but actually remains constant until more than three quarters of the surface is covered (see Fig. 6.4). [54, 60] In this section we propose a model to explain the different behaviors of the growth rate. After a brief review of the other models, we give a special focus on a model proposed by Aspnes *et al.* involving strictly surface related reactions without decomposition of the precursor in the gas phase to explain the growth rate profiles [60]. This model is the only one that was deliberately

designed around the premise of modeling the linear Ga incorporation during TMGa exposure for the ALE of GaAs.

6.2 Literature review

6.2.1 Other models

The first reported attempts at modeling the time dependence of the Ga incorporation during TMGa exposure [12, 61] have used standard kinetic adsorption theory. This approach states that the probability of adsorption of molecule reacting with the surface is proportional to the fraction of unoccupied sites. The rate of adsorption is therefore large initially and continuously decreases as the surface becomes covered with adsorbates. On a plot of surface coverage as a function of time, an exponential dependence is expected. The main concern of these early models was to determine the steady state coverage of the surface and to model the time required to deposit 1 ML of material. The details of the initial moments of the incorporation were neglected.

Later some observations were reported stating that the rate of deposition of Ga on GaAs when the surface is exposed to a flow of TMGa remains constant for a significant part of the coverage [54, 60]. This difference was investigated by several groups who tried to gain some insight into the underlying mechanism. Creighton and Bansenauer [62] supposed that the growth proceeded in two separate phases without attempting to explain how. They proposed two different schemes where one had a linear incorporation in the early stage and found that it produced a better agreement with their experimental growth rates measurements. Yu [63] has gone a little further by introducing a steric factor to simulate the blocking effect that an adsorbed TMGa molecule has on the sites immediately adjacent to its position. The model also includes a term representing the desorption of methyl-Ga groups from the surface which is responsible for the self limiting behavior of the growth. Neither of these models was used to directly simulate the time dependence of the Ga incorporation. This task was undertaken by Aspnes *et al.* in detail. Their model uses strictly surface based reactions to reproduce the RDS signal during TMGa exposure. The following section will

outline the main features of their model and set the stage for our own explanation for the linear incorporation behavior.

6.2.2 Precursor mediated approach

Since the experiments from reference 60 were performed at very low temperature (370°C), the authors have assumed that all the chemical reactions were taking place at the growth interface and neglected any gas phase processes. This assumption is supported by observations at low temperature of a GaAs surface covered mostly with physisorbed TMGa molecules. The basic idea behind the model is that physisorbed molecules, because of their size, effectively cover a certain number of surface sites. The molecule can then decompose and the Ga atom can incorporate at any of the surface sites located anywhere in the "covered" area. This subtle change greatly modifies the dependence of the Ga chemisorption probability on the surface coverage. Whereas under the standard models this probability is simply proportional to the fraction of available sites, it is greatly increased by permitting the Ga to effectively "sample" several sites before desorbing to the gas phase. Using θ as the Ga surface coverage the probability of incorporation of a given Ga is given under standard adsorption theory by:

$$P(\theta) \propto (1-\theta). \quad (6\text{-}5)$$

When the same Ga is allowed to react with n different sites it will chemisorb with a probability given by:

$$P(\theta, n) \propto \left(1-\theta^n\right). \quad (6\text{-}6)$$

which remains close to unity even for significant values of coverages as n increases. This characteristic influences the growth rate in such a way as to make it almost independent of surface coverage at least for small values of θ. Using such a framework Aspnes *et al.* [60] have found that the value of n that reproduced the data with the best agreement was 5. This value is reasonable for the number of sites that are covered by an non-decomposed TMGa molecules.

If we try to use this type of model to reproduce our data we encounter several problems. First our growth temperature of 470°C is beyond the range where the surface is expected to be covered mainly by TMGa molecules. It is in fact mainly covered by Me_1Ga and some Me_2Ga [64]. The site blocking process is therefore unlikely to act in the same fashion under those conditions. Also at that temperature we already see some signs of saturation in the MOCVD growth rate meaning we are in a mass transport limited regime. In their model, Aspnes *et al.* [60] have assumed that the boundary layer did not exist and that the rate of arrival of the molecules at the surface could be deduced by gas kinetics. Since ALE of GaAs is performed at temperature where some degree of mass transport is observed, this assumption cannot be used. A different approach must be proposed to explain the linear behavior in the Ga incorporation.

Our method of tackling the problem is to go to the other extreme. Let's assume that no molecules are dissociated at the surface but that all cracking of the precursors happen in the gas phase. When the temperature in the gas becomes high enough, all the molecules dissociate and the growth rate simply depends on the rate at which they can reach the surface. At lower temperature, partial decomposition of the molecules are responsible for a decrease in the growth rate. The molecules can reach the surface with the same rate but only a fraction of them are dissociated and in a state that permits them to chemisorb. This assumption is not as unreasonable as it may seem. Our observations on the growth rates of MOCVD and ALE strongly suggest that diffusion plays an important role in ALE as well. When we compare the rate of incorporation of Ga at the inital instant of TMGa incorporation, we find that it is within a factor 2 of the measured MOCVD growth rate under the same conditions. Since MOCVD is assumed to be diffusion limited, ALE must be governed by the same dynamics since the growth rates are so similar.

6.3 Gas phase based model

6.3.1 Theoretical description

When the gas is traveling through the growth chamber (Fig. 4.2), it reaches the susceptor with some vertical velocity but is then deflected towards the edges and the exhaust. Near the surface of the susceptor there is a region where the vertical component of the gas velocity is negligible. The region is called the stagnant or boundary layer. In this layer the gas can be considered to be static and the dominating transport mechanism of the dilute species is diffusion. In the framework of our model it is during this diffusion that the TMGa molecules will sometimes undergo a pyrolytic fission of a methyl-Ga bond. This is an important difference with the model of Aspnes *et al.* [60] where all dissociations happen at the surface exclusively. A schematic view of the overall process is shown in Fig. 6.1.

Consider a TMGa molecule that arrives at the top of the boundary layer where it starts to diffuse through the H_2 carrier gas. At some point along the way there is a probability that the molecule will decompose via pyrolysis and lose one or more of its methyl radicals. Once it has crossed the boundary layer and reached the surface, we suppose that it will incorporate into the crystal according to the following probability;

P=1 if the molecule has lost at least one methyl radical

P=0 otherwise.

We also suppose that the incorporation proceeds instantly so the surface is always considered "bare" and that there is no adsorbed molecules, neglecting any sort of site blocking effects. Finally our picture assumes that each molecule reaching the surface reacts with it in a Langmuir type of interaction meaning that the probability of incorporation depends on the coverage according to equation (6-5).

Since molecules are continuously swept away at the growth interface, a concentration gradient is established across the boundary layer and a net flux of molecules appears. Using simple diffusion theory the flux of molecules through a surface in the gas phase and the ideal gas law the flux is given by Fick's law [65]:

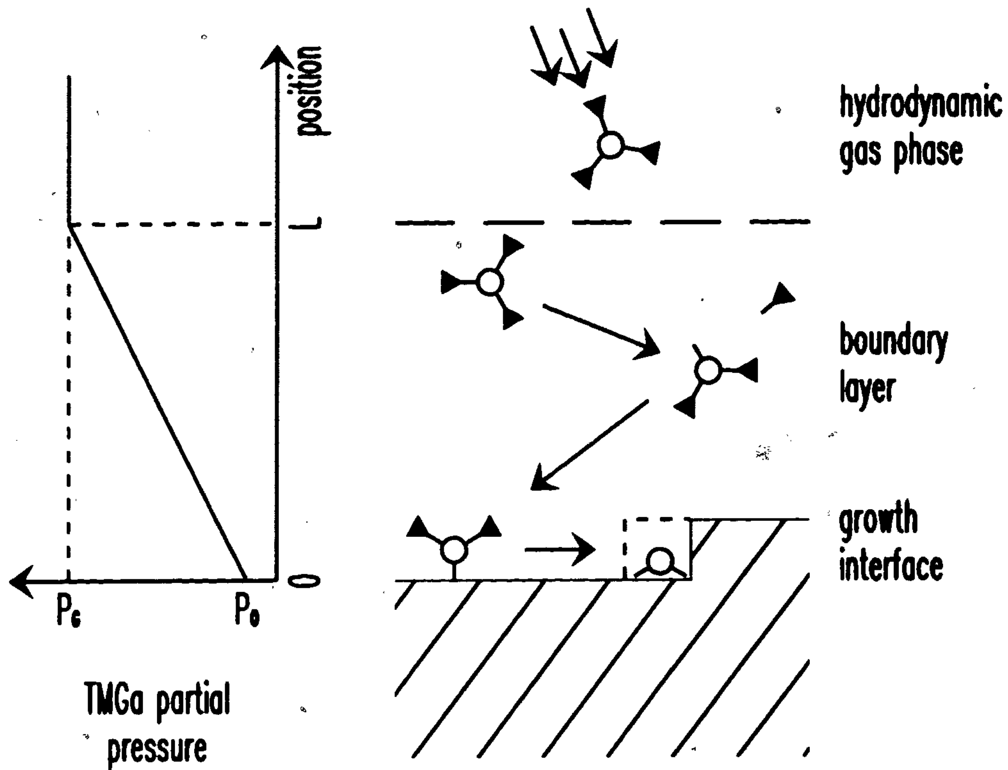

Fig. 6.1 Schematic view of the gas dynamics near the surface during the MOCVD process. On the left side a graph gives a qualitative illustration of the precursor partial pressure as a function of distance from the surface.

$$J = -\frac{D}{kT}\frac{dp}{dx}, \tag{6-7}$$

where p is the precursor partial pressure and D the diffusion constant for TMGa in H_2. In the boundary layer the molecules migrate by diffusion driven by the incorporation of Ga in the crystal, lowering the partial pressure at the surface and creating a pressure gradient. In the mass transport limit of the growth in MOCVD the effective partial pressure at the surface drops to zero and the growth rate depends only on the diffusion

coefficient which has a weak temperature dependence. This explains the relative constant growth rate at high temperature.

From the conservation of chemical species the flux across the boundary layer must be equal to the rate of incorporation. Replacing the flux term with the coverage rate we get;

$$n_s \frac{d\theta}{dt} = -\frac{D}{kT}\frac{\partial p}{\partial x}. \quad (6\text{-}8)$$

In the equation n_s represents the density of sites on the surface of the crystal. Since the flux of molecules is constant across the boundary layer we can substitute the concentration gradient with an expression involving the TMGa partial pressure at the top of the boundary layer (p_G) and immediately over the surface (p_o).

$$n_s \frac{d\theta}{dt} = -D\frac{(p_G - p_o)}{kT\delta}, \quad (6\text{-}9)$$

where we have used δ as the thickness of the boundary layer. The exact value of δ is difficult to determine because its very definition is arbitrary. In his book Stringfellow [1] defines the boundary layer as the region in the gas where the vertical velocity is less than 99 % of its maximum value. We assume in our model that it is an area next to the surface where the gas is essentially stationary and all molecular transport is done via diffusion. This argument is not rigorously justified but constitutes a useful first order approximation. The hydrodynamic equation can be solved exactly for a vertical reactor and the value of δ is given by:

$$\delta = 2.4\sqrt{\frac{\upsilon}{a}}, \quad (6\text{-}10)$$

where a is a constant and υ is the kinematic viscosity, defined as the ratio of the dynamic viscosity to the mass density of the gas:

$$\upsilon = \frac{\eta}{\rho}. \quad (6\text{-}11)$$

We also assume that the gas flow through the chamber is perfectly laminar and that no recirculation is present. The effective TMGa partial pressure over the surface is therefore given by the expression:

$$p_o = p_G - \frac{kT\delta n_s}{D}\frac{d\theta}{dt}. \quad (6\text{-}12)$$

This expression illustrates the mass transport effect on the partial pressure of the different vapors over the growth surface. As the molecules are incorporated into the crystal with a faster rate, the concentration of molecules over the surface decreases. Using the classical kinetic theory of gases to obtain the rate of collision of the molecules in the gas phase per unit area of the surface as a function of partial pressure we obtain:

$$\frac{1}{A}\frac{dN}{dt} = \frac{p}{\sqrt{2\pi MkT}}. \quad (6\text{-}13)$$

The growth rate is proportional to the number of decomposed molecules that hit the surface per unit time so we must introduce a term showing the fraction of all molecules that will be in a reactive state when they do interact with the prospective sites. This fraction can simply be expressed in the Arrhenius form with an attempt frequency ν and an energy of activation E_d. The growth rate is then given by:

$$n_s\frac{d\theta}{dt} = \frac{p_o}{\sqrt{2\pi MkT}}\nu\tau\, e^{-E_d/kT}(1-\theta). \quad (6\text{-}14)$$

We have used $\tau = \delta^2/D$ as the residence time of the molecules in the boundary layer and the term $(1-\theta)$ is the probability of the reacting surface site of being unoccupied by a Ga atom. The activation energy defined here is different than the one used by Aspnes *et al.* in the sense that it represents the dissociation of the molecule through collisions in the gas phase, not on the surface. It should be noted that we are not using any multiple site sampling in our model as was the case with the one used by the same authors. It will shown later that it is not necessary to introduce that effect in our model to obtain the long linear incorporation rate in ALE.

Using equation 6-14 for the expression of p_o and rearranging the terms we obtain a differential equation for the coverage of the surface.

$$\frac{d\theta}{dt}=\frac{p_G}{\sqrt{2\pi MkT}}\frac{\delta^2}{Dn_s}\left[\frac{1}{1+\left(\frac{\delta^3}{D^2}\sqrt{\frac{kT}{2\pi M}}\right)\nu\, e^{-E_d/kT}(1-\theta)}\right]\nu\, e^{-E_d/kT}(1-\theta) \qquad (6\text{-}15)$$

The strong temperature dependence in the denominator of the factor in square brackets is responsible for the transition from the kinetically limited to the mass transport limited growth modes as the right side term becomes comparable to or larger than unity. In the low temperature range the term is negligible compared to unity and the factor can be discarded so the growth rate is approximated by:

$$\left.\frac{d\theta}{dt}\right|_{T\to 0}=\frac{p_G}{\sqrt{2\pi MkT}}\frac{\delta^2}{Dn_s}\nu\, e^{-E_d/kT}(1-\theta), \qquad (6\text{-}16)$$

which has the proper exponential temperature dependence of the kinetically limited growth regime. On the other hand at high temperature the exponential term becomes much larger than unity and the growth rate takes the form:

$$\left.\frac{d\theta}{dt}\right|_{T\to\infty}=\frac{p_G D}{n_s\delta kT}. \qquad (6\text{-}17)$$

The temperature dependence in this case is weak and corresponds to the mass transport limited growth mode where the growth rate is determined by the number of molecules that can diffuse through the boundary layer per unit time.

The diffusion coefficient D can be obtained from the empirical expression [6]:

$$D=\frac{2.23\times 10^{-5}\,T^{1.73}}{P}\,cm^2/s, \qquad (6\text{-}18)$$

where the pressure is given in atmospheres.

The adjustable parameters in the model are: δ, ν , and E_d. From equation 6-17 we can see already that the high temperature asymptotic limit of the growth rate will determine the value of δ. The other two parameters are somewhat more complicated to differentiate. In the low temperature region both will affect the growth rate. The attempt frequency shifts the whole curve because of its direct effect on the number of decomposed molecules. When the frequency is increased the number of decomposed molecules goes up as well, affecting the growth rate. The activation energy affects the

growth rate in a different fashion but its main effects can be observed in the same region as the attempt frequency. At very low temperature the slope of the growth rate curve in the Arrhenius plot is determined by this energy. It is in the transition region, where ALE of GaAs is usually performed that all the parameters are important and only a curve fit will provide meaningful information on the processes involved. The following section gives the results of such fits on the growth rate for the MOCVD growth of GaAs using both TMGa and TNPGa. In the first case the parameters are close to previously reported values. By using some of the values obtained, we then attempt to deduce some information on the poorly characterized TNPGa precursor.

6.3.2 Comparison with growth rate data

Before attempting to simulate the growth rate data we must first reflect on the order of magnitude of the values we expect to find for the different parameters. Many efforts have been devoted to the numerical modeling of the gas dynamics in MOCVD reactor chambers [4–8, 66]. For a horizontal reactor operating at atmospheric pressure with helium as the carrier gas the value of the boundary layer was found to be millimeters [67]. The kinematic viscosity depends on the pressure through the density term and on the nature of the carrier gas. Helium has a dynamic viscosity twice as large as hydrogen [68] and the pressure in our case is an order of magnitude smaller. These two combine to produce a value for δ that is expected to be about 3 times larger. The value for a vertical reactor might be significantly different as well.

The values for the energy of activation and the attempt frequency differ depending on the source. Jacko and Price [52] have characterized the pyrolysis of TMGa and obtained 59.5 kcal/mol and 3.5×10^{15} s^{-1}. DenBaars *et al.* have obtained a value of 58 kcal/mol by studying the decomposition of TMGa in heated hydrogen. [69] Activation energy values obtained during the MOCVD process are in the range 40-45 kcal/mol and are usually deduced from the slope of the Arrhenius plot at low temperature.

The best fit of equation 6-15 with the growth rate data using TMGa is given in Fig. 6.2. We attempted to fit the MOCVD and not the RDS/ALE data because the

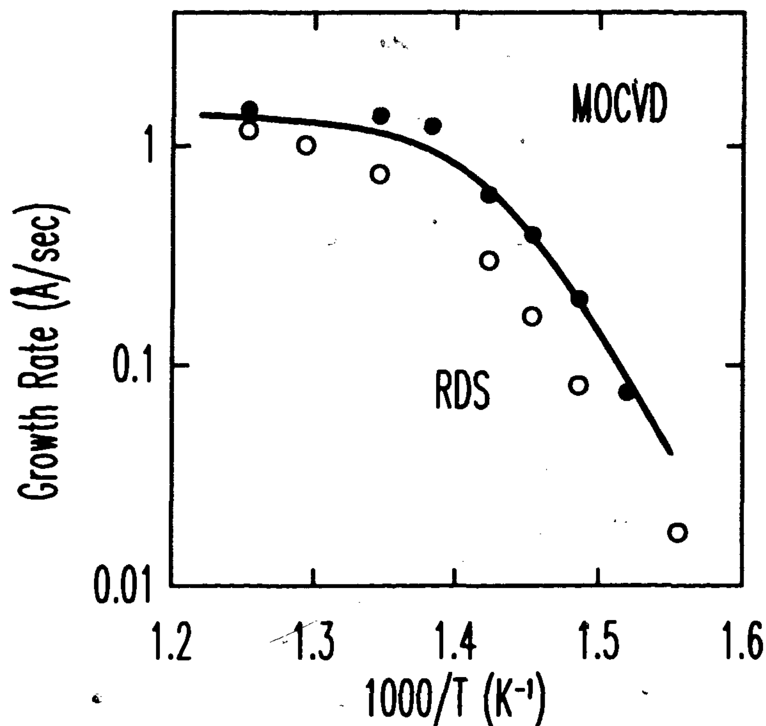

Fig. 6.2 Growth rate measurements for GaAs grown with TMGa as a function of temperature obtained by XRD (solid dots) and RDS (circle). The solid line shows the best fit using the model outlined in the text.

values obtained by RDS are not an actual direct measurement of the growth rate at zero coverage. As we have explained earlier the RDS measures only the time required to deposit one complete layer of Ga. It is not a measurement of the rate of incorporation in the very first moments of the exposure. The MOCVD data is more significant in this regard. The quality of the fit is quite satisfactory considering the approximations involved in the model. The model exhibits the required qualitative behavior through the whole temperature range. The values of the adjustable parameters are given in table 6.1. A value of 15 mm for the boundary layer thickness seems to be larger than expected. This is understandable considering the crudeness of our approximation in the definition of this parameter.

The TMGa partial pressure was 0.14 Pa according to the manufacturer's data. The values of the activation energy and the attempt frequency (57 kcal/mol, and 1.2×10^{16} s^{-1} respectively) are surprisingly close to the values of both Jacko and Price and DenBaars *et al.*. [61] In fact the lower value of the attempt frequency found by the first authors is probably due to the fact that their experiment was performed at 13 Torr

and ours at 50 Torr. They also differ considerably from the values we obtain directly from the low temperature slope of the Arrhenius plot (49 kcal/mol). This result could explain why the activation energies obtained from the growth rates are all lower than the value yielded by the pyrolysis experiment. It seems that in the region where the slope was computed the value of the correction term in equation 6-15 is not close enough to unity justify the approximation of a true exponential behavior. The slope is

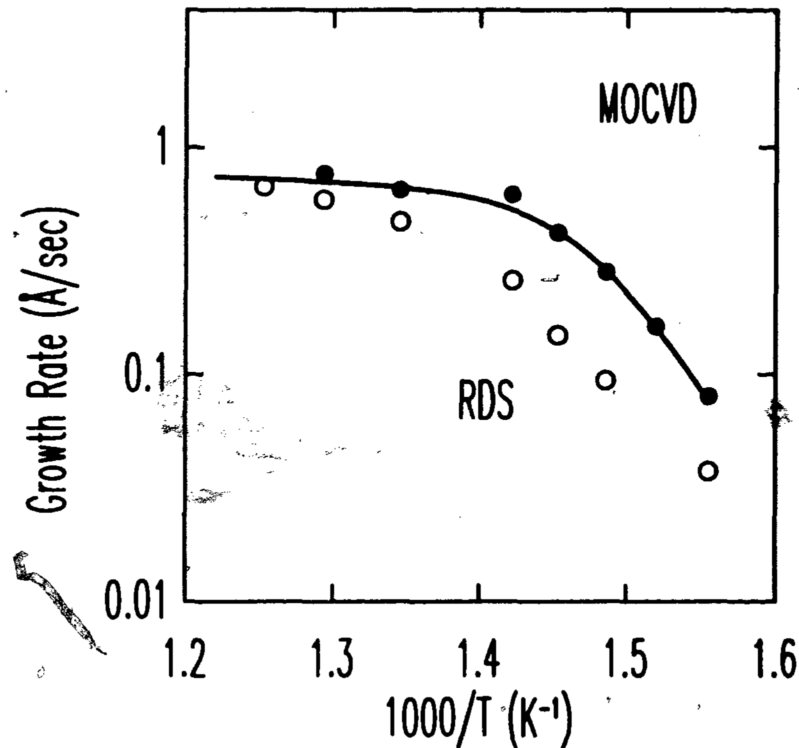

Fig. 6.3 Growth rate measurements for GaAs grown with TNPGa as a function of temperature obtained by XRD (solid dots) and RDS (circle). The solid line shows the best fit using the model oulined in the text.

modified by some contribution from the mass transport.

The task of modeling the growth rate data using TNPGa is complicated by the

	TMGa	TNPGa	Literature
p_G *(Pa)*	0.14	**0.075**	n/a
δ *(mm)*	**15**	15	a few mm's [67]
E_d *(kcal/mol)*	**57**	**54**	59.5 [52]
ν (s^{-1})	**1.2×10^{16}**	1.2×10^{16}	3.5×10^{15} [52]

Table 6-1 Fitting parameters used to model the growth rate data. The values in bold were allowed to vary while the other values were kept constant.

fact that we do not have a reliable value of p_G. The exact value of the diffusion coefficient is not known either so we chose to use the same value as for TMGa. In order to circumvent the unavailability of the partial pressure data we make that quantity a variable parameter and instead fix the value of the boundary layer thickness at 15 mm for this fit as well. Also we decided to use the same value for the attempt frequency because we can expect the process to be similar. The resulting fit to the data is shown in Fig. 6.3. The values corresponding values of the activation energy and the partial pressure are 54 kcal/mol and 0.075 Pa respectively. As can be expected from bond strength argument, the activation energy for TNPGa is lower than TMGa. A summary of the physical parameters for both sources is given in table 6.1. The values shown in boldface are the parameters that were allowed to vary during the fit.

6.3.3 Comparison with ALE growth rate

Using the parameters obtained by the fit to the MOCVD growth rate we have

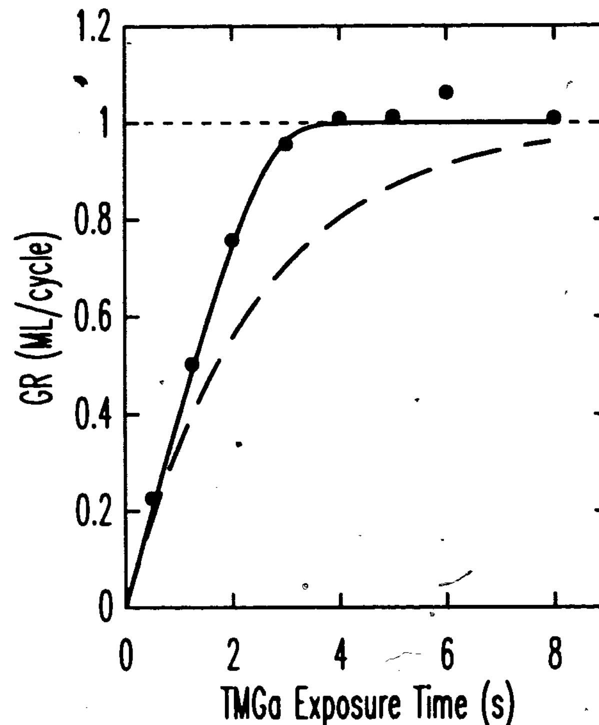

Fig. 6.4 ALE growth rate of GaAs using TMGa as the group III precursor. The solid line is the fit from the model outlined in the text. The dotted line shows the prediction of the standard Langmuir theory.

integrated equation 6-15 and plotted the evolution of the Ga coverage as a function of TMGa exposure time and the result is shown in Fig. 6.4. The agreement is striking especially since it was achieved using parameters from the fit to the MOCVD growth rates. This constitutes a confirmation that the processes governing the growth rates of MOCVD are the same as in ALE, at least for our temperature regime and reactor conditions. The gas phase model completely reproduces the long linear incorporation at low coverage. The reason for such a behavior is simple. As the surface becomes covered with Ga there is an increased number of decomposed TMGa molecules that are returned to the gas phase because they did not find an available site. This has the effect of increasing the partial pressure of decomposed TMGa molecule immediately over the surface and consequently the number of molecules hitting the surface per unit time. The two effects end up canceling each other and the incorporation rate remains roughly constant even for large coverages. The difference with the simple adsorption model given by the dashed line is obvious.

6.4 Conclusion

This chapter reported on the study of the kinetics of growth in ALE. Using RDS to measure the time needed for saturating the surface with Ga during exposure to TMGa we have shown that the growth rates calculated from these measurements were qualitatively similar to the MOCVD results. Using the same procedure we could show that TNPGa had the same behavior as TMGa and that its decomposition energy was lower as expected from bond strength arguments.

Several models have been suggested to explain ALE experimental growth rate measurements results such as ours. One of them, proposed by Aspnes *et al.* [60] assumed that in ALE the molecules strictly decompose at the surface and that no diffusion limited regime is present. Starting from the RDS monitoring of the surface during TMGa exposure in ALE of GaAs they proposed a model to explain the sustained constant Ga incorporation rate up to more than 0.8 ML of surface coverage. Since the Langmuir approach taken literally fails to reproduce such results, they mad the assumption that a TMGa molecule adsorbed on the surface can chemisorb at any of

the sites that lies underneath it. This picture which is credible at low growth temperature breaks down under normal GaAs ALE conditions where a significant number of TMGa molecules are at least partly decomposed when they reach the surface. Furthermore, growth rate measurements in MOCVD show that diffusion plays an important role at normal ALE temperature and that these effects must be considered.

We have proposed a model that assumes that the TMGa molecules are decomposed only in the gas phase and that the growth rate at short exposure times is determined by the rate of diffusion as in standard MOCVD. The surface reactions were assumed to be instantaneous and depended only on the state of decomposition of the molecule and on the surface coverage. From such a picture we were able to extract physical parameters that were in agreement with previous experimental measurements. It is however true that the surface is mostly covered with TMGa molecules at low temperature. Our model cannot pretend to explain the situation then. Some reported values for the decomposition energy as measured from the slope of the Arrhenius plot seem to be lower than the value obtained from gas phase measurement. Our model suggests that this is due to the fact that the region where the slope is measured still involves significant gas phase decompositions. The real situation most likely involves both gas phase and surface reactions.

The measured ALE Ga incorporation profile was also reproduced by our simple model. The fit was very good considering that the parameters used were taken from conventional MOCVD results and none of them was allowed to vary to fit the data. The multiple site sampling effective in the surface reaction model is not necessary in our model to reproduce the data. Again the reality is probably a superposition of both effects since the molecules have a certain mobility on the surface permitting the interaction with more than one potential site. On the other hand at higher temperature the molecules are mostly decomposed in the gas so their mobility is reduced by the presence of dangling bonds interacting with the surface.

Fig. 6.5 shows an interpolation of our MOCVD growth rate data as a function of temperature. Both Aspnes *et al.* [60] and Dapkus *et al.* [10] argue that at low

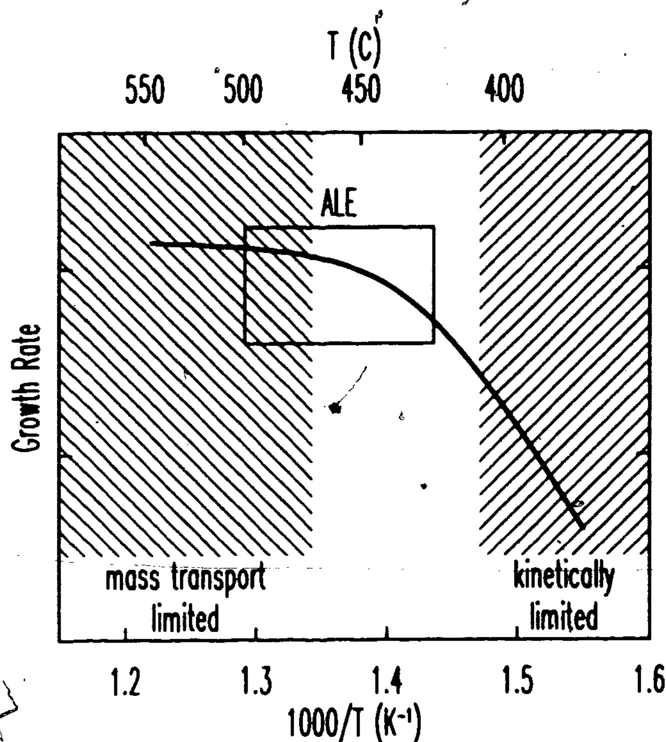

Fig. 6.5 Temperature dependence of the growth rate. The cross hatched regions indicate purely limited regimes. The square shows approximately the temperature window for ALE of GaAs.

temperature, the TMGa molecules reach the surface intact and that diffusion does not play a role in limiting the growth rate. In both cases however the experiments were performed at temperatures below 400°C which is well outside the usual ALE window for GaAs (430°C-500°C) represented by a box in Fig. 6.5. At such low temperatures, the ALE growth rate is generally observed to saturate well below 1 ML/cycle because of the large amount of undecomposed TMGa molecules adsorbed on the surface that inhibit further reactions with available sites. [10] This mechanism is usually identified as steric hindrance. At the high temperature end of the ALE window the MOCVD growth is already observed to saturate, just like the ALE saturation time (see Fig. 6.4), indicating the gas phase diffusion is playing a significant role in limiting the growth rate. The mass transport limited and kinetically limited growth regions are identified by crosshatched patterns.

7. Heteroepitaxy

One of the principal reasons for using a technique such as ALE for the growth of epitaxial structures is the potential control of the layer composition and thickness with monolayer accuracy. The reality is somewhat less ideal and absolutely abrupt interfaces are still a challenge for ALE. Even though ALE can effectively eliminate basic problems common in conventional MOCVD such as depletion of precursors leading to lateral variations in the growth rate, turbulent flows and limits in the gas switching speed, there are a number of problems that remain to be investigated and solved and one of them is the segregation of atoms at the growth front.

In order to lower its total surface energy, a crystal might find it favorable to rearrange its top few layers of atoms by bringing the species with a lower surface energy to the surface and burying the ones with a higher surface energy. This process is called segregation and has generated a lot of interest recently. Segregation effects have been observed in different systems with detrimental effects on interface quality and alloy composition. The first section of this chapter will discuss such a phenomenon as seen by RDS. This constitutes the first reported *in situ* monitored segregation effect in MOCVD.

The idea behind the use of quantum wells (QW) in semiconductors is to take the carrier movement from the 3 dimensions of the normal crystal and confine it in the 2 dimensions of a thin well. In doing so the quantum mechanical picture of the carrier behavior changes, resulting in very high carrier confinement which is useful for many device applications. When the thickness of the well becomes comparable to the size of the wavefunctions of the carriers we also observe a modification of that wavefunction

and the energy attributed to it as well. One of the systems that has been investigated extensively is the InAs quantum well in a GaAs matrix. From the point of view of strain the critical layer thickness of about 1.5–2 ML makes that system one of the most strained of all in the field of III-V semiconductors. Significant efforts have been devoted to the study of the InAs/GaAs system and many interesting effects are observed. The growth of those extremely thin structures is very well suited for the advantages of ALE so we have done some work on the RDS characterization of the ALE of InAs single ML's in GaAs. The second and last section of this chapter will report our results from the study.

7.1 Indium segregation

7.1.1 Background

When a compound A is grown over a different material B several forces enter the picture affecting the growth patterns like the growth mode or the stoichiometry of the crystal. In the case of heterostructures the interface abruptness is one of the critical parameters that needs to be controlled. Conditions such as lattice mismatch, surface energy and reconstruction can affect the way the atoms from compound A wet the surface of B.

The total energy stored in the dangling bonds of the surface is called the surface energy. Its value depends on the strength of the individual bonds. In the case of InAs/GaAs heterostructures, two types of bonds need to be considered. Since the Ga-As bond is much stronger than the In-As bond, the surface energy of GaAs is expected to be larger than that of InAs. In the growth of these heterostructure, when a situation arises where one material is deposited on the other, the system will try to rearrange itself in order to minimize its surface energy. For example, if Ga is deposited on InAs, the system will try to lower the surface energy by bringing the In atoms from the bulk to the surface and burying the Ga atoms. This process is called segregation.

Surface segregation is well known in heterostructures and has been initially observed and studied in metals [70]. The first observations of such an effect in III–V

semiconductor epitaxy involved the surface stoichiometry of ternary compounds. The surface composition of $Ga_{0.7}Al_{0.3}As$ is found to have a higher Ga concentration than the bulk and In containing compounds such as $Ga_{0.5}In_{0.5}As$ and $Al_{0.5}In_{0.5}As$ are observed to have In–rich surfaces [71, 72]. The lower surface energy of Ga in the first case and In in the second, forces them to the surface. Similarly the smearing of heterointerface by the migration of group III atoms to the surface has been known for several years for a variety of structures such as GaAs on InAs [73], AlAs on GaAs [74], and GaSb on AlSb [75]. In this work we give special attention to the InAs/GaAs heterointerface. The ultimate goal is to grow a single or submonolayer InAs QW in GaAs.

Several reports have claimed that InAs forms clusters nanometers in size when thin (1-2 ML) layers are deposited on a GaAs matrix [76–80]. The effects of this clustering on the interface quality is still being debated at this time. The islands are mostly monolayer thick and are elongated towards the $(\bar{1}10)$ crystal direction. Their size varies with total InAs coverage but in the first stages of island widths of 4 nm in the (110) direction have been observed prior to GaAs burial. [76] All these results point to a significant difference in surface dynamics in heteroepitaxy. The main reason that makes InAs ultrathin QW's so attractive is their high photoluminescence efficiency. Short period superlattices with a period made of 1 ML of InAs and 4 ML's of GaAs have been successfully used to fabricate lasers [81].

7.1.1.1 Segregation models

Different approaches have been used to explain segregation in heteroepitaxy. The simplest has been based on a phenomenological picture where a fixed fraction of the low surface energy atoms travels to the surface when a different type of material is deposited over it. If for example, GaAs is deposited on top of InAs, which corresponds to the studied case here, some of the In from the covered layer will exchange with the Ga on the surface due to the lower surface energy of InAs as discussed in section 7.1.1. Let σ be the probability of an In atom of exchanging when

GaAs is deposited on top of it and x_{si} the fraction of In on the surface after deposition of the i th GaAs monolayer. Before GaAs is added to the crystal we have:

$$x_{s0} = 1 . \qquad (7\text{-}1)$$

In the subsequent layers the surface composition varies as:

$$x_i = \sigma^i . \qquad (7\text{-}2)$$

If we now look at the actual In amount left behind the growth front when GaAs is grown, we obtain for the resulting In profile:

$$x_i = (1-\sigma)\sigma^i , \qquad (7\text{-}3)$$

and by making this relation continuous an exponential decay in the direction of the growth z is obtained:

$$x(z) = (1-\sigma)e^{\frac{z}{d}(\ln\sigma)} , \qquad (7\text{-}4)$$

where d is the thickness corresponding to 1 ML.

Other models using more physical arguments have been proposed [82–84] but due to the simple qualitative nature of our study we will restrict ourselves to the phenomenological picture. The only parameter of interest in the model is the segregation coefficient σ.

7.1.2 *In situ* study

The ALE sequence for inserting one plane of In a GaAs matrix is very simple: we replace one of the TMGa pulses of the GaAs ALE by a TMIn pulse. If the exposure is long enough we should have a complete ML of InAs in the crystal. From previous work we have determined the optimal conditions for the ALE of GaAs [85] and InAs [86]. Using this information we chose the conditions for the growth of the quantum wells. We used 390°C as the growth temperature in order to keep the thermally activated segregation to a minimum. A growth rate of 0.8 ML per cycle was measured for GaAs at that temperature but it is very sensitive to temperature because of the exponential dissociation of the TMG precursor. It is therefore expected to vary somewhat from sample to sample. Thus we are not truly in ALE mode for the measurements, but more accurately flow modulation epitaxy. Two types of

heterostructures were grown for comparison. In each case one group III pulse is replace by the other element with an exposure time that is expected to include 1 ML of material in or around the well.

The structures were grown using the following growth sequence:

"B" layer in "A" matrix

1) "A" buffer layer grown at 560°C.
2) Temperature lowered to 390°C.
3) 4 "A" ALE cycles.
4) 1 "B" ALE cycle
5) 40 "A" ALE cycles
6) "A" cap layer grown at 500°C.

note: the ALE growth sequence were (H_2:III:H_2:V): 2:8:2:4 for GaAs,
2:3:2:4 for InAs

The labels "A" and "B" represent either GaAs or InAs depending on the structure. Fig. 7.1 shows a schematic view of the structure. The energy chosen for monitoring the surface state depends on the nature of the host crystal. For the InAs layers inserted in GaAs (A: GaAs, B: InAs) the energy was 2.6 eV and 2.3 eV was used for the complementary structure (A: InAs, B: GaAs). These energies are related to transitions in the As dimers of the host crystal but are also affected by changes in the Ga (or In) dimer structures (see Figs 3.2, and 5.2). The evolution of the RDS signal during the growth of a InAs QW is shown in Fig. 7.2. The origin for the time axis has been set at the point of the TMIn pulse.

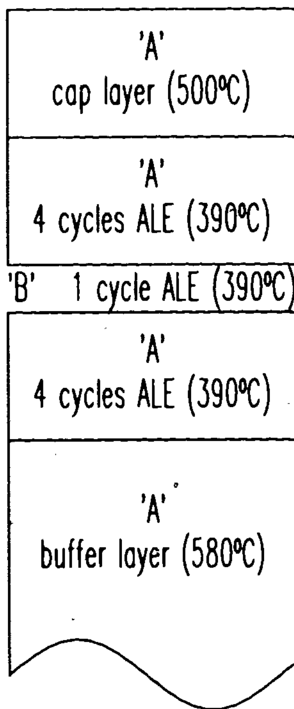

Fig. 7.1 Schematic view of the heterostructure.

The RDS transients preceding the well are highly reproducible, a testimony to the stability of the growth conditions during ALE. The RDS response corresponding to each individual cycle is identical to the others. When one TMGa pulse is replaced by a TMIn pulse the RDS

signal is shifted upwards and remains modified during several of the following cycles. Even after more than 20 cycles the RDS signal is still slightly modified.

The shape of individual cycles is also strongly perturbed beyond the growth of the well. The general shape of the cycles is not only shifted upwards but the signal transient is modified. The biggest difference happens during the TMGa pulse in the few cycles that follow the In insertion. After this perturbation has disappeared, the cycle shape is still shifted upwards. It appears the this shift starts to decrease only once the cycle has recovered somewhat the right shape. This could be due to the presence of In clusters on the surface. Since these clusters are probably more than 1 ML thick the self-limiting behavior of TMGa may be disrupted because the surface is no longer atomically flat. The RDS signal is then perturbed during the TMGa exposure. Once a few ML's have been laid on top of the In clusters, the only In remaining on the surface is segregating and lies in the Ga plane as an alloy. This situation, where the surface is flat again, allows the TMGa to remain self-limiting. The data does not permit us to draw any conclusions on the origin of that perturbation but, as will be shown later in this section, it is related to the amount of In on the surface in excess of 1 ML.

Since white light penetrates well into the layer it could be argued that the

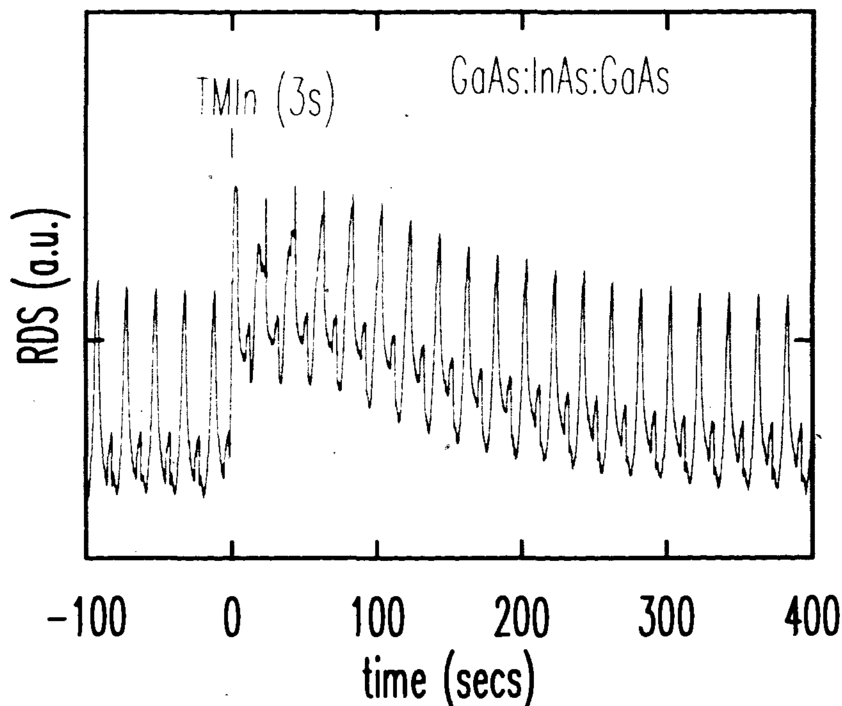

Fig. 7.2 RDS signal measured at 2.6 eV during the growth of a InAs SMQW in GaAs.

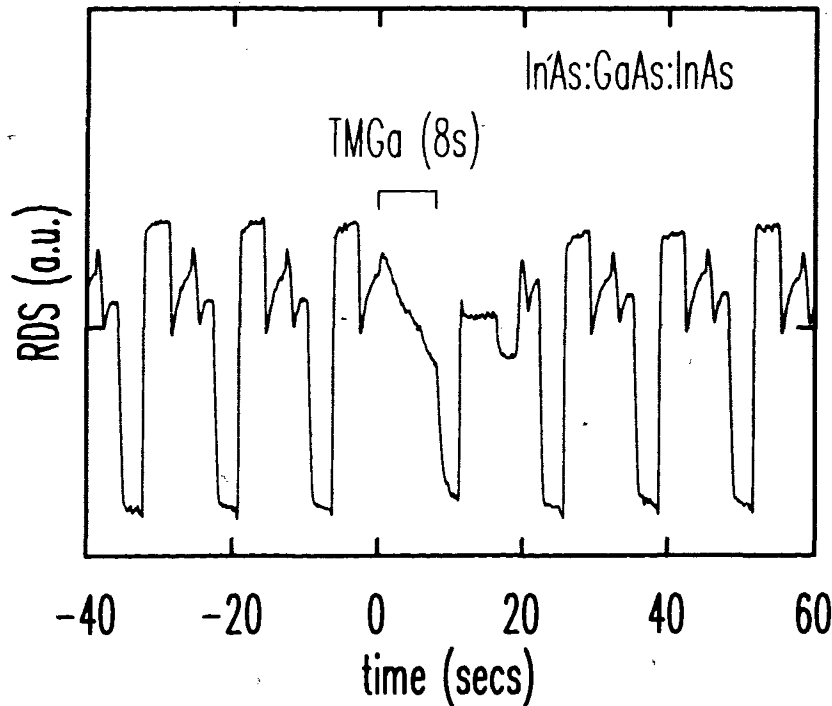

Fig. 7.3 RDS signal measured at 2.6 eV during the growth of 1 ML of GaAs in InAs.

assumption stating the bulk is isotropic in the case of the zincblende structure breaks down in the well and the contribution to the signal is expected to show on the RDS response until the amount material covering the well is thicker than the penetration depth. The obvious way to verify that RDS is really only sensitive to the surface composition is to grow the complementary InAs/GaAs/InAs "antiwell" structure which is not expected to show segregation.

We have done the experiment and the results are illustrated in Fig. 7.3. Here again the cycles are reproducible before the inserted layer but in this case when TMGa is introduced in the chamber the signal is modified for the remainder of that cycle only. The following cycles are virtually identical to those preceding the Ga insertion. Subsequent XRD measurements confirmed that close to 1 ML of GaAs was incorporated in the crystal, confirming that RDS remains effectively a surface measurement even for heterostructures. It should be noted though that the total amount of material in the both structures does not surpass the critical thickness of 2 ML so the inserted layers are pseudomorphically strained.

The stoichiometry of the surface has also been monitored by interrupting the growth after each cycle. The procedure consisted of two parts. The RDS signal was monitored during the ALE cycle until the TBAs exposure step was reached. At that point the ALE was stopped and the surface was kept under TBAs until the RDS stabilized. A RDS energy spectrum was then measured and the process was repeated for every cycle until the RDS signal had returned to the normal ALE shape.

With the results we can push our understanding a little further. The spectra for the InAs QW structure are summarized in Fig. 7.4. The measured growth rate during GaAs ALE in those conditions is 0.8 ML/cycle. The estimated cap layer thickness is labeled beside each spectrum. The top spectrum labeled "GaAs" was taken after the

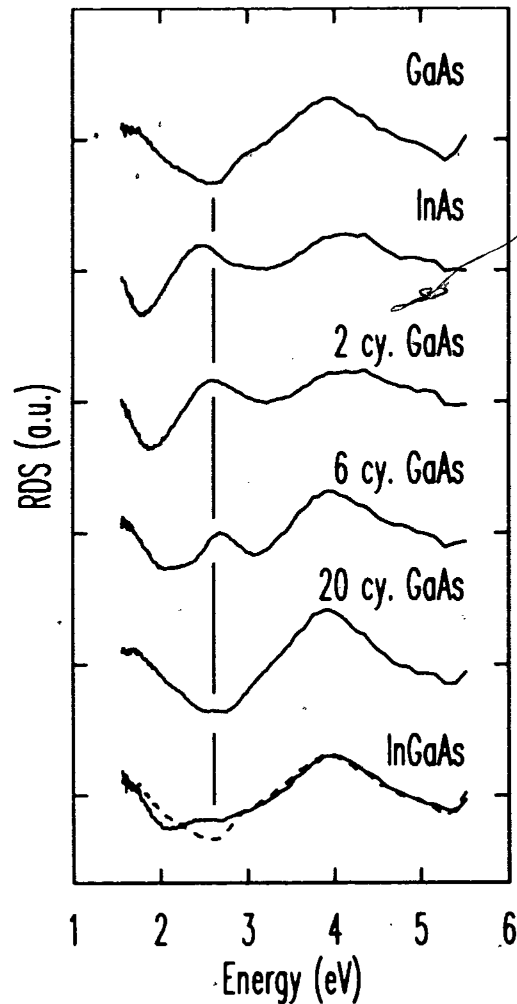

Fig. 7.4 RDS energy spectra of the TBAs exposed surface as a function of the number of ALE cycles for the InAs SMQW in GaAs.

last cycle preceding the In insertion. It corresponds to the now familiar d(4×4) surface that is observed at this low temperature. The following spectrum (InAs) shows a strongly modified spectrum with several new features. At this point a strong new feature is present at 2.4 eV which is very close to the normal InAs As dimer feature at 2.3 eV. This feature is also observed after more cycles have been deposited on top of the In with a slight change in energy position. Its intensity is observed to decrease with cap layer thickness to be almost unobservable after 20 cap layer cycles.

The presence of In on the surface alters the As dimer structure on the top layer. The bottom spectrum shows the RDS signature of a 50 Å $In_{0.11}Ga_{0.89}As$ coherently strained layer on a GaAs substrate where we observe the same feature which confirms our argument for the presence of In on the top layer of the crystal.

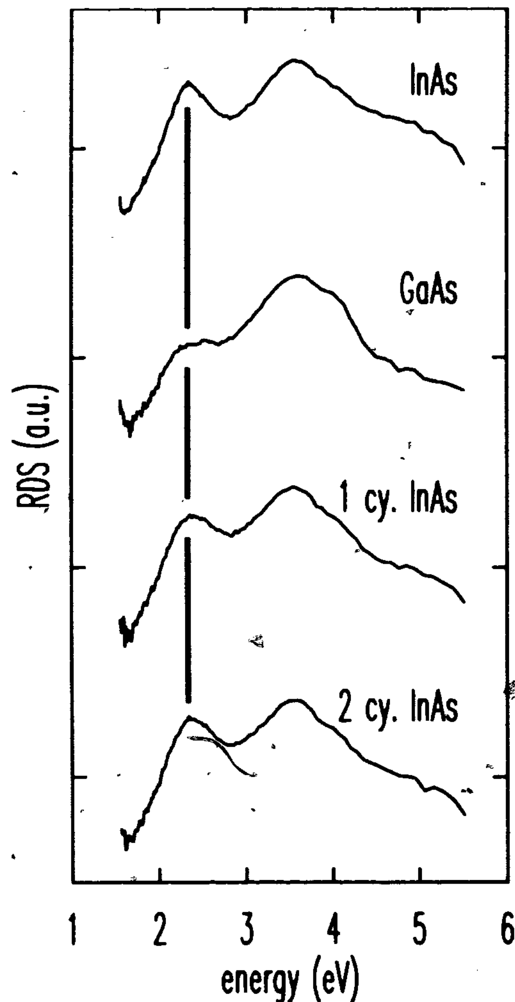

Fig. 7.5 RDS energy spectra of the TBAs exposed surface as a function of the number of ALE cycles for the GaAs ML in InAs.

The difference in the InAs/GaAs/InAs structure is even more obvious. Fig. 7.5 shows the same spectra taken during the growth of such a structure. The surface has the normal As super rich configuration under TBAs before the Ga insertion but is only slightly modified after the deposition of the GaAs ML. The same main features are still present albeit somewhat disturbed but far from a GaAs–like surface. The deposition of only 1 ML of InAs is enough to return the surface to its normal InAs–like shape. The similarity of the GaAs spectrum with InAs can in fact be expected from In segregation as well. When the GaAs layer is grown, the underlying In travels to the surface and exchanges sites with the Ga atoms of the top layer. The surface therefore remains almost Ga free even after TMGa exposure. This result means that In segregation is present in both structures but with very different results. For the InAs QW some fraction of the In travels to the surface when a GaAs ML is deposited and the phenomenon is repeated each time a new GaAs ML is grown to bury the InAs, resulting in a much larger deviation from the nominal structure in this case.

7.1.2.1 Measurement of the segregation coefficient

We have monitored the RDS signal during the growth of the GaAs/InAs/GaAs structure for different TMIn pulse lengths. The amount of In in the structure was then measured by XRD using the procedure described in chapter 4. The results are presented in Fig. 7.6. The measured In content of each structure along with the TMIn pulse length is given beside each transient. We observe that the number of disrupted cycle transients increase with the total In inserted in the crystal. The only case where the perturbation is absent is for an In content of less than 1 ML. This supports the hypothesis of In clustering on the surface and destroying the self-limiting deposition of Ga.

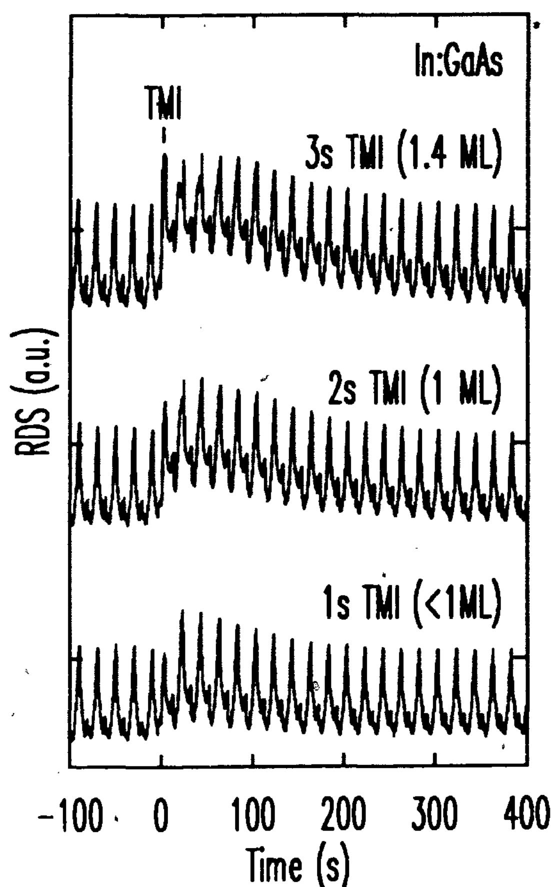

Fig. 7.6 RDS signal at 2.6 eV monitored during the growth of InAs/GaAs heterostructures with different TMIn pulse durations.

As expected the RDS signal of each cycle is shifted more as the amount of In is increases. The recovery of the signal to the original ALE shape has a shape that is close to be exponential. Using the phenomenological model oulined in section 7.1.1.1, and more specifically equation (7-4) we can obtain an estimate of the segragation coefficient from the RDS data. In order to reproduce the change in RDS intensity at every cycle we have plotted the RDS signal at the end of the TBAs exposure for each cycle. The results for the 3 structures shown in Fig. 7.6 are given in Fig. 7.7. The solid lines are least square fits to the data using equation (7-4). The fits do not reproduce the data for the first few cycles where the shape of the signal during TMGa exposure is disrupted. Since this effect is probably related to a flatness effect due to uneven In distribution we decided to leave this part of the signal out of the fit. The segregation coefficient that we obtained through this procedure is 0.74±0.08. There was no

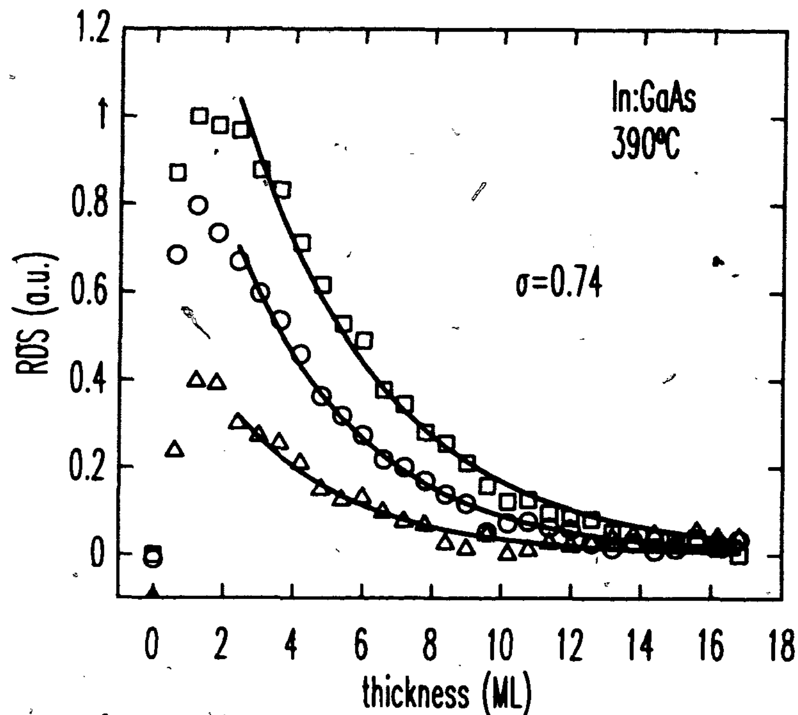

Fig. 7.7 Variation of the shift in the RDS signal as a function of growth thickness for the heterostructures of Fig. 7.5. The solid lines represent a least square fit to the data.

appreciable variation between the structures with different In content. Early work in MBE using surface probes such as XPS and Rutherford back scattering (RBS) gave a value of 0.8±0.1 for growth at 480°C [87] and more recently Muraki *et al.* have obtained a value 0.7±0.1 at 370°C in good agreement with our results. [88]

7.1.3 Conclusions

In the preceding section we have shown the presence of In segregation during the growth of InAs/GaAs heterostructures. RDS can be used to monitor the ALE growth of heterostructures and constitutes an efficient probe for interface quality measurements. Even though ALE should, in principle, provide perfect control on interface abruptness due to its sequential nature, thermodynamic effects participate and alter the results. RDS is a powerful technique that can be used *in situ* to monitor the presence of segregation. It can also be used in the search for ways of improving interface quality. Because it is non invasive several sets of parameters can be tested on the same sample. As long as the surface of the wafer remains smooth, a buffer layer

can be deposited over the previous structure and a new one can be grown with different conditions without the need to prepare a new wafer. Using such a procedure we were able to achieve the growth of single and submonolayer InAs QW's in GaAs which displayed very narrow and strong PL features [89].

Surface effects such as In segregation in heterostructures have been monitored *in situ* for the first time. RDS transients during ALE of GaAs were modified after the insertion of an In layer in the structure. Using the *in situ* RDS measurements as a probe of the In concentration of the surface we were able to measure a value for the phenomenological segregation coefficient that is consistent with previously reported results.

With the treatment outlined in chapter 4, we have demonstrated that XRD is only sensitive to the total phase shift created by the inserted In in the structure. The lattice constant perpendicular to the surface of an InGaAs layer coherently strained on a GaAs matrix varies linearly with the fraction of In. Each monolayer of material in the structure has a modified lattice constant depending on its In content and each subsequent. The shift in the position of the planes of the cap layer correspond to the total contribution of each plane near the region of inserted InAs that contains In. XRD can therefore only detect the total amount of In and cannot provide any information on the distribution through the crystal. If we follow the phenomenological model and assume that the segregation proceeds homogenously, our measured value of the segregation coefficient suggests that the In is spread over several monolayers in the crystal and that each individual monolayer consists of a dilute InGaAs alloy. However, the fact that the first few RDS cycles are modified during TMGa exposure might be an indication that the segregation does not proceed evenly during the growth. For example the segregating In might be composed mainly of the "extra" In contained in the several ML's thick InAs clusters that form during the TMIn exposure. The "base" of these clusters might stay within the original layer without segregating, creating an In rich layer followed by a series of very dilute InGaAs layers. More local types of measurements such as extended x-ray absorption fine structure (EXAFS) or x-ray standing wave will be needed to settle these questions.

7.2 Breakdown of self-limiting behavior for ALE heteroepitaxy

The advantage of ALE for the growth of heterostructures is the total control over the nature of the vapors arriving at the surface. We have demonstrated in the last section that despite the fact that the crystal is grown one atomic layer at a time the interface quality can be altered by other effects such as segregation. Another condition that needs to be controlled for proper ALE to be performed is the preservation of a self–limiting growth mode throughout the structure. In order to keep the surface atomically smooth it is imperative to suppress the formation of droplets during exposure to the group III vapor. As we have seen earlier the mechanisms for self–limiting growth are complex and may be disrupted easily.

The well controlled ALE of both GaAs and InAs is possible under the proper conditions. Since their respective self–limiting growth temperature windows are separated [14] the proper choice of growth temperature for heteroepitaxy of both is difficult. The temperature that was chosen in this work was at the higher end of InAs ALE (390°C). At this temperature GaAs grows with only partial ML coverage during each cycles (0.8 ML/cycle). InAs on the other hand is self–limiting at this temperature [86]. In a previous report GaAs was shown to partially lose its self–limiting characteristics when grown on an InAs substrate [14]. We will show here that the same type of breakdown in the growth behavior is observed with InAs grown on GaAs.

A study of the RDS monitoring of the growth of heterostructures at different temperatures gives some evidence of a similar phenomenon. Fig. 7.8 shows the RDS trace taken at 2.6 eV during the ALE of InAs single ML QW's at different temperatures. The time axis has been normalized to the number of cycles. The lowest trace shows a structure grown at 370°C. At this temperature the conditions produce around 0.4 ML per cycle. The segregation seems to carry over several cycles but due to the partial coverage of Ga at each exposure, real assessment of segregation is ambiguous. The remaining traces all produce 1 ML/cycle of GaAs with a 1 ML InAs cycle inserted in the structure.

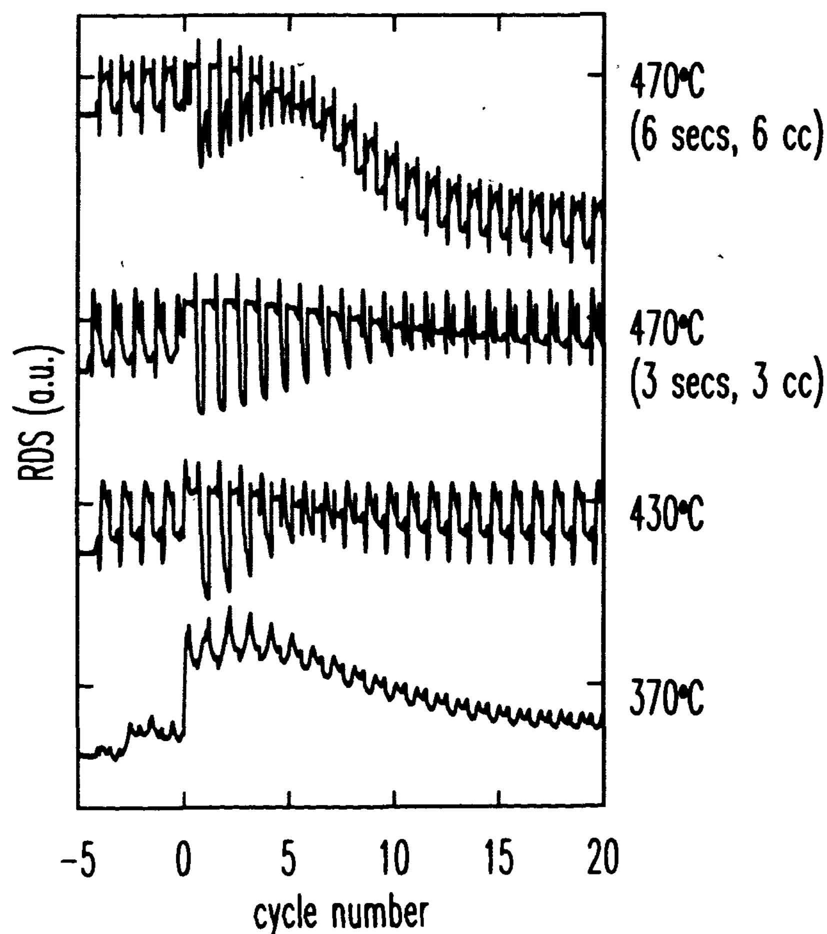

Fig. 7.8 RDS signal monitored at 2.6 eV during the ALE growth of InAs SMQW's in GaAs at different growth temperatures. The time axis has been normalized to the number of cycles.

The structure grown at 430°C takes approximately 10-12 cycles for the RDS signal to return to the normal GaAs ALE. At 470°C such a recovery takes more than 20 cycles. This temperature dependence of the segregation goes against early reports that claimed that segregation did not vary between 420°C and 560°C [87] but agrees with most recent studies which observe an increase in the segregation at high temperature [82,88]. The top two traces show results for structures grown under identical conditions except that the topmost structure has four times the TMGa dose (twice the flow, twice the time) of the lower one. In both cases the ALE preceeding the In insertion is stable and self-limiting. After the In is deposited though, the first few cycles of the high dose structure show an increasing shift of the RDS signal, indicating

the presence of surface roughness. The shift stops increasing after 12-15 cycles and the shape of each cycle returns to the one preceeding In insertion. Some surface roughness could be noted on the surface after the growth. These data indicate that the GaAs cycles lose their self–limiting character when In is present on the surface. The following section will study the incorporation of In on a GaAs surface.

7.2.1 Experimental results

Figs 7.9 and 7.10 show the XRD measured growth rate for both homo– and heteroepitaxy for InAs at 360°C and 390°C respectively. For both temperatures the homoepitaxial growth rates show self–limiting behavior, saturating at 1 ML per cycle. The In incorporation shows the same features as observed in GaAs i.e. the rate of incorporation remains constant until more than C.8 ML of In has entered the surface. On the other hand the incorporation of In on GaAs is not saturating at all. In is deposited with a rate that remains constant up to several ML's. The 360°C data show a linear incorporation up to 4 ML's with no signs of saturation. All this indium comes from a single TMIn exposure.

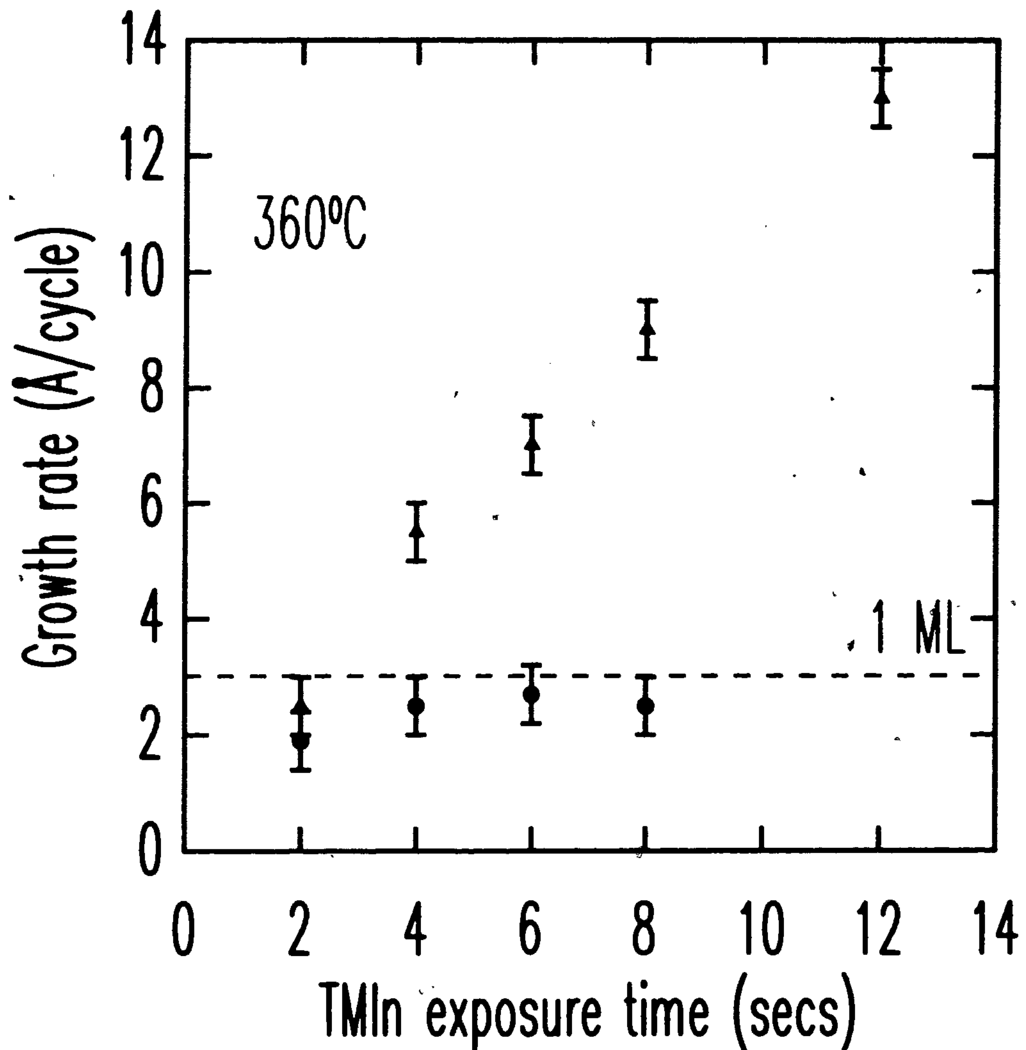

Fig. 7.9 Growth rate measurements for homo- (dots) and heteroepitaxy (triangles) of InAs by ALE at 360°C.

If a single TMIn exposure of 6 s is replaced by two cycles with a 3 s exposure which correspond to 1 ML of InAs each, the total In is the same as can be seen by the star in Fig. 7.10. The In incorporation is therefore insensitive to the surface coverage or to the amount of As available for reaction. Under these condition every TMIn reaching the surface results in a In atom added to the crystal. According to our data the rate of incorporation of In is not different on GaAs than on InAs. Both growth rate profiles agree within experimental uncertainty which differ from the results of Brandt *et al.* [90] who have observed a decrease in the growth rate for In deposited on GaAs under MBE conditions.

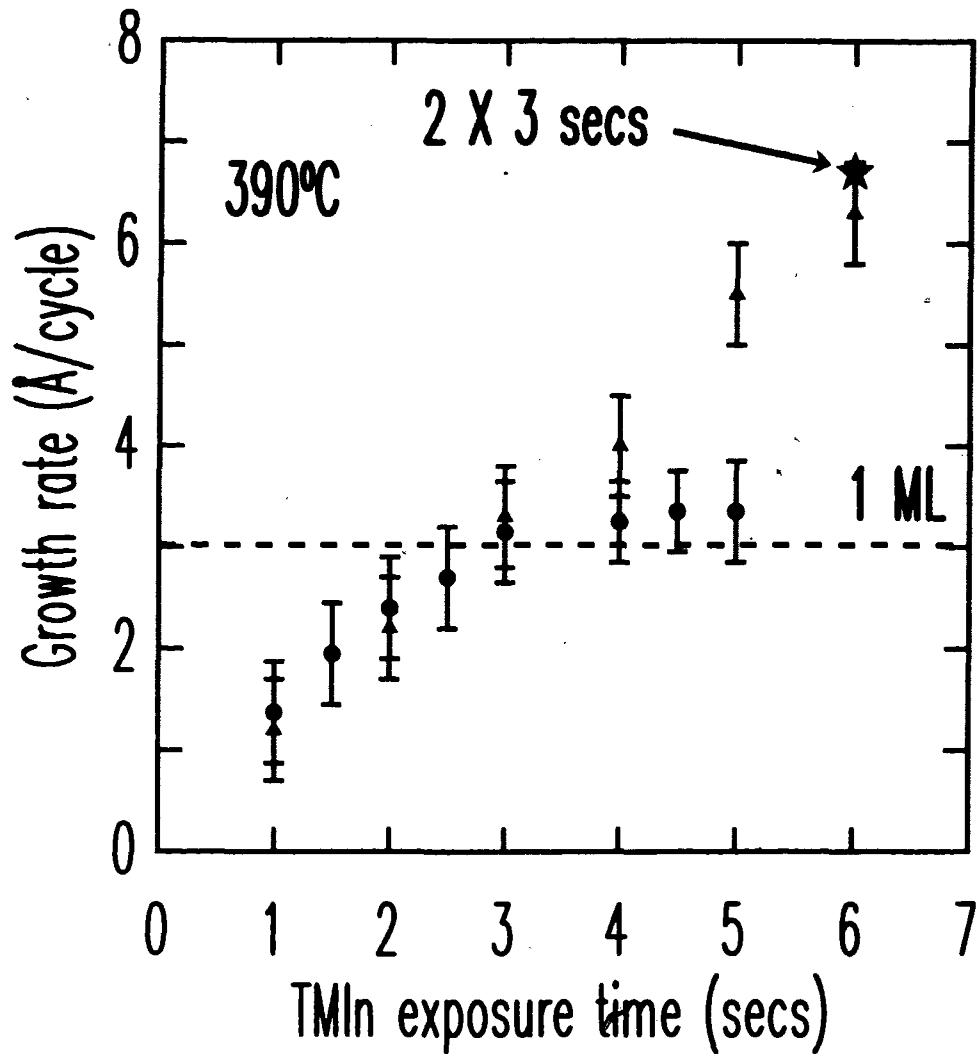

Fig. 7.10 Growth rate measurements for homo- (dots) and heteroepitaxy (triangles) of InAs by ALE at 390°C.

Photoluminescence characterization of the same structures was performed by Dr. Yves Lacroix from Prof. Mike Thewalt's group and the results are presented in Fig. 7.11. The TMIn exposure time is given beside each emission spectrum. The main QW luminescence emission feature is labeled by an asterisk in the short exposure spectra in order to differentiate it from the underlying GaAs spectrum. The excitonic and donor acceptor pair luminescence for the bulk GaAs are labeled "X" and "DAP" respectively.

We observe a continuous shift of the luminescence towards lower energies in accordance with larger well widths confirming the XRD results. There is a large difference in the emission linewidth between the 4 s and the longer exposures. The longer exposure times exhibit a much wider emission band. This is due to the extremely thin well (<20 Å) compared with the size of the free exciton wave function

(200 Å). As the well becomes thinner the fraction of the exciton wave function that overlaps it becomes smaller and variations in the effective width due to interface roughness have less effects on the emission energy. Another reason for this big difference in emission peakwidth could be partial relaxation of the layer, since the total indium content approaches and even surpasses the 1.5-2 ML critical thickness for TMIn exposure time longer than 4 s.

However, from the XRD rocking curves of the structures we did not observe

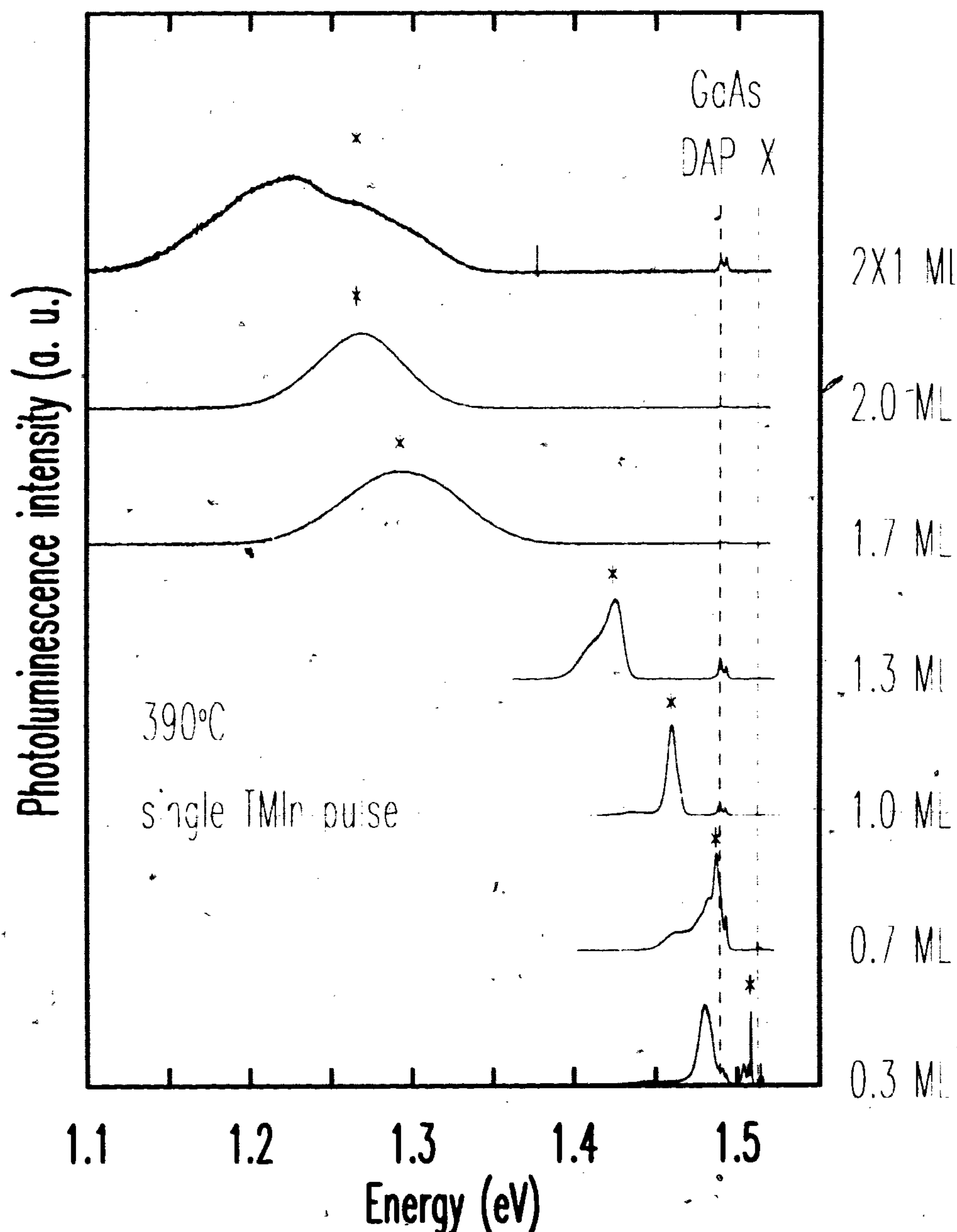

Fig. 7.11 Low temperature photoluminescence emission spectra of InAs SMQW's in GaAs as a function of TMIn pulse length. The asterisk identifies the QW related emission.

any appreciable relaxation of the layers even at high In content. The reported critical layer thickness is around 2 ML for the InAs/GaAs system. At 360°C, even for 4 ML of InAs the crystal remained coherent. This is probably due to the formation of InAs clusters during the long TMIn exposure which provide partial strain relief at their boundary with the host crystal without introducing dislocations. These clusters have recently been observed by AFM for similar structures. [91] As was explained in section 4.3.2.1 the XRD signal originates only from the substrate and cap layer. The region of inserted In only influences the shape of the rocking curve by decoupling the two GaAs layers.

A comparison of the 6 s and the "2×3 s" TMIn exposure PL spectra shows that the latter has two distinct PL emissions for the QW. The higher energy emission of the "2×3 s" sample coincides with the QW luminescence of the 6 s sample but the spectrum also has an emission band at a slightly lower energy. Clustering is probably responsible for this extra emission as well. It seems that in the "2×3 s" sample there are two distinct phases in the well. The emission energy is lower in the clusters where the effective well width is larger than nominal, and higher in the regions around the clusters where the well is either closer to its nominal width or consists of an InGaAs well with a larger band gap than pure InAs. The main point of the PL study is the finding that In is continuously incorporated in the crystal during TMIn exposure even though there is only 1-2 ML of As available to form the crystal at that moment. It appears that the In droplets are dissociated and replaced by InAs clusters during the following TBAs exposure. A detailed study of the emission linewidths of these structures, especially for the submonolayer structures has been published. [89]

The temperature dependence of the In incorporation rate on GaAs is illustrated in Fig. 7.12. There is no noticeable difference between 360°C and 390°C. A 2 s TMIn exposure at 470°C confirms that even at higher temperature In incorporates into the layer with the same rate. The rates were fitted with a straight line and gave 1.02±0.05 Å/s at 360°C and 1.03±0.04 Å/s at 390°C.

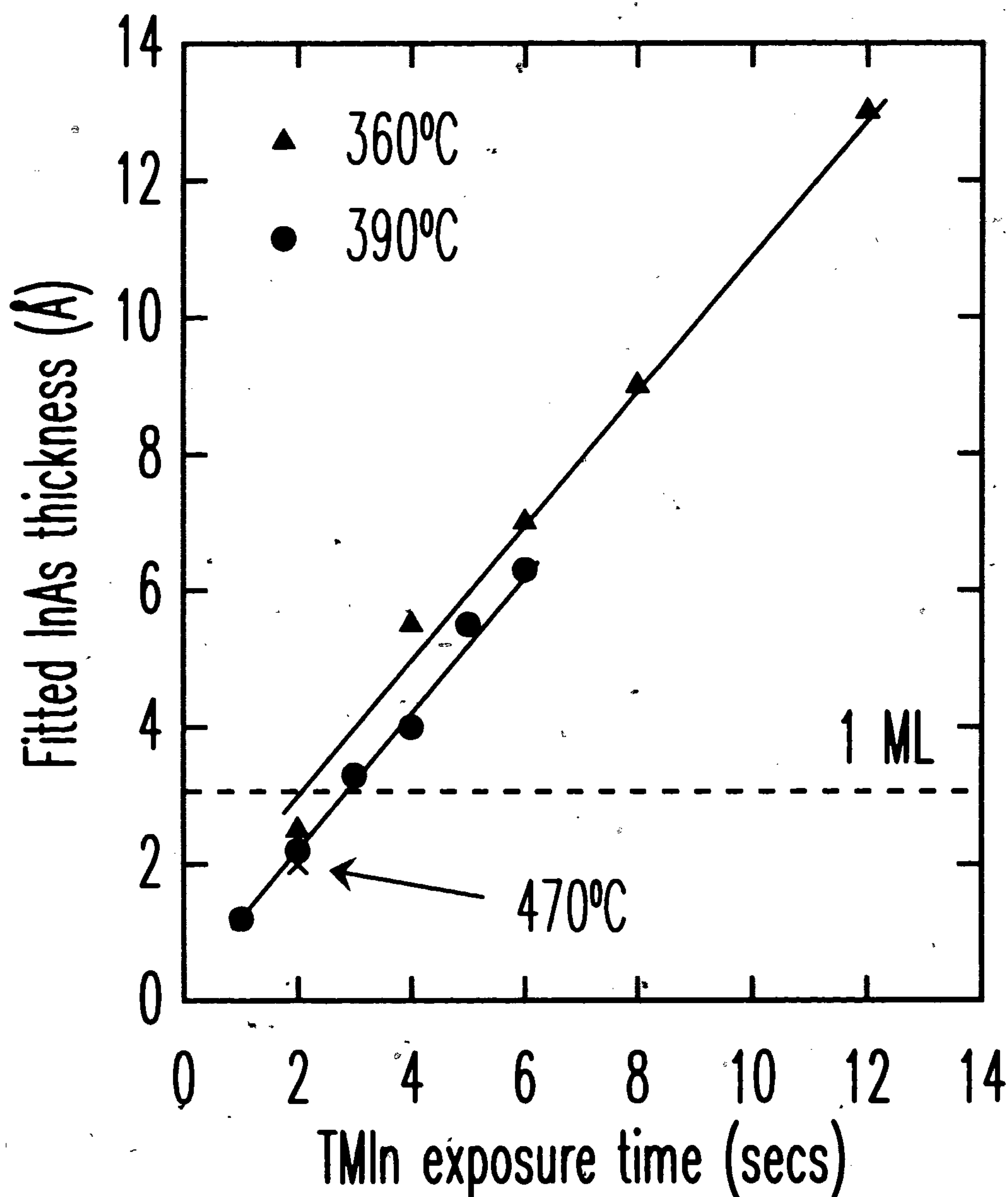

Fig. 7.12 Comparison of heteroepitaxial growth rate of InAs on GaAs at 360°C and 390°C. The lines are linear square fits to the data. The cross symbol shows a result at 470°C.

7.2.2 Conclusions

We have characterized the incorporation of In on a GaAs surface under ALE conditions. The In is observed to incorporate with a constant rate that is independent of temperature. Photoluminescence results show that the In forms a quantum well with increasing width as more atoms are incorporated. The formation of clusters is believed to explain the large peak width observed for In content exceeding 1 ML.

8. Concluding remarks

In the recent years several new diagnostics tools have emerged to help crystal growers improve their understanding of the epitaxy process. This change has had dramatic effects in the field of vapor phase epitaxy like MOCVD where most of the understanding had been acquired in a post growth setting. Until *in situ* monitoring was made available to the growers the optimization of the growth had proceeded in a hit and miss fashion reminiscent of an art such as cooking. The layers were grown with conditions chosen by the operator and the result was evaluated after the growth. Conclusions were then drawn from the characterization results and new parameters were chosen for the next try.

Very few means were available to detect systematic problems such as hardware drift, and the intuition and experience of the crystal grower were his or her main assets. Nowadays several tools can be installed on the growth reactor to monitor the stability and reproducibility of the machine from growth to growth, such as IR or UV absorption units to monitor systematic characteristics such as the stability of gas flows or the line transients. Optical techniques have opened a new variety of possibilities for MOCVD growers since they can be used under atmospheric or slightly sub-atmospheric pressures in effect during growth. Of these techniques relatively few have a strong selectivity for information coming from the surface. RDS is one of them. This characteristic combined with its non invasive nature make it a privileged tool to study a process so intimately tied to surface reaction such as ALE.

We have mounted the RDS setup on our newly acquired reactor in the first weeks following the first growth. Since that day RDS has been used as a routine

monitoring tool for every growth regardless of the nature of the technique. It has proven itself extremely useful to detect subtle effects such as slow roughening of the surface when a buffer layer is grown on a badly cleaned substrate. Variations in the mass flow controller outputs have been detected during our experiments with the growth of GaSb. In retrospect RDS has turned out to be a very useful tool for us.

In the case of the present work the technique was applied to the study of a specific process, ALE. The growth of GaAs by ALE being the most documented, we focused most of our attention on this material. We have shown that contrary to the current beliefs the surface of GaAs retains its double layer of As as its termination even after the 2 s purge following exposure to TBAs. Most previous interpretation were discarding this possibility because it was believed that every As on the surface would participate in the inclusion of a Ga atom in the crystal. A growth rate of 1 ML per cycle could not be explained with the presence of almost 2 ML of As when the Ga atoms arrive at the growth front. Our work has shown that not only is the presence of second layer of As a fact in ALE but it is critical for the establishment of a 1 ML/cycle growth mode. The second layer of As, because of its relatively stable bond structure to the underlying first layer atoms inhibits their desorption. This desorption would occur under normal single layer termination because of charge neutrality arguments and reconstruction of the surface.

The interactions between the Ga atoms on the surface with their As neighbors have been shown to be important. The second layer As leave the surface more readily when there is some Ga present. We have attributed this effect to a combination of displacement of As by incorporated Ga and a facilitation of As desorption by the formation of a methyl-As bond.

The Ga gradually covers the surface until a complete ML is included. Here again the natural coverage for an adsorbate-free surface is not 1 ML but 0.75 ML for the normal Ga rich reconstruction. The presence of methyl radicals attached to the Ga atoms changes the conditions and permits a full ML of Ga to enter the layer and remain there to complete the cycle. This constitutes the second role played by the methyl radicals. Their third and most important role was demonstrated in a surface

morphology study that we performed on GaAs surface saturated with Ga. We were able to show that the presence of methyl radicals on the surface inhibits the formation of Ga droplets and maintains the self-limiting character of the growth.

The important role of methyl radicals on the controlled ALE growth has several repercussion on the future of the technique as a candidate for specific applications. The high concentrations of residual carbon in GaAs grown by ALE has been a major factor in the relative lack of interest of the industry for the technique. From the result of this work and others it seems that methyl radicals which are thought to be responsible for the incorporation of carbon, are also essential to the self-limiting behavior of the growth. This tradeoff constitutes a significant hurdle to overcome if the technique hopes to achieve high purity material. The solution might lie in a different type of precursor. The configuration of the molecule should allow it to dissociate through homolytic fission to keep some radical attached to the Ga upon incorporation in order to maintain self-limiting growth and to allow the formation of a reconstruction with 1 ML of Ga. The same radical must then have a bond to the Ga that is weak enough to be easily desorbed during the subsequent purge.

On the other hand the microscopic process by which the carbon is incorporated is not known. The residual levels of doping correspond to a 1 ppm concentration approximately. This is several orders of magnitude smaller than the methyl concentration during the process. The radical removal is therefore relatively efficient. There might be some specific microscopic environment that retains the radical at the surface and permits its decomposition and the incorporation of the carbon atom. Experiments on miscut substrates have shown that the carbon incorporation is not affected by a larger concentration of step edges. The mysterious favorable sites are not simple step edges as one might suggest.

In the study of self-limiting growth the proposed role of the radicals have been manifold. One of these roles was to cover the surface and block a certain number of sites from reacting with other TMGa molecules. This argument was used to explain the constant Ga incorporation rate during group III exposure in ALE. We have demonstrated that for GaAs the temperatures used for ALE are high enough for gas

phase reactions to take place. The ability to fit the growth rate data of other models relying exclusively on surface dynamics has been used as an argument to claim their pertinence. We have shown that a model using exclusively gas phase reactions can also reproduce the same results and even explain the ALE data. We think that this demonstrates that a complete picture of ALE should include both kinds of reactions. The reality seems to be much more complex for ALE than was first thought.

Finally the potential of RDS as an *in situ* probe for the growth of complex structure was demonstrated in the monitoring of the surface during the growth of SMQW of InAs in GaAs. The presence of In segregation in those systems has been indirectly inferred in the past from post growth *ex situ* measurements but we have shown that RDS is indeed exclusively sensitive to the top few angstroms of the crystal and can be very efficient in detecting processes such as segregation.

Appendix A: Electronic feedback for the RDS setup.

Since the RDS setup measures the ratio $\Delta R/R$ two different approaches are possible to accurately do so. Both values of the ratio can be measured independently, allowing for more flexibility in the use of the setup and providing accurate information of both the Ac and DC signals, or one value can be kept constant by some kind of electronic control and the other measured. The second method has the advantage of being simpler and easier to implement and is the one that we have chosen for our experiments. This appendix describes the electronic circuit that was used to control the level of the DC signal. Fig. A.1 shows a simplified flow chart of the different components of the circuit as well as the current and voltage levels around the feedback loop. The programmable power supply is controlled by a DC voltage between 0 and 3 V corresponding to a supply voltage of 1500 and 600 V respectively. The current output of the PMT is converted to voltage and the DC part of the signal is extracted by a low pass filter. This signal is then compared to a reference signal by a differential amplifier and, in the case of a discrepancy, a signal is sent to the programmable power supply to change the PMT gain. Fig. A.1 shows the schematics of the electronic feedback circuit that we have built to control the DC signal. It uses analog electronics to control the gain of the PMT through a programmable gain power supply in order to keep the DC signal level constant. The circuit behaves well for the requirements of the system. No oscillation of the feedback loop is observed even during the rapid changes of the response when the spectrometer is quickly repositioned to the start of a new scan.

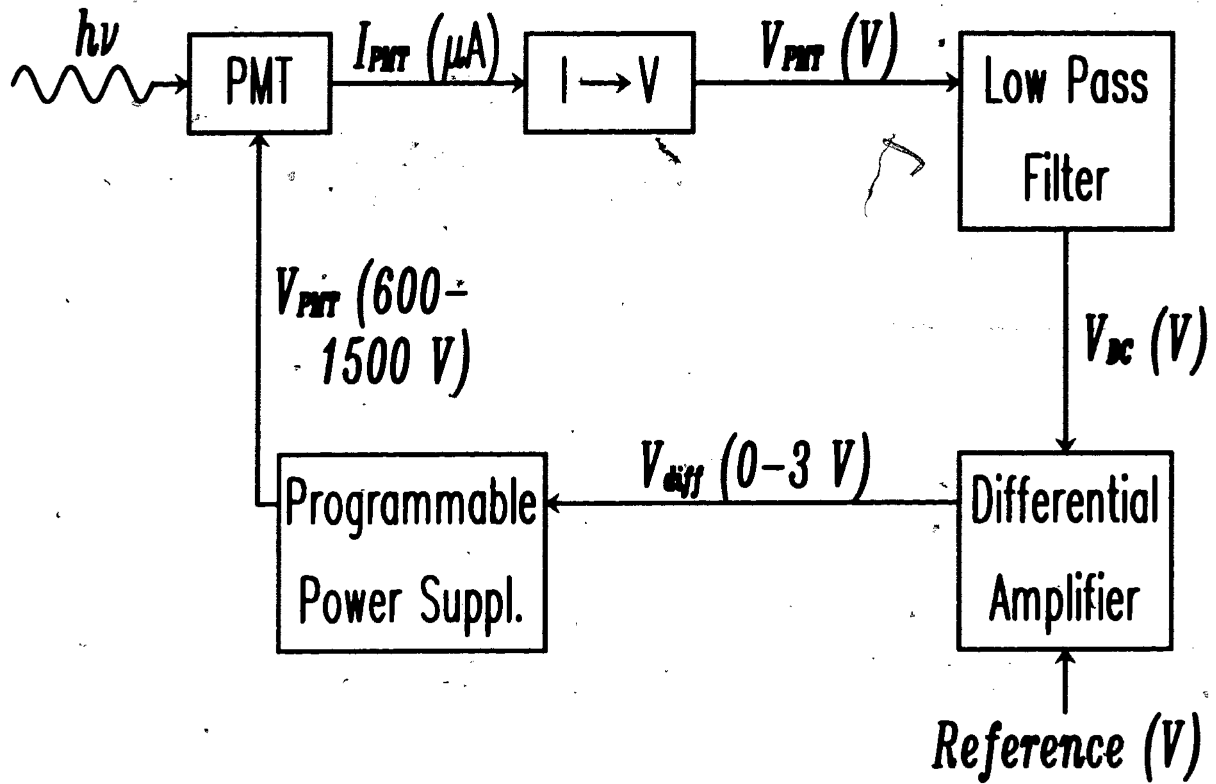

Fig. A.1 Simplified schematic representation of the circuit detailed in Fig. A.2.

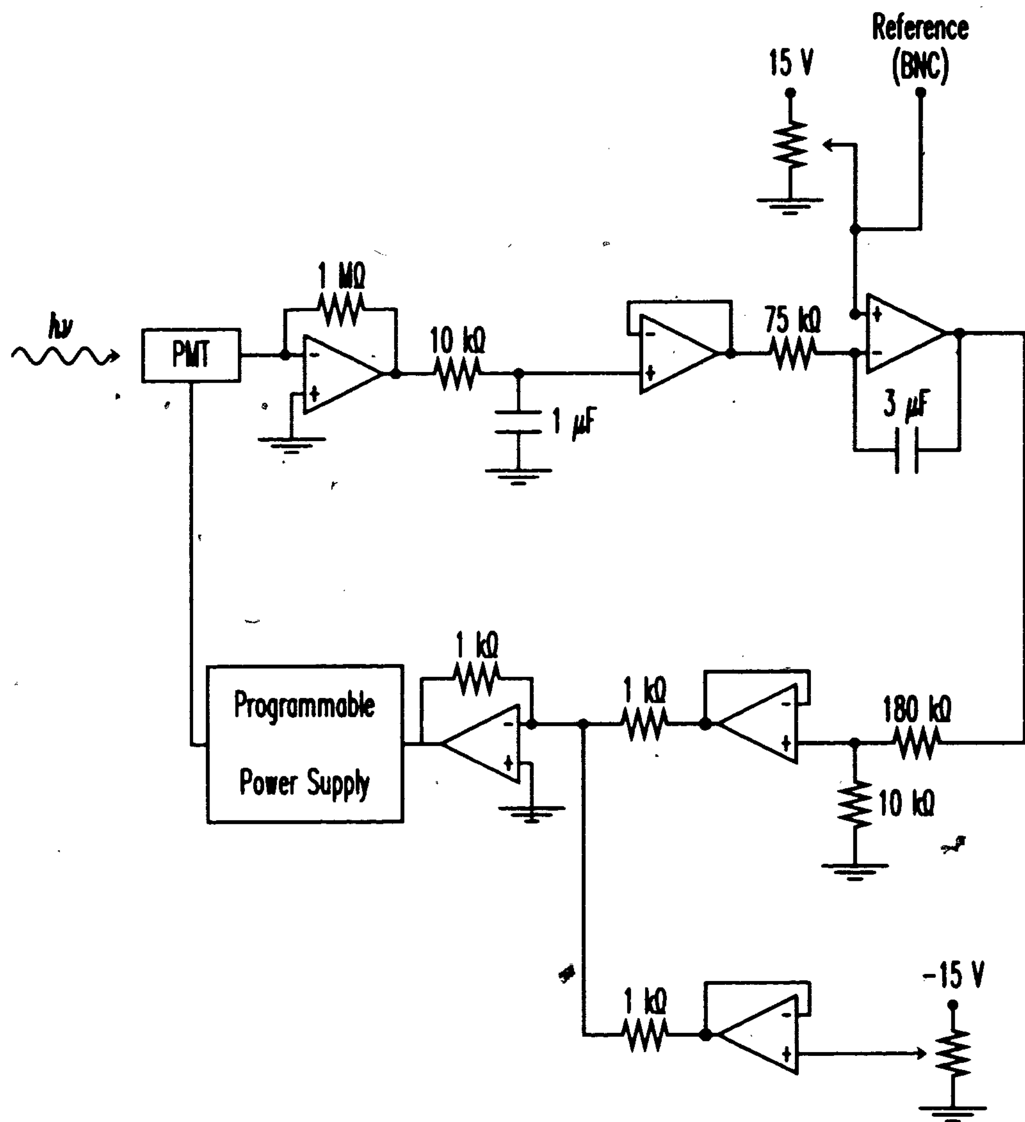

Fig. A.2 Electronic circuit used to regulate the DC signal in the RDS setup.

References

1 G. B. Stringfellow, *Organometallic Vapor Phase Epitaxy: Theory and Practice.*, (Academic Press, London, 1989). p. 1.

2 T. Suntola, J. Anston, A. Pakkala, and L. Lindfors, *SID 80 Digest*, 108 (1980). (cited from G. B. Stringfellow, *Organometallic Vapor Phase Epitaxy: Theory and Practice*, (Academic Press, London, 1989).

3 H. Watanabe and A. Usai, *Inst. Phys. Conf. Ser.*, **83**, 1 (1987).

4 C. A. Wang, S. H. Groves, S. C. Palmateer, D. W. Weyburne, and R. A. Brown, *J. Cryst. Growth*, **77**, 136 (1986).

5 S. Patnaik, R. A. Brown, and C. A. Wang, *J. Cryst. Growth*, **96**, 153 (1989).

6 H. K. Moffat, and K. F. Jensen, *J. Cryst. Growth*, **77**, 108 (1986).

7 J. Van de Ven, G. M. J. Rutten, M. J. Raaijmakers, and L. J. Giling, *J. Cryst. Growth*, **76**, 352 (1986).

8 H. Watanabe, and A. Usai, *Inst. Phys. Conf. Ser.*, **83**, 129 (1987). reference taken from G. B. Stringfellow, *Organometallic Vapor Phase Epitaxy: Theory and Practice*, (Academic Press, London, 1989). p.367.

9 B. Y. Maa, and P. D. Dapkus, *J. Electron. Mater.*, **19**, 289 (1990).

10 P. D. Dapkus, B. Y. Maa, Q. Chen, W. G. Jeong, and S. P. DenBaars, *J. Cryst. Growth*, **107**, 73 (1991).

11 J. R. Creighton, and B. A. Banse, *Mat. Res. Soc. Symp. Proc.*, **222**, 15 (1991).

12 M. Ozeki, K. Mochizuki, N. Ohtsuka, and K. Kodoma, *Appl. Phys. Lett.*, **53**, 1509 (1988).

13 M. L. Yu, N. I. Buchan, R. Souda, and T. F. Kuech, *Mat. Res. Soc. Symp. Proc.*, **222**, 3 (1991).

14 M. Ozeki, *Mat. Sci. Rep.*, **8**, 97 (1992).

15 E. Colas, R. Bhat, B. J. Skromme, and G. C. Nihous, *Appl. Phys. Lett.*, **55**, 2769 (1989).

16 D. E. Aspnes, J. P. Harbison, A. A. Studna, and L. T. Florez, *J. Vac. Sci. Technol. A*, **6**, 1327 (1988).

17 A. J. Pidduck, D. J. Robbins, A. G. Cullis, D. B. Gasson, and J. L. Glasper, *J. Electrochem. Soc.*, **136**, 3083 (1989).

18 Y. Horikoshi, H. Yamaguchi, F. Briones, and M. Kawashima, *J. Cryst. Growth*, **105**, 326 (1991).

19 D. E. Aspnes, W. E. Quinn, and S. Gregory, *Appl. Phys. Lett.*, **57**, 2707 (1991).

20 T. Stehlin, M. Feller, P. Guyot-Sionnet, and Y. R. Shen, *Opt. Lett.*, **13**, 389 (1988).

21 L. P. Sadwick, K. L. Wang, D. L. Joseph, and R. F. Hicks, *J. Vac. Sci. Technol. A*, **7**, 273 (1989).

22 H. H. Farrell, J. P. Harbison, and L. D. Peterson, *J. Vac. Sci. Technol. B*, **5**, 1482 (1987).

23 D. J. Chadi, *J. Vac. Sci. Technol. A*, **5**, 834 (1987).

24 M. D. Pashley, K. W. Haberern, W. Friday, J. M. Woodall, and P. D. Kirchner, *Phys. Rev. Lett.*, **60**, 2176 (1988).

25 D. K. Biegelsen, R. D. Bringans, J. E. Northurp, and L. E. Swartz, *Phys. Rev. B*, **41**, 5701 (1990).

26 J. D. E. McIntyre, and D. E. Aspnes, *Surf. Sci.*, **24**, 417 (1971).

27 P. Yeh, *Surf. Sci.*, **96**, 41 (1980).

28 R. M. A. Azzam, and N. M. Bashara, *Ellipsometry and Polarized Light*, (North Holland, Amsterdam, 1977), chap. 4.

29 D. E. Aspnes, J. P. Harbison, A. A. Studna, and L. T. Florez, *Phys. Rev. Lett.*, **59**, 1687 (1987).

30 I. Kamiya, D. E. Aspnes, L. T. Florez, and J. P. Harbison, *Phys. Rev. B*, **46**, 15894 (1992).

31 I. Kamiya, L. Mantese, D. E. Aspnes, D. W. Kisker, P. H. Fuoss, G. B. Stephenson, and S. Brennan, *J. Cryst. Growth*, **163**, 67 (1996).

32 Y. C. Chang, and D. E. Aspnes, *Phys. Rev. B*, **41**, 12002 (1990).

33 S. Brennan, P. H. Fuoss, J. L. Kahn, and D. W. Kisker, *Nucl. Instr. Meth. Phys. Res. A*, **291**, 86 (1990).

34 D. E. Aspnes, *IEEE J. Quantum Electron.*, **25**, 1056 (1989).

35 D. E. Aspnes, I. Kamiya, H. Tanaka, and R. Bhat, *J. Vac. Sci. Technol. B*, **10**, 1725 (1992).

36 D. E. Aspnes, I. Kamiya, H. Tanaka, R. Bhat, L. T. Florez, J. P. Harbison, W. E. Quinn, M. Tamargo, S. Gregory, M. A. A. Pudensi, S. A. Schwarz, M. J. S. P. Brasil, and R. E. Nahory, *Thin Solid Films*, **225**, 26 (1993).

37 L. Tafter, and K. Ploog, *Phys. Rev. B*, **40**, 9802 (1989).

38 L. Tafter, M. Ospelt, and H. von Känel, *J. Appl. Phys.*, **67**, 1298 (1990).

39 I. Kamiya, D. E. Aspnes, H. Tanaka, L. T. Florez, J. P. Harbison, and R. Bhat, *J. Vac. Sci. Technol. B*, **10**, 1716 (1992).

40 D. W. Kisker, G. B. Stephenson, I. Kamiya, P. H. Fuoss, D. E. Aspnes, L. Mantese, and S. Brennan, *Phys. Stat. Sol. A*, **152**, 9 (1995).

41 Y. Yamaguchi, K. Uwai, and N. Kobayashi, *Jpn. J. Appl. Phys.*, **32**, 3363 (1993).

42 A. Sakamoto, S. Otake, and I. Iwasa, *Jpn. J. Appl. Phys.*, **32**, L1318 (1993).

43 M. Zorn, J. Jönsson, W. Richter, J.-T. Zettler, and K. Ploska, *Phys. Stat. Sol. A*, **152**, 23 (1995).

44 S. M. Scholz, A. B. Müller, W. Richter, D. R. T. Zahn, D. I. Westwood, D. A. Woolf, and R. H. Williams, *J. Vac. Sci. Technol. B*, **10**, 1710 (1992).

45 J. Drowart, S. Smoes, and Vanderauwera-Mahieu, *J. Chem. Thermodyn.*, **10**, 453 (1978). Referenced from ref. 41.

46 E. N. Vigdorovich, V. V. Popov, M. M. Artamonov, and V. M. Andreev, *Izv. Akad. Nauk. SSSR Neorg. Mater.*, **9**, 771 (1973). Referenced from ref. 41.

47 A. Dip, G. M. Eldallal, P. C. Colter, N. Hayafuji, and S. M. Bedair, *Appl. Phys. Lett.*, **62**, 2378 (1993)..

48 M. Mochizuki, M. Ozeki, K. Kodoma, and N. Ohtsuka, *J. Cryst. Growth*, **93**, 557 (1988).

49 P. Yeo, R. Arès, and S. P. Watkins, *J. Electron. Mater.*, submitted (1997).

50 C. A. Tran, R. Arès, S. P. Watkins, G. Soerensen, and Y. Lacroix, *J. Electron. Mater.*, **24**, 1597 (1995).

51 B. Y. Maa, and P. D. Dapkus, *Appl. Phys. Lett.*, **58**, 2261 (1991).

52 M. G. Jacko, and S. J. W. Price, *Can. J. Chem.*, **41**, 1560 (1963).

53 N. Kobayashi, *J. Cryst. Growth*, **145**, 1 (1994).

54 P. E. Gee, H. Qi, and R. F. Hicks, *Surf. Sci.*, **330**, 135 (1995).

55 Y. Sakuma, S. Muto, K. Nakajima, and N. Yokoyama, *Appl. Surf. Sci.*, **82/83**, 239 (1994).

56 J. R. Creighton, *Appl. Surf. Sci.*, **82/83**, 171 (1994).

57 J. R. Creighton, *Surf. Sci.*, **234**, 287 (1990).

58 H. Yokoyama, M. Tanimoto, M. Shinohara, and N. Inoue, *Appl. Surf. Sci.*, **82/83**, 158 (1994).

59 C. R. Abernathy, P. W. Wisk, A. C. Jones, and S. A. Rushworth, *Appl. Phys. Lett.*, **61**, 180 (1992).

60 D. E. Aspnes, R. Bhat, E. Colas, V. G. Keramidas, M. A. Koza, and A. A. Studna, *J. Vac. Sci. Technol. A*, **7**, 711 (1988).

61 S. P. DenBaars, and P. D. Dapkus, *J. Cryst. Growth*, **98**, 195 (1989).

62 J. R. Creighton, B. A. Bansenauer, *Thin Solid Films*, **225**, 17 (1993).

63 M. Yu, *Thin Solid Films*, **225**, 7 (1993).

64 J. Nishizawa, and T. Kurabayashi, *J. Cryst. Growth*, **93**, 98 (1988).

65 A. W. Adamson, *A Textbook of Physical Chemistry*, 2nd ed. (Academic Press, New York, 1979).

66 S. H. Groves, S. C. Palmateer, J. W. Caunt, and D. L. Hovey, *J. Cryst. Growth*, **93**, 242 (1988).

67 S. Berkman, V. S. Ban, and N. Goldsmith in *Heteroepitaxial Semiconductors for Electronic Devices*, ed. by G. W. Cullen and C. C. Wang, (Springer Verlag, New York 1978), p. 264.

68 S. W. Benson, *The Foundations of Chemical Kinetics*, (McGraw Hill, New York, 1960), p. 175.

69 S. P. DenBaars, B. Y. Maa, P. D. Dapkus, A. D. Danner, and H. C. Lee, *J. Cryst. Growth*, **77**, 188 (1986).

70 *Adsorption on Metal Surfaces*, ed. by J. Bénard (Elesevier, New York, 1983).

71 T. C. Chiang, R. Ludeke, and D. E. Eastman, *Phys. Rev. B*, **25**, 6518 (1982).

72 J. Massie, F. Turco, A. Salettes, and J. P. Contour, *J. Cryst. Growth*, **80**, 307 (1987).

73 C. Guille, F. Houzay, J. M. Moison, and F. Barthe, *Surf. Sci.*, **189/190**, 1041 (1987).

74 R. A. Stall, J. Zilko, V. S. Swaminathan, and N. Schumaker, *J. Vac. Sci. Technol. B*, **3**, 524 (1985).

75 C. Raisin, H. Tegmousse, and L. Lassabatère, *Vide Couches Minces*, **41**, 241 (1986).

76 V. Bressler-Hill, A. Lorke, S. Varma, P. M. Petroff, K. Pond, and W. H. Weinberg, *Phys. Rev. B*, **50**, 8479 (1994).

77 M. A. Alonso, M. Ilg, and K. Ploog, *Phys. Rev. B*, **50**, 1628 (1994).

78 P. D. Wang, N. N. Ledentsov, C. M. Sotomayor Torres, P. S. Kop'ev, and V. M. Ustinov, *Appl. Phys. Lett.*, **64**, 1526 (1994).

79 N. Ikoma and S. Ohkouchi, *Jpn. J. Appl. Phys.*, **34**, L724 (1995).

80 S. Fafard, R. Leon, D. Leonard, J. L. Merz, and P. M. Petroff, *Phys. Rev. B*, **52**, 5752 (1995).

81 N. K. Dutta, N. Chand, J. Lopata, and R. Wetzel, *Appl. Phys. Lett.*, **60**, 924 (1992).

82 H. Yamaguchi and Y. Horikoshi, *J. Appl. Phys.*, **68**, 1610 (1990).

83 J. M. Moison, F. Houzay, F. Barthe, J. M. Gérard, B. Jusserand, J. Massie, and F. S. Turco-Sandroff, *J. Cryst. Growth*, **111**, 141 (1991).

84 N. Grandjean, J. Massie, and M. Leroux, *Phys. Rev. B*, **53**, 998 (1996).

85 R. Arès, C. A. Tran, and S. P. Watkins, *Can. J. Phys. suppl. 1*, **74**, S85 (1996).

86 C. A. Tran, R. Arès, S. P. Watkins, and G. Soerensen, *J. Electron. Mater.*, **24**, 11 (1995).

87 J. M. Moison, C. Guille, F. Houzay, F. Barthe, and M. Van Rompay, *Phys. Rev. B*, **40**, 6149 (1989).

88 K. Muraki, S. Fukatsu, Y. Shiraki, and R. Ito, *J. Cryst. Growth*, **127**, 546 (1993).

89 C. A. Tran, R. Arès, V. A. Karasyuk, S. P. Watkins, G. Létourneau, and R. Léonelli, *Phys. Rev. B*, **55**, 4633 (1997).

90 O. Brandt, L. Tapfer, R. Cingolani, K. Ploog, M. Hohenstein, and F. Phillipp, *Phys. Rev. B*, **41**, 12599 (1990).

91 P. Yeo, private communication.